Sudan University of Science and Technology

College of Graduate Studies

Removal of Heavy Metals from Oil Fields Drilling Mud Wastewater Using Zeolite.

إزالة العناصر الثقيلة للمخلفات الطينية المائية للحفر فى حقول البترول بأستخدام الزيولايت

A Thesis Submitted for the Fulfilment of the Requirement for the Degree of Doctor of Philosophy in Chemistry

By

Sahl Ibrahim Bakhit Yasin

BSc. M.Sc. (Chemistry)

Supervisor: Dr. Elmugdad Ahmed Ali

Co- Supervisor: Dr. Adil Elhag Ahmed

Jan 2017

Sudan University of Science & Technology

College of Graduate Studies

بسم الله الرحمن الرحيم

كلية الدراسات العليا

جامعة السودان للعلوم

والتكنولوجيا

كلية الدراسات العليا

Approval Page

Name of Candidate: Sahl Ibrahim Bakhit Yasin

Thesis title: Removal of Heavy Metals from Oil Fields Drilling Mud Wastewater Using Zeolite

Approved by:

1. External Examiner

Name: Elshiekh Elgilany Elbasher

Signature: ..... Date: 21.03.2017

2. Internal Examiner

Name: Mohammed Elmubark Osman

Signature: ..... Date: 01/03/2017

3. Supervisor

Name: Elmugdad Ahmed ALi

Signature: ..... Date: .....

الاية

أَوَلَمْ يَسِيرُوا فِي الْأَرْضِ فَيَنظُرُوا كَيْفَ كَانَ عَاقِبَةُ الَّذِينَ مِن قَبْلِهِمْ وَكَانُوا أَشَدَّ مِنْهُمْ قُوَّةً ۚ وَمَا كَانَ اللَّهُ لِيُعْجِزَهُ مِن شَيْءٍ فِي السَّمَاوَاتِ وَلَا فِي الْأَرْضِ ۚ إِنَّهُ كَانَ عَلِيمًا قَدِيرًا

سورة فاطر الاية 44

Dedication

To

The soul of my mother,

To

my Father,

sisters,

and brothers

Acknowledgments

I gratefully acknowledge my supervisor Dr.Elmugdad Ahmed Ali my research guide, for the fruitful guidance and extended inspiration provided for my research work. He has always encouraged me to work on the problems of my choice and never forced his opinions and views on me. He gave me a lot of confidence and freedom to work, and I really enjoyed working with him.

I would like to thank my Co-supervisor Dr. Adil Elhag Ahmed, the man who thought different, rich in knowledge and helpful.

I would like to thank deeply the staff of the chemistry department (SUST).

I would like to thank Abdeazem Eldoma of the Central Forensic Lab. for running (SEM&EDX) spectra.

I cannot forget the tremendous help I received from my friends.

Special thanks to Hala and Marwan Awad for their continuous assistance.

Abstract

The aim of this research work was to study the potential capability of zeolites and kaolin to remove some, heavy, metals from drilling mud wastewater.

Four samples were used, (three zeolites and one kaolin). Two natural zeolites (Stablite and Stellerite) collected from Al Gadaref state (East Sudan), synthesized zeolite from fly ash using sodium hydroxide under hydrothermal conditions. Kaolin sample collected from Elmerkhiat mountain (North-East Omdurman Sudan).

X-ray diffraction (XRD) was used to indicate crystal structure and ascertain zeolites and kaolin quality, the result shows that stablite (ZN1), have monoclinic, for stellerite (ZN2) similar to orthorhombic, synthesized zeolite (SZ) attributed to hexagonal and for natural kaolin (ka) triclinic. X-ray fluorescence (XRF), shows that major constituents of sample are SiO_2 and Al_2O_3, in addition some other oxide, such as MgO, CaO, Fe_2O_3, TiO_2 and Na_2O were also detected. The main constituents were confirmed by scanning electron microscopy (SEM), and Energy Dispersive (EDX) analysis to be oxygen, silicon and aluminum, and the main function group of samples were determined using, Fourier Transform Infrared (FT-IR) analysis to determine framework of sample (SiO_4 and AlO_4) from 681cm^{-1} to 698cm^{-1}. The morphology of samples investigated using (SEM) to show a profound crystalline property of the samples. In addition, specific surface area, pore size and pore volume of samples investigated by N_2 (adsorption- desorption) analysis, surface area of ZN1 was 20.44m^2/g, ZN2 26.88m^2/g, SZ 40.717m^2/g and Ka 14.73m^2/g, the pore size was 11.8 nm, 12.69nm, 13.8 nm and 18.02nm respectively. Some parameters such as pH, concentration and contact time were optimized for efficiency, from stander solutions of (Cr^{3+}, Co^{2+}, Zn^{2+} and Fe^{2+}), the optimum condition for removal were 4.5 to 6.0 pH, metal concentration of 200ppm and 80 minutes. These conditions were adopted to minimize the level of targeted heavy metals in wastewater of drilling mud (fluid) collected from oil filed. The experimental data showed that the respective efficiency

percent of those species were 66.6%, 80, 80%, 50% and 77% for ZN1, 83.8%, 96.8%, 38.4%, and 38.3% for ZN2, 99%, 97%, 98% and 80% for SZ and 72.8%, 78.6%,77.9% and 39% for Ka. Synthesized zeolite showed high affinity to remove heavy metals due to increased surface area 40.317m^2/g.

المستخلص

يهدف البحث الى دراسة قدره الزيولايت والكاولين على إزاله بعض العناصر الثقيله من مخلفات سوائل الحفر. أستخدمت أربعه عينات عينات, ثلاثة عينات من الزيولايت وعينه من الكاولين.

الزيولايت الطبيعى تم جمعه من منطقة ودكولى (ولايه القضارف- شرق السودان) , والزيولايت الصناعى تم تحضيره من مخلفات الفحم الحجرى باستخدام هيدروكسيد الصوديوم فى درجات حرارة مختلفة, جمعت عينه الكاولين الطبيعى من منطقه المرخيات (شمال أم درمان- السودان).

تم إستخدام الاشعه السينية المتشتته لقياس التراكيب البلورية ومعرفة كمية الزيولايت والكاولين, أظهرت النتائج بإن النوع الاول من الزيولايت الطبعيى ينتمى الى آحادى الميل والنوع الثانى الطبيعى المعين المستقيم, اما الزيولايت المصنع تركيبه سداسى , والكاولين الطبيعى ثلاثى الميل.

الاشعه الفلورنسية اكدت بان العينات أحتوت على نسب من أوكسيد السيلكون وأوكسيد الالمونيوم بكميات, وبعض اكاسيد الفلزات مثل اوكسيد المغنزيوم و الكالسيوم والحديد والتاتنيوم تم تحديدها.

كمية العناصر الاساسية تم التحقق منها بواسطة جهاز التصوير الدقيق وجهاز الالكترونات المتباعده أظهرت النتائج بان الاوكسجين والسيلكون والالمونيوم عناصر ذات تراكيز اعلى فى العينات.

المجموعات الوظيفية قيست بواسطة جهاز الاشعة تحت الحمراء وحددت أيضا التركيب الاساسى للعينات التى كانت فى المدى بين $681cm^{-1}$ to $698cm^{-1}$

أما الشكل الخارجى للعينات تم التحقق منه بواسطة جهاز التصوير الدقيق الذى أكد ايضاّ عمق التراكيب البلورية للعينات. أما مساحة السطح الكلية وحجم ومساخه الفتحات الداخلية قيست بواسطه جهاز أمتزاز النتروجين, مساحة سطح النوع الاول الطبيعى كانت حوالى $20.44m^2/g$ وللنوع الثانى الطبيعى $26.88m^2/g$ وللزيولايت المصنع $40.317m^2/g$ وللكاولين كانت $14.73m^2/g$.

بعض العوامل مثل الاس الهيدروجينى والتركيز وزمن الالتصاق أثرت فى عملية الازالة للمحاليل المائية المحضره من الكروم و الكوبالت والخارصين والحديد. أفضل عوامل الازاله كانت 4.5 الى 6.0 على مستوى الحموضة وبتركيز قدره 200 جزء من المليون فى زمن قدره 80 دقيقة, هذه العوامل تم التاكيد عليها لازاله العناصر الثقيله من مخلفات سوائل الح9فر التى جمعت من الحقل , واظهرت النتائج نسب الازاله كاتى:

للنوع الاول الطبيعى 66% , 80% , 50% , 77% , أما النوع الثانى الطبيعى كانت 83.8% , 96.8% , 38.4% , 38.3% , وللزيولايت المصنع 99% , 97% , 98% , 80% , وللكاولين 72.8% , 39% .

أظهر الزيولايت المصنع قدره عالية على الازاله نسبه لزياده مساحة سطحه التى تعادل حوالى $40.317m^2/g$.

Table of Contents

List of Tables

List of figures

Abbreviations

ZN1*:* Natural zeolite (stablite)

ZN2: Natural Zeolite (Stellerit)

SZ: Synthesis zeolite

Ka: Kaolin

RH : Rice husk

ANA	Analcime
BIK	Bikitaite
CAN	cancrinite
EDI	Edingtonite
FAU	NaX
FRA	franzinite
GIS	Gismondine
GME	Gmelinite
JBW	NaJ
LAU	laumonite
LEV	levyne
LIO	liottite
LOS	losod
LTA	linde type A
LTN	NaZ-21
NAT	Natrolite
PAR	partheite
PHI	philipsite
ROG	Roggianite
SOD	Sodalite

WEN	Wenkite
THO	Thomsonite
TSC	Tschornerite
ABW	Li-A(BW)
AFG	afghanite
BHP	linde Q
BOG	boggsite
BRE	brewsterite
CAS	aluminosilicate
CHA	chabazite
CHI	chiavennite
DAC	dachiardite
EMT	hexagonal faujasite
EPI	epistibite
ERI	erionite
FAU	faujasite,NaY
FER	ferrierite
GOO	goosecreekite
HEU	heulandite
KFI	ZK-5
LOV	lovdarite
LTA	Lind A
LTL	linde L
MAZ	mazzite
MEI	ZSM-18
MER	merlinoite
MON	montasommaite
MOR	mordenite

OFF	offretite
PAU	paulingite
RHO	Rho
STI	stibnite
YUG	yugawaralite

DAM : dehydro-aromatization of methane

SS : suspended solids

COD : chemical oxygen demand

Chapter one

Introduction and

Literature Review

1.1. Introduction to chemistry of zeolite

The term zeolite was originally coined in the 18th century by a Swedish mineralogist named Cronstedt who discovered the first zeolite minerals Staiblie (kind of natural zeolite),he suggested zeolites as new class of minerals containing hydrated aluminosilicate alkali and earth alkali.(Flanigen et al. 2010).

Zeolites are micro porous crystalline aluminosilicates, composed of TO_4 tetrahedral (T = Si, Al) with O atoms connecting neighboring tetrahedral. For a completely siliceous structure, combination of TO_4 (T = Si) units in this fashion leads to silica (SiO_2), which is an uncharged solid. Upon incorporation of Al into the silica framework, the 3^+ charge on the Al makes the framework negatively charged, and requires the presence of extra framework cations (inorganic and organic cations can satisfy this requirement) within the structure to keep the overall framework neutral. The zeolite composition can be best described as having three components:

$$M^{m+}_{n/m} \qquad (Si_{1-n}\ Al_nO_2) \qquad nH_2O$$

Extra framework • cations framework • sorbed phase

The extra framework cations are ions exchangeable and give rise to the ion-exchange chemistry of these materials. The important of zeolites stems from their microporosity which is theresult of the topology of the framework. The amount of Al within the framework can vary over a wide range, with Si/Al = 1 to l, the completely siliceous form being polymorphs of SiO_2. Lowenstein proposed that the lower limit of Si/Al = 1 of a zeolite framework arises because placement of adjacent AlO_4^- tetrahedra is not favored because of electrostatic repulsions between the negative charges. The framework composition depends on the synthesis conditions. Post synthesis modifications that insert Si or Al into the framework have also been developed. As the Si/Al ratio of the framework increases, hydrothermal stability as well as hydrophobicity increases.(Auerbach 2003)

Zeolites are crystallized, hydrated alumosilicate alkalines and earth alkalnies cations which possess endless three-dimensional crystal structures which make them hard in water and insoluble which enables them to exchange their ions with suitable structure. zeolites, are contain (Si/Al)/O ratio must equal 1:2. The alumino-silicate structure is negatively charged and attracts the positive cations that reside within. Unlike most other tectosilicates, zeolites have large vacant spaces or cages in their structure that allow space for large cations, such as sodium, potassium, barium, calcium, and even relatively large molecules and cation groups such as water, ammonia, carbonate ions, and nitrate ions. In the more useful zeolites, the spaces are interconnected and form long wide channels of varying sizes depending on the mineral. These channels allow the easy movement of the resident ions and molecules into and out of the structure. The process of ions exchange is a heterogeneous process, while the zeolite structure (the changer of ion) practically does not change (Cejka et al. 2007).

1.2. Zeolite structure and composition

The best criteria for distinguishing zeolites and zeolite–like materials (porous tectosilicates) from denser tectosilicate is the number of tetrahedraly atoms per 1000 $A^{\circ 3}$. This number, which known as the framework density, is less than 21 T atoms per 1000$A^{\circ 3}$ for porous tectosilicates. The angle around T atoms in the TO_4 tetrahedral can vary over a wide range. IUPAC recommendations for nomenclature of structural and compositional characteristics of order micro porous and mesoporous materials with inorganic hosts with particular attention to the chemical composition of both host and guest species.(Auerbach 2003).

In addition, zeolite is crystalline aluminosilicate with a 4-connected tetrahedral framework structure enclosing cavities occupied by large ions and water molecules, both of which have considerable freedom of movement, permitting ion exchange and reversible dehydration. From this definition, we see that a zeolite contains three components: a 4-connected framework, extra frame work cations, and an adsorbed phase (in this case, the water molecules). Also it has to be noted that by definition a zeolite has an open structure with pores and voids where ions

and molecules can move. An example of a material that fits this definition, the zeolite mineral gismondine $|Ca^{2+}4(H_2O)_{16}|$ $[Al_8Si_8O_{32}]$. This formula means that in a unit cell of gismondine the tetrahedral framework contains eight aluminates ($[AlO_{4/2}]$) and eight silicate ($[SiO_{4/2}]$). Four extra frame work calcium cations balance the negative charge of the framework, and there are 16 water molecules in the cavities.(Cejka et al. 2007). All zeolite frameworks can be built by linking in a periodic pattern a basic building unit (BBU), the tetrahedron. In the center of the tetrahedra there are atoms with relatively low electronegativities (Si^{IV}, Al^{III}, P^{V}, Zn^{II}, etc.) and in the corners, there are oxygen anions (O^{-2}). These combinations can be depicted as $[SiO_4]$, $[AlO_4]$, $[PO_4]$, etc., and the term TO_4 is used to describe, tetrahedral in general, where T stands for any tetrahedral species. The notation $[TO_{4/2}]$ is often used to emphasize that each oxygen atom is coordinated to two T atoms. Considering each apical oxygen is shared with the adjacent tetrahedron and as a consequence the framework of zeolite materials always has a metal-to-oxygen ratio of 2. In general, the (O-T-O) angle is closed to the ideal value of 109° 28` for geometrical perfect tetrahedron and deviations of more than a few degrees. The T-O bond length depends on the particular metal cation, for (SiO_4) tetrahedral. The d(Al-O) is usually ≈ 1.73 A° whereas, the d(Zn-O) is ≈ 1.95 A°. More complex composite building units can be formed by linking groups of BBUs together. The simplest examples of CBUS are rings. All zeolite structures can be viewed as if they formed of tetrahedral rings of different sizes. In general, a ring containing n tetrahedral is called an n ring. The most common rings contain 4, 5, 6, 8, 10, or 12 tetrahedra (Fig. 1.1). However, materials with rings formed of 14, 18, up to 20 tetrahedra have also been prepared. Materials with 3-, 7- or 9- rings, are rare when a ring defines the face of a polyhedral unit, it is also called a window. More often they have more complicated shape and geometry. Elongated rings and rings that are puckered out of a plane are very common. The next levels of complexity are obtained by constructing larger CBUs from n rings giving rise to diverse and interesting sets of structures. Polyhedral cages characterized by too narrow rings that are too narrow to allow the passage

of molecules larger than water it is usually considered that 6-rings are the limited ring size to form a cage. Cavities are polyhedral units that differ from cages by containing windows that allow the passage of molecules in and out of the cavities, it should not be infinitely extended and should be distinguished from other units such as pores and channels. In case of zeolite A cavities ($4^{12}6^{8}8^{6}$) Linde Type A (LTA) , the cavities contain six 8-rings through which water molecules, linear alkanes, and small molecules like CO_2 and N_2 can penetrate. Since the cavities are connected to one another via the 8-ring molecules diffuse within the zeolite crystal by jumping between adjacent cages.

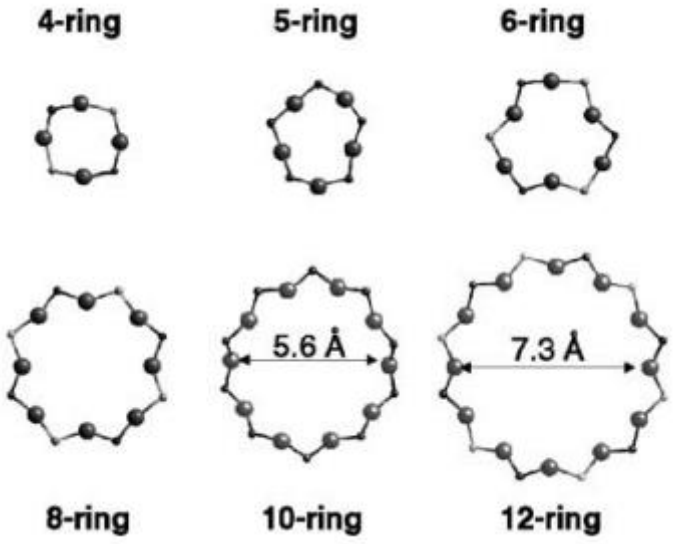

Fig (1.1) Relative sizes of n-rings frequently found in zeolites

A channel is pore that is infinitely, extended in at least one dimension with a minimum aperture size (n ring) that allows gust molecules to diffuse along the pore. In many zeolites the channels intersect forming two-and three-dimensional channels systems, the dimension of the pore is one of the critical properties of zeolite materials since this dimension determines the maximum size of the molecule that can enter from the exterior of the zeolite crystal into its microspores.(Auerbach 2003). Channels and cages of a zeolite framework are usually filled with extra-framework species such as exchangeable cations, which balance the negative charge of the framework, removable water molecules, and or

organic species. These may come from the synthesis mixture or they may be the result of a post-synthesis treatment. Whatever their origin, it is often of interest to know where they are located. Modern crystallographic techniques generally allow such information to be extracted from diffraction data, but there are some limitations that should be appreciated. The primary problem is the fact that extra-framework species do not generally follow the high symmetry of the framework, so they are what is called "disordered" (A.Martens 1987), (Cejka et al. 2007).

1.3. Types of zeolite

1.3.1 Natural zeolite:

The first natural microporous aluminosilicate, i.e., natural zeolite, was discovered more than 200 years ago. After long-term practical applications, the intrinsic properties of natural zeolites such as reversible water-adsorption capacity were fully recognized. By the end of the 19th century, during exploitation of ion-exchange capacity of some soils, it was found that natural zeolites exhibited similar properties: some cations in natural zeolites could be ion-exchanged by other metal cations. Natural zeolites were formed by the long-lasting effect of mineral alkaline solutions on various petrographic types of rocks of different ages at increased temperatures. Interestingly, these aluminium silicates are located near hot mineral springs or volcanic craters. However, the environment in which they were formed reflects their structure and chemical composition. In a natural environment zeolites, do not occur in a pure state but usually together with other minerals and rocks. Each deposit contains rocks with a specific structure. This fact explains the importance of comprehensive research focused on the properties of natural zeolites and options for their use. In the early decades of their discovery, natural zeolites could adsorb water, methanol, ethanol, and formic acid vapor, but could hardly adsorb acetone, diethyl ether, or benzene. Soon afterwards, scientists began to realize the importance of such features, and use these materials as adsorbents and desiccants. Later, natural zeolites were also used widely in the field of separation and purification of air. (Barlokova, 2008). With geological exploration and study on minerals, more and more natural zeolites have been

discovered. Up to now, over 40 types of natural zeolites have been found, but fewer than 30 of them have had their structures solved. Recently, many natural zeolite resources have been discovered, and the applications of these natural species are drawing increasing attention. At present, natural zeolites are, widely, used in the fields of drying and separation of gases and liquids, softening of hard water, treatment of sewage, and melioration of soils. Some well selected or modified natural zeolites are also used as catalysts or supports of catalysts in industry. Abundant natural zeolites were found later in sedimentary rocks. Since these zeolite deposits were usually located near the surface of the earth, it was concluded that they had been produced at temperatures and pressures which were not very high. During a study on strata of Triassic rocks, it was found that zeolites were somehow in a chemical equilibrium state when they were formed. Although, compared with natural zeolites, synthesized zeolites have many advantages such as high purity, uniform pore size, and better ion-exchange abilities. Natural zeolites are more applicable when there are huge demands and fewer quality requirements. The reason is that natural zeolites are often located near the surface of the earth and can be easily exploited and used after some simple treatments, which lead to lower costs . Therefore, natural zeolites have a good prospect of application especially in the fields of agriculture and environmental protection (Auerbach 2003).

1.3.1.1 Families of natural zeolite

There are about 45 natural minerals that are recognized members of the zeolite group

●1/The Analcime family:

-Analcima (Hydrated sodium Aluminum silicate)

-Pollucite (Hydrated Cesium Aluminum silicate)

-Wariakite (Hydrated Calcium sodium aluminum silicate)

- Bellbergite (Hydrated Potassium Barium Strontium Sodium Aluminum silicate)

-Bikitaite (Hydrated Lithium Aluminum Silicate)

-Boggsite (Hydrated Calcium Sodium Aluminum Silicate)

Brewesterite (Hydrated Strontium Barium Sodium Calcium Aluminum Silicate)

●2/ The Chabazite family

-chabazite (Hydrated Calcium Aluminum Silicate)

-Willhendersonite (Hydrated Calcium Sodium Potassium Aluminum Silicate)

-Cowlesite (Hydrated Calcium Aluminum Silicate)

-Dachiardite (Hydrated Calcium Sodium Potassium Aluminum Silicate)

-Edingtonite (Hydrated Barium Calcium Aluminum Silicate)

-Epistibite (Hydrated Calcium Aluminum Silicate)

-Erionite (Hydrated Sodium Potassium Calcium Aluminum Silicate)

-Faujasite (Hydrated Sodium Calcium Magnesium Aluminum Silicate)

- Ferrierite (Hydrated Sodium Potassium Magnesium Calcium Aluminum Silicate)

●3/ The Gismondine family

-Amicite (Hydrated Potassium Sodium Aluminum Silicate)

- Garronite (Hydrated Calcium Aluminum Silicate)

-Gismondine (Hydrated Barium Calcium Aluminum Silicate)

- Gobbinsite (Hydrated Sodium Potassium Calcium Aluminum Silicate)

-Gmelinite (Hydrated Sodium Calcium Aluminum Silicate)

-Gonnardite (Hydrated Sodium Calcium Aluminum Silicate)

-Goosecreekite (Hydrated Calcium Aluminum Silicate)

●4/ The Harmotome family

-Harmotome (Hydrated Barium Potassium Aluminum Silicate)

-Philipsite (Hydrated Potassium Sodium Calcium Aluminum Silicate)

-Wellsite (Hydrated Barium Calcium Potassium Aluminum Silicate)

●5/ The Heulandite family

-Clinoptiloite (Hydrated Sodium Potassium Calcium Aluminum Silicate)

-Heulandite (Hydrated Sodium Calcium Aluminum Silicate)

-Levyne (Hydrated Calcium Sodium Potassium Aluminum Silicate)

-Mazzite (Hydrated Potassium Sodium Magnesium Calcium Aluminum Silicate)

-Merlinoite (Hydrated Potassium Sodium Calcium Barium Aluminum Silicate)

-Montesommaite(Hydrated Potassium Sodium Aluminum Silicate)

-Mordenite (Hydrated Sodium Potassium Calcium Aluminum Silicate)

●6/The Natrolite family

-Mesolite (Hydrated Sodium Calcium Aluminum Silicate)

-Natrolite (Hydrated Sodium Aluminum Silicate)

-Scolecite(Hydrated Calcium Aluminum Silicate)

-Offretite (Hydrated Calcium Potassium Magnesium Aluminum Silicate)

-Paranatrolite (Hydrated Sodium Aluminum Silicate)

-Paulingite (Hydrated Potassium Calcium Sodium Barium Aluminum Silicate)

-Perlialite (Hydrated Potassium Sodium Calcium Strontium Aluminum Silicte)

●7/ The Stibite family

-Barrerite (Hydrated Sodium Potassium Calcium Aluminum Silicate)

-Stibite(Hydrated Sodium Calcium Aluminum Silicate)

-Stellerite(Hydrated Calcium Aluminum Silicate)

-Thomsonite(Hydrated Sodium Calcium Aluminum Silicate)

-Tscherichite(Hydrated Calcium Aluminum Silicate)

-Yugawaralite (Hydrated Calcium Aluminum Silicate)

Most zeolites known to occur in nature are of low Si/Al ratios. Table (1-1) indicates the neutral zeolites, sometimes natural zeolites are found as large single crystals (Colella, 2005)

Table (1-1) types of zeolites Si/Al ≤ 2

ANA	Analcime
BIK	Bikitaite
CAN	cancrinite
EDI	Edingtonite
FAU	NaX
FRA	franzinite
GIS	Gismondine
GME	Gmelinite
JBW	NaJ
LAU	laumonite
LEV	levyne
LIO	liottite
LOS	losod
LTA	linde type A
LTN	NaZ-21
NAT	Natrolite
PAR	partheite
PHI	philipsite
ROG	Roggianite
SOD	Sodalite
WEN	Wenkite
THO	Thomsonite
TSC	Tschornerite
ABW	Li-A(BW)
AFG	afghanite

Table (1-2) types of Zeolite (2< Si/Al ≤ 5) content

BHP	linde Q
BOG	boggsite
BRE	brewsterite
CAS	aluminosilicate
CHA	chabazite
CHI	chiavennite
DAC	dachiardite
EMT	hexagonal faujasite
EPI	epistibite
ERI	erionite
FAU	faujasite,NaY
FER	ferrierite
GOO	goosecreekite
HEU	heulandite
KFI	ZK-5
LOV	lovdarite
LTA	Lind A
LTL	linde L
MAZ	mazzite
MEI	ZSM-18
MER	merlinoite
MON	montasommaite
MOR	mordenite
OFF	offretite
PAU	paulingite
RHO	Rho
STI	stibnite
YUG	yugawaralite

1.3.2. Syntheses of zeolites

Zeolite synthesis is an active field of research because zeolites with uniform micropores are important in many industrial processes in catalysis, adsorption and separation, a large number of zeolites with new framework topologies, compositions, and properties have been, successfully, prepared. Up to now, thousands of zeolite materials have been prepared, which correspond to 174 types of structure (each being assigned a three-letter code by the Structure Commission of the International Zeolite Association). Since the pioneering work of Barrer and Milton (1959) on the synthesis of zeolites. The hydrothermal synthetic technique has become the basic route for zeolite synthesis. Hydrothermal synthesis usually refers to reactions occurring under conditions of high temperature–pressure >100°C >1 bar in aqueous solutions in a closed system. Hydrothermal synthetic techniques have been applied not only in the preparation of zeolites and related porous materials, but also in the preparation of most other important inorganic materials, such as superionic conductors, chemical sensors, electronically conducting solids, complex oxide ceramics and fluorides, magnetic materials, and luminescence phosphors. According to reaction temperature, the hydrothermal synthesis can be classified into subcritical and supercritical synthetic reactions. In subcritical synthesis, the temperature is in the range of 100 – 240 ℃, while in supercritical synthesis, the temperature could reach 1000 ℃ and the pressure may increase up to 3000 bar. Water can act as a mineralizer or a catalyst under elevated pressure–temperature conditions. The thermodynamic and transport properties of supercritical water are remarkably different from those of ambient water. The solubility of nonpolar species increases whereas that of ionic and polar compounds decreases. Under hydrothermal conditions, the physical and chemical properties of reactants are also significantly changed. High temperature and pressure hydrothermal conditions accelerate the reaction rate among the complex ions, intensify the hydrolyzation reaction, and significantly change the redox potential of the reactants. Consequently, hydrothermal conditions can promote the reactivity of reactants with low solubility at ambient temperature (Cejka, 2007).

Many kinds of zeolites can be synthesized for example from fly ash. (Gougazeh & Buhl 2014). (Mohamed et al. 2015).

1.3.2.1 Fly ash

Fly ash is mainly composed of some oxides derived from inorganic compounds, which remain after combustion of the coal. The amounts of the main components of ash viz. SiO_2 and Al_2O_3 and other metal oxide such as CaO, Fe_2O_3 and MgO, although some show few variations with the type of coal. The similar chemical composition of fly ash and some volcanic rocks prompted several research groups to attempt making zeolite from fly ash. The alkali–fly ash mixture facilitates the formation of highly active Na-aluminate and silicates, which are readily soluble in water and enhance zeolite formation. Using fusion followed by hydrothermal process, the investigators developed low silica, X-type zeolite selectively. KOH and NaOH can be used as activators to synthesize zeolite using both open and closed system.

Zeolite can be synthesized from other sources of silica and aluminum like rice husk (RH). RH is an agricultural residue abundantly available in rice producing countries. Much of the husk produced from the processing of rice is either burnt or dumped as waste. Even though some of this husk is converted into end products such as feedstock. Temperature can used to convert RH to gel or zeolite, it would be beneficial to the environment to recycle the waste to produce eco-material having a high end value (Mohamed et al. 2015)

1.3.2.2. Mineralizers

A mineralizer is a chemical species which makes possible the formation of a more stable solid phase from a less stable solid phase, through a dissolution precipitation or crystallization process. Thus, it allows the formation of a supersaturated solution, generally from a gel. In the case of zeolite synthesis mixtures, the solution contains, besides the poly condensable (useful) silicate and aluminosilicate species, other species which are in equilibrium with the former. One of the roles of the mineralizer is to increase the overall solubility, i.e. the concentration of all the species. It may be assumed that the mineralizer not only

increases the dissolution and condensation rates but also the conversion rates between the different species in the solution. It thus maintains the availability of the useful species at the level needed for nucleation and crystal growth. The mineralizer inters the dissolution during the transformation of crystallization, the low negative elements i.e Si, Al and P are present as silica and aluminasilicate anions in alkaline solutions, whereas OH- increase the solubility of silica by ionizing the silenol groups and breaking silozane bonds.

$SiOH + OH^- \longrightarrow SiO^- + H_2O$ (1)

$Si\text{-}O\text{-}Si + OH^- \longrightarrow SiO^- + HO\text{-}Si$ (2)

Thus, the monomeric silicic acid $Si(OH)_4$ which is sparingly soluble at pH 7 (= $2.\ 10^{-3}$ mol $^{-1}$) forms highly soluble silicate anions at high pH, but with fewer silanol groups

$Si(OH)_4 + nOH^- \longrightarrow Si(OH)_{4-n}O_n^{n-} + nH_2O$ (n=1-4) (3)

These anions are in equilibrium with oligomeric anions which have chain, cyclic or polyhydric structures. High concentrations and not too akaline pH values favor these oligomeric species. The presence of organic cations such as Me_4N^+ or Pr_4N^+ modifies the distribution of these species and may lead to the formation of specific species (e.g., double four- or five-membered rings). The condensation of the silicate and aluminate anions to form aluminosilicate anions and then the zeolite framework needs the presence of hydroxide groups. When the concentration of OH- increases, the silicate species will be less and less able to condense (the SiO^- / SiOH ratio increases), however alumina rich- zeolite observed at high pH and low pH favoring silica rich, although OH^- ions liberated by the transformation of non-bridge $=SiO^-$ groups, at high pH the low concentration of polycondesable silicate species may favor the formation of stable and dense phase. Other differences may be noticed when P^{3-} is used in place of OH^-. According to the stability of the different fluoro complexes it may be concluded that F^- is a mineralizer suitable for the synthesis of silica-rich zeolites. Fluoride allows

incorporation of soluble cations which are such as(Co^{2+}) and insoluble like $NH^{+}_{4.}$ (Wang & Peng 2010).(Anthony R. West 2014).

1.3.2.3. Templates

The contribution of template during synthesis facilitates the stability of the crystal solid and allow their formation. According to the nature of the T elements the charge density of the framework and the shape of the micro porous spaces, different stabilizing interactions can be produced by template-template bonds and/or template-framework bonds (cation-anion, dipole-ion, hydrogen and/or van der Waals bonds). However, many type of inorganic template like Na^{+} and Ca^{2+} which make framework charge, organic template such as alkayl ammonium, H_2O and amines are molecule template, NaCl and Pr_4NF as ion pair template **.**(Auerbach 2003).

1.4. Characterization of zeolite

Physical characterization of a materials, such as a zeolite begins in principle by visual inspection. This inspection can be refined by the use of instruments which enlarge small particles. Such instruments may be: an ordinary microscope, an electron microscope, or a raster scan electron microscope. Crystalline materials may often be identified by the shape of a crystal which also may give information concerning the presence of crystalline impurities. Furthermore, from the shape of the crystals and their size distribution conclusions may even be drawn which render information concerning the conditions of crystallization or later transformations which will take place, and the colour of the crystals reveals the presence of ionic impurities (Niwa and Katada, 2013). Scanning electron microscopy (SEM) is the method of choice for determining the size and morphology of zeolite crystallites. High-resolution transmission electron microscopy has been extensively used to study intergrowth fault planes and stacking faults and recently for structural analysis. Common spectroscopic methods for analyzing zeolite structure, include magic angle spinning ^{29}Si and ^{27}Al nuclear magnetic resonance (NMR) spectroscopy. Information regarding the coordination environment around Si and Al and the framework Si/Al ratio can be

obtained. Infrared spectroscopy via the frequencies of structure-sensitive bands provides information regarding framework properties, including Si/Al ratios and nature of acidity by the -OH stretching vibration. Other techniques used include Raman spectroscopy, which provides information complementary to infrared, electron paramagnetic resonance for analyzing the coordination environment of non-framework and framework metal ions, X-ray fluorescence spectroscopy for elemental analysis, and X-ray photoelectron spectroscopy for surface analysis (Akimkhan 2012).

1.4.1. X ray Diffraction

With improvements and computerization of the single-crystal X-ray diffractometric (XRD) technique in the last decades, large progress has been made in the structure determination of crystalline materials. However, zeolite research has not benefited much from this progress since zeolite crystals of good quality and large size needed for single-crystal XRD are available only in exceptional cases. Thus, most of the structural information on zeolites was derived from powder. XRD and neutron diffraction, generally applied in combination with other techniques such as MASS NMR spectroscopy, adsorption methods etc. XRD provides information about the Bragg angles, of the reflection of an incident monochromatic X-ray beam on crystal planes, according to Bragg's equation:

$$n\lambda = 2d \sin \theta \qquad (5)$$

Where (n) represents the order of reflection. Also, the wavelength of the incident X- ray beam and d the spacing between reflecting crystal planes. Also, information is provided about the intensities of the reflected X-rays, An XRD pattern provides, in principle, all data necessary to solve crystal structures. However, powder patterns of complex structures with low symmetry might consist of a great number of Bragg reflections with either severe peak overlap or of very low intensity. Thus, in most cases it would be practically impossible to obtain information on the precise position and intensity of enough individual reflections. Powder XRD is not only the current method in structural investigations of zeolites, but is also

widely used for the identification, quantitative determination and characterization of zeolitic phases. Since a typical XRD pattern is obtained for each crystalline phase, the pattern feature may be regarded as a "fingerprint" of the respective material. Thus, zeolite structures can be easily identified by comparison of the d-spacing or 26 positions of the typical Bragg reflections with those given for known zeolites in straightforward compilations. Even in mixtures with other zeolites or crystalline materials the identification of a zeolitic phase generally does not encounter difficulties. In zeolite synthesis, powder XRD is an, indispensable, analytical method which allows a quick identification of the prepared crystalline phases and monitoring the progress of crystallization processes. The relative intensities, i. e., the intensity distribution in diffractometric patterns, are not affected when the absorption coefficient is changed due to variation of the chemical composition of the zeolitic material. The absolute values of integrated intensities, however, significantly depend on compositional changes of the crystal lattice, especially if constituents are involved which contribute by highly different degrees to the coefficient as, for example, in the case of Na^+ , Cs^+ ion exchange. In general, the larger the nuclear charge number of the constituents of the particular material, the higher the degree of absorption. (Kokotailo & Fyfe 1995) (Treacy & Higgins 2001) and (Auerbach 2003).

1.4.2. Infrared and Raman Spectroscopy

Infrared spectroscopy (IR) is one of the most widely used techniques in zeolite chemistry and catalysis. Due to its ready availability of instrumentation, IR has been used in almost all aspects of zeolite chemistry, for information on zeolite formation, framework vibrations, surface property, adsorption and catalysis. IR spectroscopy is arbitrarily divided into three categories based on the instrumental designs: near-IR (>3,000 cm^{-1}), mid-IR (4,000–400 cm^{-1}) and far-IR (<300 cm^{-1}). In general, near-IR spectroscopy deals with overtones of fundamental vibrations and provides information on adsorbed species such as water, organic molecules and small gas molecules, etc. in zeolite cavities or channels. Mid-IR spectroscopy is fruitful for zeolite chemistry and provides information on surface OH groups,

adsorbed molecules and framework vibrations. Far-IR spectroscopy has been used to study framework oxygen and charge-balancing cations in zeolite structures.

Raman spectroscopy has become popular in recent years due to the development in instrumentation. The replacement of the mercury lamp by lasers and the use of charge couple device (CCD) detectors and notch filters increase the Raman sensitivity and spectral range dramatically. Similar to IR, Raman spectroscopy gives vibrational information but, due to its different selection rule from that of IR, dipole moment vs. polarizability, the information obtained is complementary to IR. Raman is preferred for studying host-guest interactions in zeolites via monitoring the guest molecules due to the very weak Raman scattering nature of the "normal" zeolite frameworks (Chester and Derouane, 2009). Both IR and Raman spectroscopies provide information on bonds between atoms. These may be atoms constituting the zeolite or molecules sorbed in the pores or at the outer surface. In case of IR spectroscopy, the information is provided by stimulating the vibration or rotation of two or more atoms in the probed matter. In case of Raman spectroscopy, it is the inelastic scattering of monochromatic light of an atom leading to an electronic excitation into a virtual state, with nearly coincident de-excitation and a change in vibrational energy leading to a lower or higher frequency compared to that of the stimulating light. The nature of stimulation is, hence, quite different in the two techniques. For a given concentration of bonds probed, the intensity of the response in an IR spectrum is proportional to the change in the dipole moment. The observed intensity in a Raman spectrum is to a first approximation proportional to polarizability of the bond by an external field. Group theory shows that IR-active vibrations are not Raman active and vice versa. This leads to drastically different sensitivities in the measured spectra, which in principal could serve as elegant tool to differentiate between functional groups on surfaces and sorbed molecules. However, Raman spectroscopy suffers from lower signal intensity, when employed under conditions appropriate to study materials as delicate as zeolites (Cejka, 2007). The framework vibrations of zeolites are observed in the spectral region 1,400– 300 cm^{-1}. Flanigen (2010). summarized the

observations for most of the early-synthesized zeolites and proposed the general assignments for the IR bands to illustrate the infrared assignments. In fig (1-2) two types of bands are observed for a zeolite framework: internal tetrahedra bands which are structure insensitive (1, solid bands) and external linkages, which are structure sensitive (2, dashed bands). The former is observed for all aluminosilicates and silicates including an amorphous silica precursors while the latter is observed only when the zeolite structure is constructed. Some researchs , studied systematically, the relationship between IR spectral features of zeolites and structural properties thus extending earlier IR investigations of silica and non-zeolitic aluminosilicate frameworks to zeolites. The bands observed in mid infrared were classified into two main categories, viz. bands due to internal vibrations of the $TO_{4/2}$ tetrahedra (T =Si or AI) and external vibrations of tetrahedra linkages, e.g., in double rings (as in A-,X-, Y-type) or pore openings (as in mordenite).

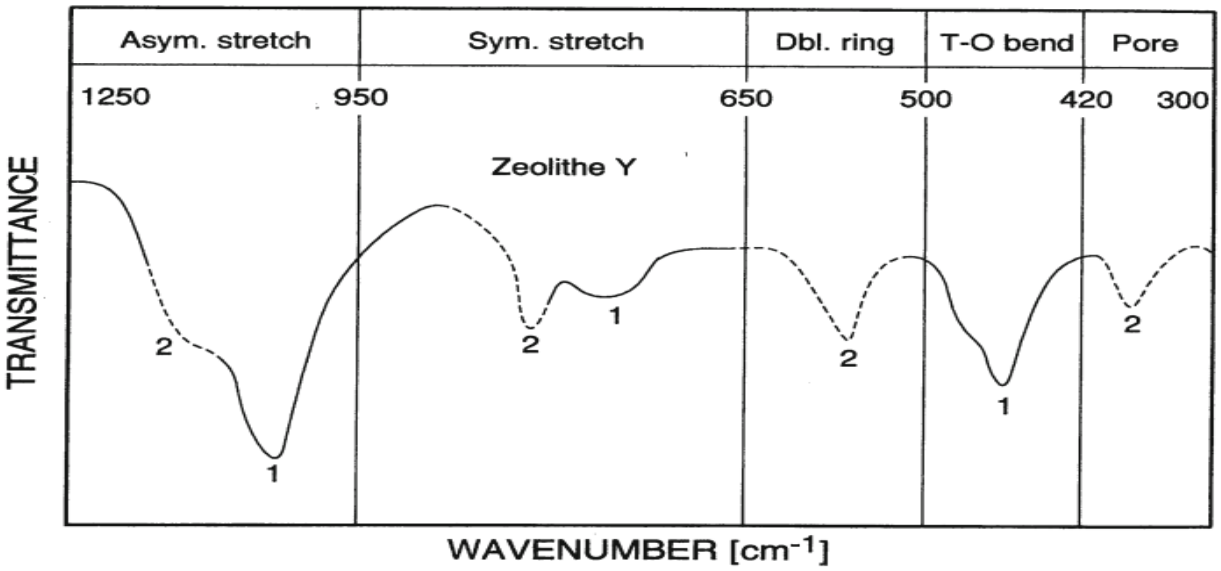

Fig (1.2) Lattice vibrations of zeolite Y (Cejka et al. 2007)

The number and position of the structure sensitive bands depend on the zeolite structure and are summarized in table 1.3 (Auerbach 2003) and (Cejka et al. 2007).

Table (1-3) Assignments of Zeolite Lattice Vibrations(Auerbach 2003)

Internal Tetrahedra	Vibrations	External Linkages	Vibrations
Asym. stretch	1250–950	Double ring	650–500
Sym. stretch	720–650	Pore opening	420–300
T–O bend	500–420	Sym. stretch	820–750
		Asym. stretch	1150–1050 sh

Numbers of the asymmetric stretch was plotted vs. the atom fraction of Al in T sites for all the zeolites studied. Very good correlations between band Al/ (Si +AI) were observed if v (asym), v (sym), v (DR) or v (pore opening) were plotted for homologous series of only one structure type such as faujasite, i.e., X and Y with different Si/Al rtios (Fig. 1.4). In fact, such relations were later on frequently used to determine the Al/(Si + Al) ratio in zeolite frameworks. The T-O bending band did not vary significantly, in particular not with the same structure and different Si/Al ratios (Weitkamp et al, 1999). IR spectroscopy is the most direct method to study the type, concentration and acid strength of hydroxyl groups in zeolite. As outlined above, the frequency of the stretching vibration of a hydroxyl group (OH) is a function of the force constant between the O and H atoms. As such, it represents the curvature of the (nonharmonic) potential well, which in turn is a function of the intrinsic chemical bond and the environment polarizing that bond. For homologous series of molecules (e.g., carboxylic acids in an a polar environment), a lower force constant indicates a higher acid strength of the hydroxyl group, i.e., a more acidic hydroxyl group, which is reflected by a lower wave number of the OH band. Again, it has to be emphasized that the position of the band cannot be used as a strict measure for the acid strength of a hydroxyl group in a zeolite, as there is no fundamental correlation between the force constant (i.e., the curvature of the OH potential well) and the heterolytic O–H

dissociation energy. Thus, state that the wave number of an O −H stretching vibration is strongly influenced by the following factors:

(i) The type of coordination of the oxygen (terminal versus bridging oxygen), (ii) The structural environment of the OH group, i.e., type of zeolite lattice, (iii) The perturbation of the OH group through the surroundings by lattice or extra-lattice oxygen. Examples to illustrate these effects are given in the IR spectra showing the typical OH stretching vibrations of zeolite Y, Ferriete and ZSM-5 and the assignment of the hydroxyl groups in Figure (1-3 and 1-4) below

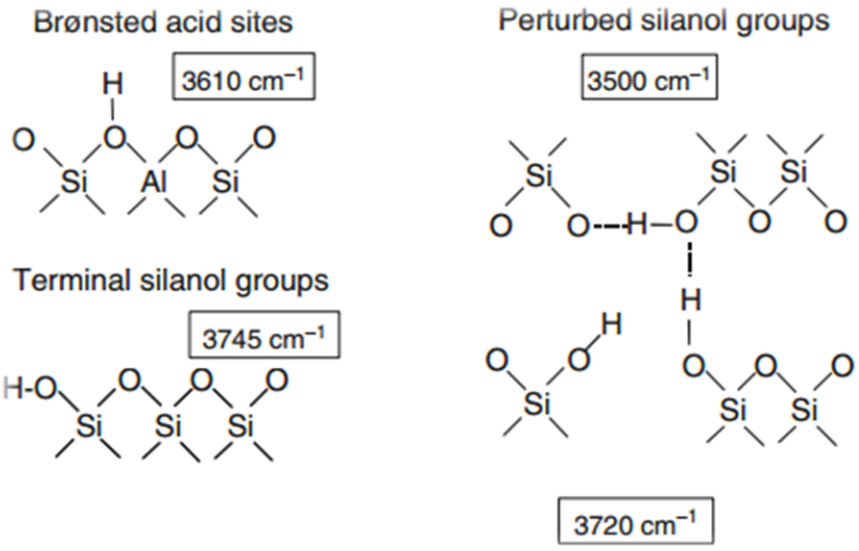

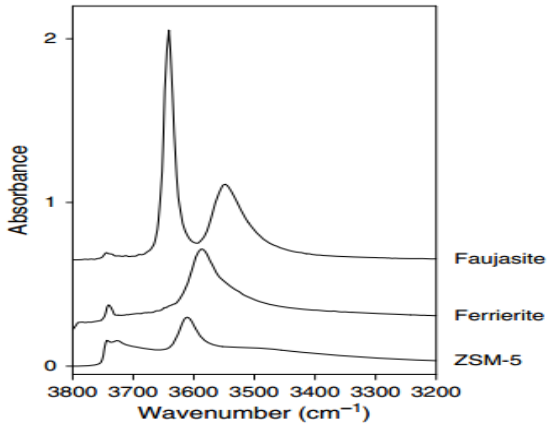

Fig (1.3)and (1.4) Comparison of the OH stretching vibrations of Faujasite, ferrierite and ZSM-5 5 (Cejka et al. 2007)

1.4.3. Solid-State NMR Spectroscopy

Nuclear magnetic resonance (NMR) is an analytical tool with a high sensitivity for chemical bonds in the local structure of the resonating nuclei, such as of framework atoms, extra-framework species, surface sites, and adsorbate complexes in zeolites. Therefore, a number of research groups utilizes solid-state NMR techniques for the characterization of these industrially very important catalysts and adsorbents. Many atoms occurring in zeolites possess isotopes with a nuclear spin, which renders these isotopes NMR-active, the most frequently investigated nuclei are summarized in Fig. 1.6 Their nuclear spins and relative sensitivities (in comparison with ^{1}H) are given in parentheses. ^{11}B, ^{17}O, ^{27}Al, ^{29}Si, ^{31}P, ^{51}V, ^{67}Zn, and ^{71}Ga isotopes are accessible for NMR spectroscopy and contribute to the framework of zeolites in a broad manner. ^{1}H, ^{7}Li, ^{23}Na, and^{133}Cs isotopes are interesting for the characterization of surface OH groups and extra-framework species, such as extra-framework cations. On the other hand, ^{1}H, ^{2}H, ^{13}C, ^{15}N, and ^{31}P isotopes allow the investigation of a wide variety of probe molecules and reactants (Arthurw et al, 2009). Recent studies have shown that the chemical shifts which characterize the ^{29}Si-NMR lines belonging to define Si(nAl) configuration were also influenced by the actual geometry of the T-O-T linkages (T=Si or Al) or by longer range structural features such as the (T-O) P ring size. This was turned to account for the effect of the actual ring structure and strains that occur in high siliceus zeolite ZSM-5 ZSM-11 silicate.

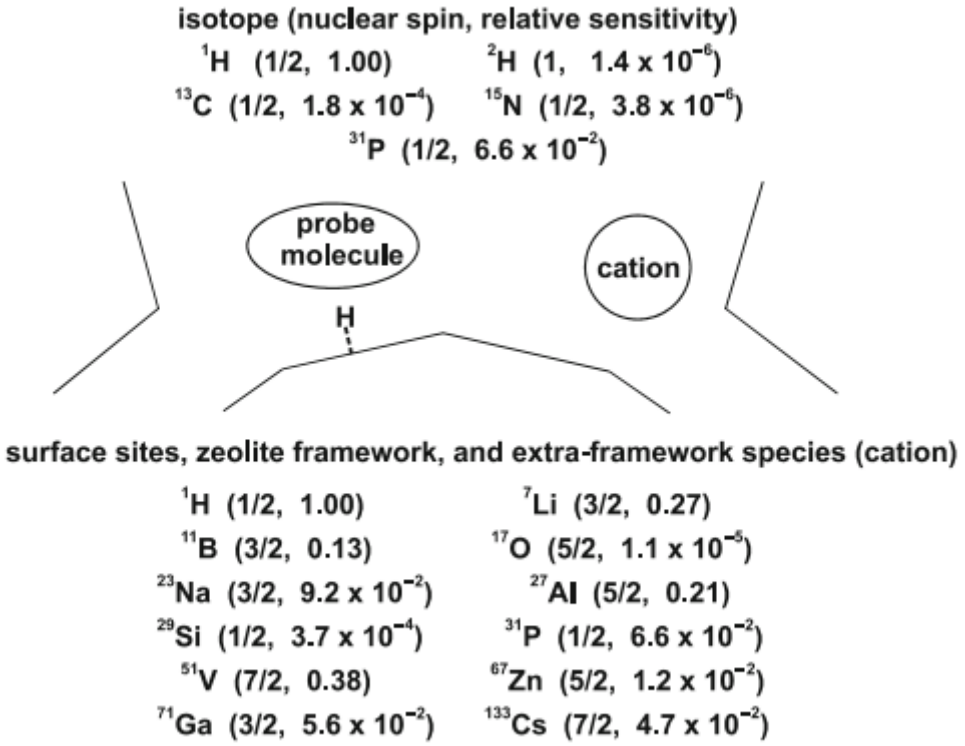

Fig (1.5) solid-state NMR spectroscopy of zeolite framework

^{29}Si nuclei can be investigated as an NMR probe of local arrangements exploiting a large set of nuclear spin interactions contained in the experimental spectrum such as isotropic chemical shift and chemical shift anisotropy (CSA), ^{29}Si–^{29}Si and ^{29}Si–^{27}Al dipole–dipole coupling, and the two bond isotropic indirect spin–spin scalar J2 (^{29}Si–O–^{29}Si) coupling between covalently bonded Si species, which have been used in 2D NMR correlation analysis. In zeolites, silicon is coordinated to four framework oxygen atoms in a tetrahedral SiO_4 coordination. The ^{29}Si NMR spectra of aluminosilicate zeolites, with a Si/Al ratio up to 10 give typically a series of peaks which correspond to SiO_4 tetrahedron five different possible environments corresponding to different number of AlO_4 tetrahedra connected to the silicon via oxygen. For simplicity, these sites will be denoted ignoring the oxygen atoms as Si (nSi, 4-nAl), where n4; for instance, Si (4Si) will be used instead of $Si(OSi)_4$, Fig 1.6 shows the ^{29}Si chemical shifts ranges for these species. Alternatively, they canbe named following the Q notation as Q^n sites, where n denotes the number of linked SiO4 tetrahedra, so that Si(4Si) environments corresponds to Q4, Si (3Si, 1Al) to Q3, and so on. Simulation of experimental spectra with individual peaks

allows to calculate the framework Si/Al molar ratio from the relative intensity of the Si (nSi, 4-nAl) peaks (Auerbach 2003) and (Colella 2005).

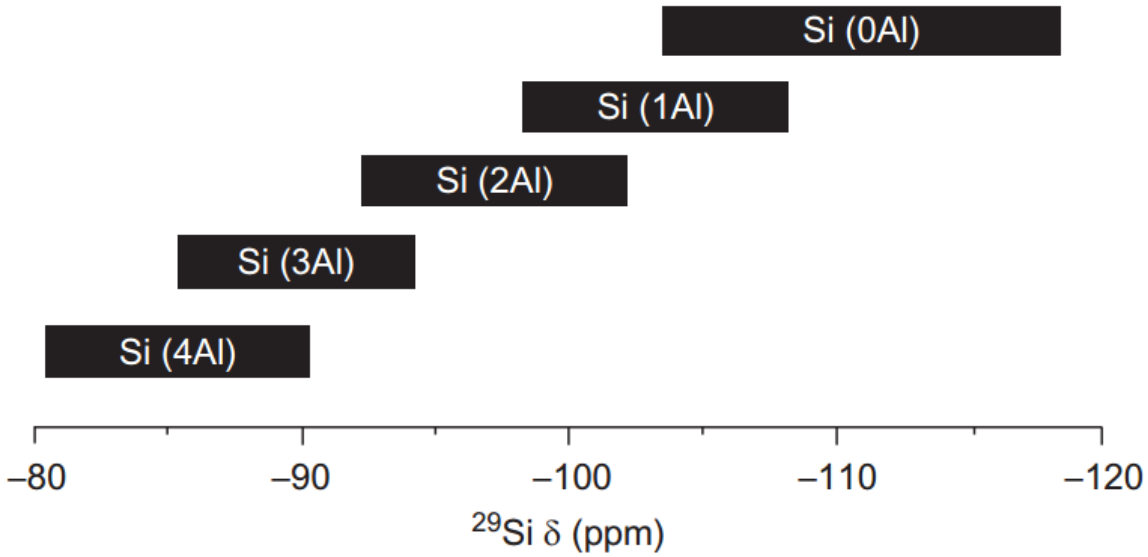

Fig (1.6) ^{29}Si NMR chemical shifts ranges of Si (nAl) species(Colella, 2005)

Table (1- 4) Connectivity of Si crystallographic sites in zeolites investigated by 2D solid state NMR methods (Auerbach, 2003)

Zeolite	***Pulse sequence used***
ZSM-29, Dodecasil-3D	COSY, DQF COSY, Spin Diffusion
ZSM-12, KZ-2	COSY, inadequate
ZSM-5	COSY, inadequate, CP-inadequate
DD3R	COSY, inadequate
Mordenite	COSY
ZSM-11	inadequate
ZSM-23	Inadequate
Ferrierite	Inadequate
SIGMA-2	Inadequate DQ-Homonuclear dipolar recoupling
ITQ-12	DQ-Homonuclear dipolar recoupling

1.5 Application of zeolites

Natural and synthetic zeolites are widely used nowadays in water treatment processes as ion-exchange and adsorption potential selectivity because zeolite based surface area distributed throughout pores with several diameters, This advantage in economic aspect of zeolite has been reported in several works that was investigated and applied to remove cation contaminants in water and wastewater, such as:-Water softening – removal of permanent hard water for drinking or industrial water preparation-water purification – removal of heavy metal cations: Fe^{3+} ,Cu^{2+}, Zn^{2+}, Mn^{2+}, Ni^{2+}, Cd^{2+}, Pb^{2+}.Zeolite softening will also remove other soluble cation species such as iron and manganese present in the raw

water and will, mechanically, retain small suspended solids. When zeolite for water softening is saturated with Ca^{2+}, Mg^{2+}, Fe^{3+}, Mg^{2+} cations, it may be backwashed with a sodium chloride solution to remove calcium,(Fansuri et al. 2008).

1.5.1. Adsorption

Adsorption is a phase transfer process, widely used in practice to remove substances from fluid phases (gases or liquids). It can also be viewed as a natural process in different environmental compartments. The most general definition describes adsorption as an enrichment of chemical species from a fluid phase on the surface of a liquid or a solid. In water treatment, adsorption has been proved as an efficient removal process for a multiplicity of solutes. Here, molecules or ions are removed from the aqueous solution by adsorption onto solid surfaces.

In adsorption theory, the basic terms shown in Figure (1-7) are used. The solid material that provides the surface for adsorption is referred to as adsorbent; the species that will be adsorbed are named adsorbate. By changing the properties of the liquid phase (e.g. concentration, temperature and pH) adsorbed species can be released from the surface and transferred back into the liquid phase. This reverse process is referred to as desorption. The amount of gas adsorbed, (n^a), by the mass, (m^s), of solid is dependent on the equilibrium pressure, p, the temperature, T, and the nature of the gas–solid system. For a given gas adsorbed on a particular solid at a constant temperature is given by:

$$n^a/m^s = f(p)\ T \qquad (1)$$

And if the gas is below its critical temperature, it is possible to write:

$$n^a/m^s = f(p/P^\circ)\ T \qquad (2)$$

Where p_o is the saturation pressure of the adsorptive. Equations (1) and (2) represent the adsorption isotherm which is the relationship between the amount adsorbed by unit mass of solid and the equilibrium pressure (or relative pressure), at a known temperature. The experimental adsorption isotherm is usually presented in graphical form. Experimental adsorption isotherms recorded in the

literature for many different gas–solid systems have various characteristic shapes. These shapes are important since they provide useful, preliminary, information about the pore structure of the adsorbent, even before any precise calculations have been carried out. The majority of vapour isotherms (i.e. at sub-critical temperatures) may be divided into nine groups in an extended IUPAC classification (see Figure 1.8). Other shapes are sometimes found and these can usually be explained as a combination of two (or more) of the nine shapes proposed and such an isotherm is then said to be composite. The five Types I, II, III, IV and V were similar to those originally proposed by Brunauer, Deming, Deming and Teller (1940), which is usually referred to as the BDDT or Brunauer classification (1945) (Duong D. Do 1998)

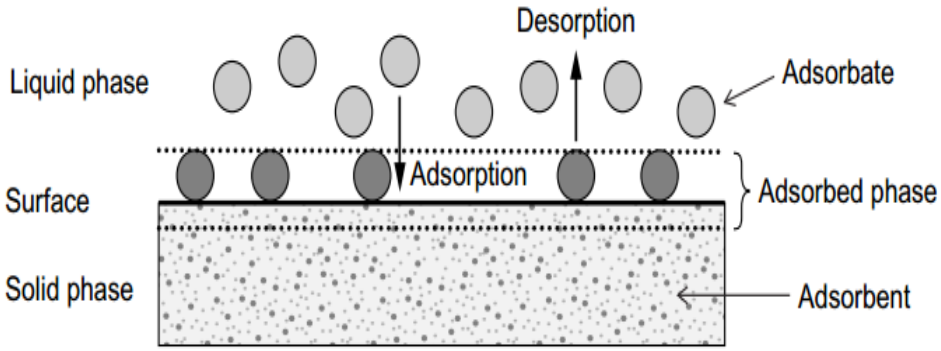

Fig (1-7) Basic terms of adsorption

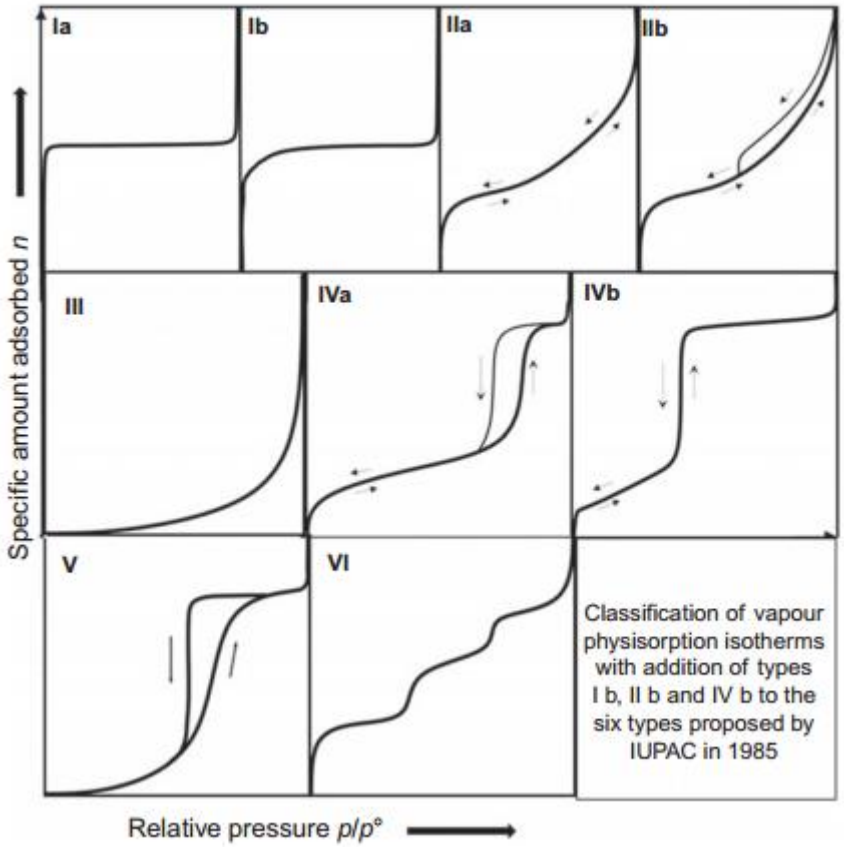

Fig (1-8) Classification of vapor adsorption isotherms combining proposals from IUPAC

A number of powders or aggregates (e.g. clays, pigments, cements) give Type II isotherms, which exhibit Type H3 hysteresis. A Type III isotherm is convex to the p/p˚ axis over the complete range and therefore has no Point B. This shape is indicative of weak adsorbent–adsorbate interactions on a non-porous or macroporous adsorbent. True Type III isotherms are not common. Type IV (a) and IV (b) isotherms, whose initial region is closely related to Type II isotherms, level off at relative high pressures with a characteristic saturation plateau, although this may be short and reduced to an inflexion point. They are obtained with mesoporous adsorbents. Type IV(a) isotherms, which are much more common than Type IV(b), exhibit hysteresis loops: the lower (adsorption) branch is obtained by the progressive addition of gas and the upper (desorption) branch by the progressive withdrawal. The hysteresis loop is associated with the filling and emptying of the mesopores by capillary condensation. Type IV(a) isotherms are common but the exact shape of the hysteresis loop varies from one system to

another, Type V isotherm is, initially, convex to the p/p° axis and also levels off at relative high pressures. As in the case of Type III isotherm, this is indicative of weak adsorbent–adsorbate interactions, but here on a microporous or mesoporous solid. A Type V isotherm usually exhibits a hysteresis loop which is associated with pore filling and emptying. Such isotherms are relatively rare. The Type VI isotherm, or stepwise isotherm, is also relatively, rare and is associated with layer-by-layer adsorption on a highly, uniform surface such as graphitised carbon. The sharpness of the steps are dependent on the system and the temperature. The above classification is necessarily somewhat idealised since, as already pointed out, many experimental physisorption isotherms have a composite nature and others are more complex than was formerly thought. (Sing & Evertt 1985). (Rouquerol Francoise 1999), (Munthali et al. 2014) .

1.5.1.2. Determination of internal surface area by BET

Adsorption methods are, universally, employed for the determination of the specific surface area of fine powders and porous solids. It must be kept in mind, however, that unless a solid material is, atomically, flat its effective 'surface area' is not a simple property. In the context of adsorption, there are two main reasons for this complexity: (1) at the molecular level, the dimensions of the solid are dependent on the convention chosen to locate the surface, and (2) the available area is dependent on the extent of surface roughness and porosity and the dimensions of the adsorbed molecules. In addition, most adsorbents, of technological importance, are in some respects heterogeneous and all experimental methods or theoretical treatments have limitations of one sort or another. For all these reasons, when reporting derived quantities such as surface area or pore size distribution it is essential to provide a detailed account of the chosen experimental technique including computational procedure used for data processing. The appearance of Langmuir's comprehensive treatment of monolayer adsorption (Langmuir, 1916, 1918) prompted several investigators to consider the possibility of using gas adsorption for surface area determination. Early attempts were made by Williams (1919) and Benton (1926), but these led to inconclusive

findings. The first significant advances were made by Brunauer and Emmett (1935, 1937) and their work paved the way for the development of the Brunauer–Emmett–Teller (BET) theory in 1938. Type II isotherms (see Figure 1.9) often display a rather long, almost linear middle range, the point at which this linear part begins was designated ‘Point B’ by Brunauer and Emmett (1937) and was shown empirically to indicate the completion of monolayer coverage and the beginning of multilayer adsorption. From the amount adsorbed at Point B, Emmett and Brunauer (1937) went on to calculate the surface area by assuming the monolayer to be molecularly close packed (Rouquerol Francoise 1999)

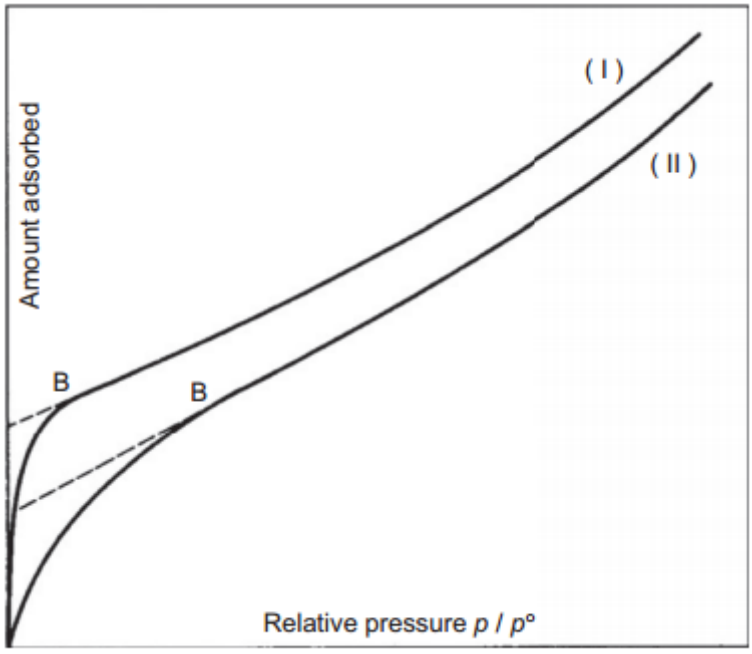

Fig (1.9) Typical Type II isotherms: (I) with sharp knee and (II) with rounded knee.

1.5.2. Ion exchange

Zeolites have an open crystal structure which is occupied by cations and water molecules. These ions and water molecules can move within the large cavities allowing ionic exchange and reversible rehydration. Zeolite exchangeable ions are relatively innocuous (Na, Ca, and K ions) makes them, particularly, suitable for removing, undesirable, heavy metal ions from industrial effluent waters. One of the earliest applications of a natural zeolite was in removal and purification of cesium (Cs) and strontium (Sr) radioisotopes. (Kim et al. 2015). The mechanism

of zeolite as cation exchanger is participating ion through the internal channels and cavities or their hindered movement through the film of ordered water which exists on the surface of the zeolite, the significance of film control is:

when concentration in solutions or small (less than 10-5 M) is rule of thumb.(Dyer 2005). Cation exchange capacity (CEC) is, directly, related to the amount of aluminum present in the framework. Properties such as Si/Al ratio, specific to the cationic species in solution and the anionic associated to them, solvent, pH, and temperature must be observed for good exchange efficiency. High charges and small radii cations are preferred by zeolites of lower Si/Al ratio such as zeolite Y. In all cases, it has been emphasized that the entering ions are preferably located in large cages such as supercages and sodalites. Exchange degree in such cages depends on the nature of each entering ion. The exchange of Na^{+} by La^{3+}, for example, preferably occurs in the supercavities and only a few cations of lanthanium may get into the sodalite cage .The La-NaY isotherms showed a very convexly upward curvature followed by a large plateau at 70% of the total exchange capacity, which agrees with the occupancy of the large cages only .As charge and hydration radius of La^{3+} (rH = 4,52 Å)-(Nightingale, 1959) are similar to Cr^{3+} (rH = 4,61 Å -Nightingale, 1959), a plateau for Cr-NaY is expected at least for low temperatures. The Cr^{3+} ion, in spite of its high charge and small size (0.64 Å), has a strong tendency to undergo hydration. In fact, for the exchange with Cr^{3+}, stated that these cations have a hexahydrated form $Cr(H_2O)^{36+}$ and are preferably present in the supercavities of zeolites NaY.(Malekian et al. 2011).

Table 1.5 show uses of some zeolites.

Table (1-5) Use of natural zeolites in ion-exchange process(Cejka et al. 2007)

Method of application	Zeolites	Field of application
Without regeneration	-Clinoptilolite -Mordenite	Cleaning of waste water from the radioactive ions ^{137}Cs ,^{90}Sr, followed by burial of zeolite treatment of domestic waste water from ammonium nitrogen when followed by the use of zeolite as ammonium fertilizer
	-Clinoptilolite	Purification of waste water from non – ferrous metals using the zeolite as a flux
With the self-refresh	-Clinoptilolite --Mordenite	The use of zeolite as filter material for zeolite treatment
	-Clinoptilolite	The introduction of zeolite in the soil to increase the duration of fertilizer
Regeneration with solution	-Clinoptilolite --Mordenite	Concentration and separation of alkali metals from technological solution and natural waters
	-Clinoptilolite	Concentration of Sr from the waste and natural waters
	-Clinoptilolite --Mordenite	Concentration of non-ferrous metals from technological solution , waste and natural waters

1.5.3 Petroleum application

Four decades ago zeolite and more, generally, molecular sieves, have been playing an increasing role in development of cleaner and more efficient refinery processes

for production of fuels and petrochemicals. However, Wang and co-workers reported for the first time in 1993 the dehydro-aromatization of methane (DAM) in the absence of oxygen at 700°C and atmospheric pressure using a Mo/HZSM-5 catalyst. The DAM reaction is thermodynamically unstable, with an equilibrium conversion of methane of about 12 % and 24 % at 700°C and 800°C respectively, and 1 atm. Besides the production of aromatics, the interest of the DAM reaction also resides in the co-production of COx-free hydrogen which may be useful for fuel cell applications. Since the initial work of Wang and co-workers, many efforts have been directed to the optimization of the Mo/HZSM-5 catalyst and reaction conditions, to understand the interactions between the transition metal and the zeolite host, and to determine the nature of the active sites and possible reaction mechanisms, as well as the role of the carbonaceous deposits formed during the reaction. The channel structure and acidity of the HZSM-5 zeolite and the state and location of Mo species play a vital role in the performance of Mo/HZSM-5 catalysts for the DAM reaction. The groups observed that the formation of hydrocarbons was preceded by an induction period, during which methane was mainly converted into coke and gaseous products (CO, H_2O, H_2 and CO) with very little hydrocarbon formation. During this period, a partial reduction of Mo^{6+} by methane occurred with formation of Mo_2C/MoO_xC_y species highly dispersed in the zeolite channels. Following the initial activation period, a benzene selectivity of about 70 % at a methane conversion of 8-10 % could be sustained for more than 16 h over a 2 wt% Mo/HZSM-5 catalyst at 700°C. It was then proposed that methane aromatization takes place through a bifunctional mechanism, where the initial activation of methane occurs on the molybdenum carbide/oxycarbide species leading to the formation of ethylene as the primary product, which then oligomerizes and cyclizes on the acid sites of the HZSM-5 zeolite to form the aromatics .The formation of acetylene as a primary product during the DAM reaction on Mo/HZSM-5, and suggested that the aromatization of methane occurs via acetylene as intermediate rather than via ethylene, (Corma and Martinez 2005). (Cejka et al. 2007)

1.5.4 Storage materials

Zeolite can be used as storage material according to it structure. hydrogen storage on porous materials has attracted considerable attention because of the great importance of hydrogen as a potential substitute for fossil fuel. Various methods for storing hydrogen including gaseous, liquid and solid-state storage based on molecular sieves have been considered. The particular interest in using zeolite-type materials as gas storage media is due to the fact that by changing the size and charge of, exchangeable, cations, the ion molecule interactions can be adjusted, and the diameter of the channels can be controlled, thus enabling the effective trapping of differently sized gas molecules. Synthetic zeolites such as A, Y, X, mordenite, chabazite, sodalite, gismondine and thomsonite, etc. were used as powder carriers for hydrogen storage. It was found that sodalite could store 9.2 cm^3/g (0.082 wt. %) of hydrogen if loaded at about 300℃ and a pressure of 100 bar. However, at very low temperatures, the storage capacity is found to be 1.2 wt. % (at-196℃ additionally, physical adsorption at low temperature is significant due to the large specific surface area of the zeolites. The specific surface area measurements of the zeolites under consideration can be plotted against hydrogen uptake values, (Fig. 1.10). As expected, the zeolites X and Y offer a maximum hydrogen storage capacity; these can be considered to be low-cost media for stationary hydrogen storage applications.(Bein, T 2005)

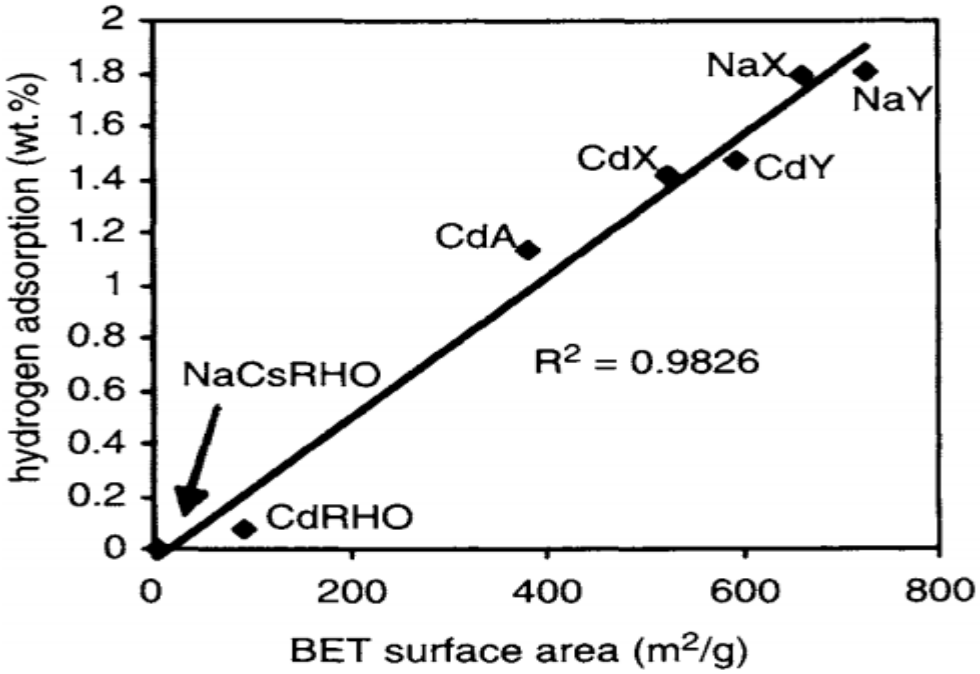

Fig (1.10) Correlation between hydrogen adsorption at-196 ~ and the BET surface area of different zeolites

1.6 Study area

1.6. 1 Elmugald Petroleum Basin

Muglad Basin, extending from the Republic of Sudan to the Republic of South Sudan, is one of a series of intra continental rift basins whose formation is linked to right-lateral movement on the Central African shear zone during opening of the South Atlantic in the Early Cretaceous. The basin is a "passive" rift structure following the definition of Sengor and Burke(1985) and can be divided into tectonic elements including the Abu Sufyan, Nugara, Fula, Bamboo and Unity sub-basins, the Kaikang Trough, Babanusa Uplift and the Abei Slope. The basin is filled with a Cretaceous Tertiary non-marine sedimentary succession which is over 13,720 m thick in the deepest parts of the Kaikang Trough depocentre. The fault-bounded Fula sub-basin is located in the NE of the Muglad Basin. Petroleum exploration in the sub-basin began in 1974 but only one wildcat well (Baleela-1, 1985) was drilled, recording very weak oil or gas shows; little further exploration work was undertaken during subsequent decades. However, a renewed exploration program including 2000 km of 2D seismic, 1334 km^2 of 3D seismic and the

drilling of 68 exploration wells has been carried out since 1996. Eleven commercial and non-commercial oilfields (Fula, Fula North, Fula Northeast, Fula South, Fula West, Moga, Keyi, Jake, Jake South, Bara and Arad) have been discovered in the sub-basin, and oil production is currently about 60,000 barrels per day. There is integrate new source and reservoir rock analytical data for the Fula sub-basin into the regional framework of the Muglad Basin, and investigate the differences between petroleum accumulations in the Fula sub-basin and those elsewhere in the Muglad Basin.

The NW-SE oriented Muglad rift basin is up to 200 km wide and over 800 km long, covering an area of at least 120,000 km^2) and may link up to the SE with the Anza Rift in Kenya. The sedimentary fill comprises three cycles of rift-related lacustrine deposits corresponding to three episodes of extension dated as Early Cretaceous (approximately 140-95 Ma). Each cycle boundary is regionally or locally expressed by an angular unconformity. The first rift phase occurred during the Barremian – Aptian. Syn-rift sediments are more than 6000 m thick in depocentres and include organic-rich shales of the Abu Gabra Formation. Overlying post-rift sediments are more than 1000 m thick, comprising medium- to coarse-grained sandstones of the Bentiu Formation. A second rift phase occurred during the Turonian – late Senonian and was characterized by widespread deposition of shallow-water lacustrine and floodplain claystones and siltstones of the Darfur Group, more than 4000 m thick. In the central Muglad Basin (Blocks 1/2/4), the Group is divided into the Aradeiba, Zarga, Ghazal and Baraka Formations. The overlying post-rift succession is composed of massive sandstones of the Amal Formation. The third rift phase began in the late Eocene – Oligocene, contemporaneous with the initial development of the Red Sea and the eastern arm of the East African Rift System. Various aspects of the Muglad Basin have been studied over the past 30 years. Schull (1988) reviewed petroleum exploration and development. The tectonic history and structural style of the basin. Throughout the Muglad Basin, organic-rich shales in the Lower Cretaceous Abu Gabra Formation have been identified as a good to excellent oil-prone source

rocks Comparison of bulk parameters and biomarker characteristics of oils and source rock extracts show that the Abu Gabra Formation is the most important effective source rock present. Major reservoir targets in the Muglad Basin are the sandstones in the Bentiu Formation and Darfur Group. Crude oil has been found over a wide stratigraphic interval in Abu Gabra, Bentiu, Aradeiba, Zarqa, Ghazal, Amal, Nayil and Tendi Formations. Oil production totalled 320,000 barrels per day in 2010, the last year for which basinwide figures are available. The largest field, Unity, was discovered in 1978 by Chevron.

The Fula sub-basin is a fault-bounded, asymmetric half-graben located in the NE of the Muglad Basin, and is up to 120 km long and 41 km wide covering an area of 3560 km^2. The sub-basin is separated from the northern part of the Kaikang Trough by the Babanusa Uplift. The Fula sub-basin can be divided into six structural units the boundary fault zone, southern faulted terrace, southern sag, central oblique anticline zone, northern sag and northern faulted terrace. The southern and northern sags occupy an area of approximately 1500 km^2 and 1000 km^2, respectively, and are bound to the west by the F1 fault. This bounding fault dips eastward at more than 50° and small-scale footwall anticlines are developed along it, Subsidence of the Fula sub-basin is linked to dextral movement on the Central African shear zone, the sedimentary column in the Fula sub-basin is up to 8400 m thick. Based on an interpretation of seismic data and drilling results, the succession. can be divided into four sequences, separated by unconformities and related conformities: Lower Cretaceous, Upper Cretaceous, Paleogene and Neogene – Quaternary. These sequences correspond to deposition during three phases of rifting and one, sag (post-rift) phase. The Early Cretaceous rift phse, during which the Abu Gabra Formation source rocks were deposited, was the most important. Balanced cross-sections indicate that about 60% of the total extension took place during this phase. At the base of the column is the syn-rift Barremian – Aptian Abu Gabra Formation which can be divided into three intervals. Medium- to coarse-grained fluvial sandstones are interbedded with thin claystones in the lower interval; thick organic rich laminated shales occur in the middle interval;

and interbedded sand stones and dark shales (and local coal shales) are present in the upper interval. The formation is about 5000 m thick. The shales in the middle interval are the main source rocks in the Fula sub-basin and throughout the Muglad Basin. The Abu Gabra Formation is bounded above by a regional unconformity, above which the post-rift Bentiu Formation comprises alluvial and fluvial-floodplain deposits. Conglomerates and coarse-grained sandstones occur in the north of the sub-basin, indicating external drainage from the north. These sandstones, up to 800 m thick, are the most important reservoir rocks in the sub-basin. The unconformably overlying syn-rift Darfur Group, up to 800 m thick, consists of fluvial floodplain and shallow-lacustrine sediments. Grey and green clay stones occur in the Aradeiba and Zarqa Formations and sand stones in the Ghazal and Baraka Formations. The Paleogene Amal Formation was deposited during thermal subsidence and is mainly composed of thick sand stones and locally thin claystones. It is less than 300 m thick. The third rift phase, represented by the Kordofan Group, is not well developed in the Fula sub-basin. The Group is about 500 m thick. Claystones are dominant in the lower interval and over lined mainly by sand stones (Kheiralla et al. 2012, Lirong et al. 2013 and Makeen et al. 2015;)

1.7drilling mud fluid

Drilling mud is a multi-component, dispersion-colloidal system of specific physical and chemical properties. It fulfills several important tasks in borehole drilling. The diversity of these tasks depend, among other things, on the kind of drilled rock, the formation thickness, the existence of formation water and its salinity, the existence of producing formations, the formation pressure, and the temperature depending on borehole depth. Good borehole penetration rates depend to a great extent on the drilling mud quality circulating in the well, and on the proper control of its properties. At the time of borehole drilling, depending on the borehole's depth and the formations drilled, generally two or three kinds of water-based drilling muds are used – bentonite drilling mud, polymer drilling mud without clays that diminish shale formation hydration, and a drill-in fluid that

prevents permeability damage as well as possessing inhibitory properties. The main ingredient of bentonite drilling mud is the bentonite, which acts as a structural building component. However, in clay-free mud the structure and viscosity is built by biopolymer-XCD, high viscosity, plant-derived organic polymers or their mixtures, aining adequate drilling fluid properties and controlling them during vertical or horizontal drilling demands the use of chemicals and drilling materials (organic natural polymers chemically modified, organic synthetic polymers, chemical compounds derived from plants, minerals, or synthetic materials such as lignosulphonates, phosphates, surfactants, defoamers, lubricants, inorganic chemicals such as salts, bases, biocides, corrosion inhibitors, weighting materials), which are also a main source of pollution due to different biodegradability and toxicity issues. After the completion of a drilling borehole section, spent drilling mud as a used-up fluid together with drilled cuttings becomes a drilling waste that is highly detrimental to the environment. The amount of drilling waste produced by a given drilling process varies because it depends on the good depth, the kind of drilled formation, and on the mud and water management regime. Field data show that drilling a length of 1 meter of borehole produces 0.6 cubic meters of waste, and 60–80% of this waste constitutes spent drilling muds. The rest is a solid waste such as cuttings spoiled by mud and hydrated mud cakes removed from borehole walls during pipe trips. In the drilling process for gas and oil exploitation, a large amount of drilling mud should be used for the requirements of balancing the reservoir pressure, carrying the drilling cuttings, cleaning the borehole bottom, cooling, and lubricating the drilling tools. Consequently, a great deal of waste drilling mud will be left on the field after the drilling process is completed. As a complex mixture, waste drilling mud contains various surfactants, hydrocarbons, and heavy metals such as Hg, As, Cr, and so on, and, hence, shows a wide range of toxicity to the surrounding environment. The waste drilling mud left on the field, which becomes a pollution threat to the adjacent water bodies and arable farmlands soil, and any failure to the control of the mud storage tanks will cause severe pollution accidents. In China, the total

emission of waste drilling mud was over 2 million m^3 annually, and nearly 50% of the amount was directly discharged to the surroundings. Therefore, the development of effective and feasible disposal methods is highly desirable. For the time being, chemical oxidation, biodegradation, chemical coagulation, and solidification are increasingly used for the treatment of waste drilling mud. The effects of chemical oxidation and biodegradation proved to be ideal. However, they are only limited to the situation with less suspended solids (SS) and low chemical oxygen demand (COD) Chemical coagulation has high removal efficiency for SS and colloid in the waste drilling mud, but the degradation effect on organic substances is unsatisfactory, and the solidification of sediments will cost much time and materials for its high-water content. Direct solidification of waste drilling mud by using lime, cement, and other coagulant aids is a cost-effective technology, but the leaching of the contaminants would be a problem. The actual waste drilling mud is a, highlym viscous suspension, composed of mud and many chemical compounds. So, based on the comparative analysis of the existing methods just mentioned, no single technology could be applied as a stand-alone treatment option. Accordingly, a sequential treatment methodology, including solid–liquid separation, Fenton oxidation coupled with biological degradation of the filtrate, and reusing of the solid mud, is proposed as an alternative to the disposal of water-based waste drilling mud. A flowchart of the whole technology is illustrated in Fig (1-11)(Afkhami et al. 2013)

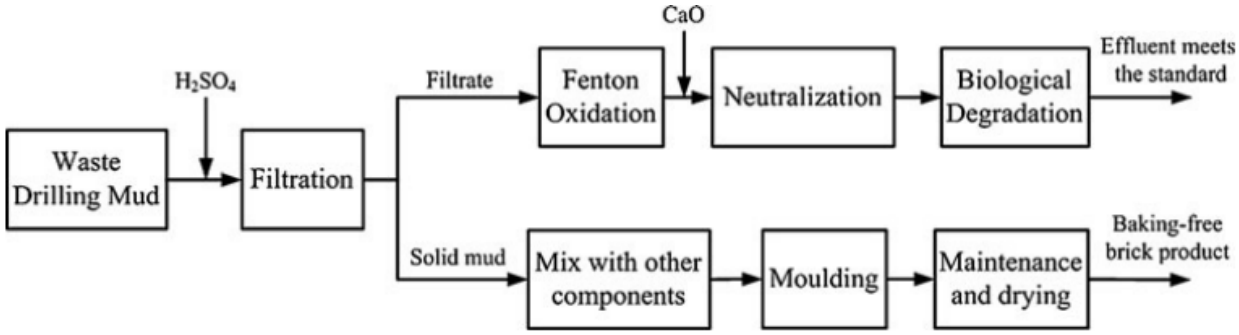

Fig (1.11) Technology Flowchart.

1.8 Literature Review

Zeolite are hot area of study according to it properties and structure, many researchers regarded application such as water treatment as removal some metals and catalysis, the history of zeolite began in 1756 by Swedish mineralogist called Cronstedt, from that time many studies started around the chemistry of zeolite including application such as adsorption properties and reversible cation exchange and dehydration. However, in 1927 X- ray diffraction entered for identification of zeolite, Richard M. Barrer was pioneer to synthesized zeolite and apply it in adsorption process. (Flanigen et al. 2010). From that time many studies on zeolite and its applications explore a new area, Mansoor (2000) prepared a new Nano-pore zeolite membrane for water-treatment, he presented that zeolite membrane are suitable for ion removal from aqueous solution, he studied also the mechanism of removal. (Kazemimoghadam, 2010 ,Jamil et al.2010). Zeolite prepared from Egyptian kaolin and experimental study for removal of heavy metals in order to apply it in industrial wastewater such as (Cd, Cu, Pb, Zn and Ni). They investigated the trace of concentration, pH, contact time and different zeolite doses. (Ibrahim et al. 2010). Ion- exchange process for removal of ammonium by natural Iranian zeolite adopted by (Malekian et al 2011), their study reported the removal ammonium NH_4^+ from aqueous solutions with different Na^+ concentrations by Iranian zeolite in nanometer particle sizes, however the study equilibrium isotherms also characterized such as Langmuir, Freundlich and Peter-Person, they suggested that natural Iranian zeolite is a suitable ion-exchanger for NH_4^+ removal (Malekian et al. 2011). Zeolites are widely used in environmental studies specially petroleum environment. (Fatima, Sahl and Mohamed 2015) used natural and modified zeolite to remove some metals from produce water, their work reported that zeolites can used for their functions as low cost adsorbed zeolites were used to remove (Ca^{2+}, Mg^{2+} and Fe^{2+}) from produced water and use the treated water again in another process.(Elbrir. Fatima A, Yasin. Sahl, 2015). In addition, synthesis of zeolite developed at last years. (Liu et al 2013) synthesis

of a new hybrid mesoporous zeolite from fly ash, the characterization of hybrid was studied by XRD, Nitrogen adsorption-desorption, FT-IR Transition electron microscopy (TEM) and NMR solid state by ^{29}Si and ^{27}Al, the experimental study used to remove Hg^{2+} from aqueous solution, thermodynamic, equilibrium and kinetics were studied(Liu et al. 2013). Recently researchers started to synthesize and facilitating surface area of zeolite and tested it in application, although, silicalaite synthesis and functionalization Nanocrystalline silicalite was synthesized and characterized by Tataurova et al 2012, they used XRD, BET surface area and NMR to investigate the interface of organic functional groups and functionalized silicate nanoparticles in D_2O(Tataurova et al. 2012). Zeolite has been surface modified to be active to remove heavy metals adopted by (Shaw et al 2016), they used it also to reduce E. Coli and other organic pollutants, zeolite modified by ZnO nanoflakes which render surface negatively charged thereby facilitating rapid adsorption process, zeolite characterized by XRD, DRS, FE-SEM and TEM, although it fitted well in Langmuir model and pseudo second order kinetics.(Shaw et al. 2016). Whereas most studies of removal metals and water treatment depend on natural and synthesize zeolite but (Matlok et al 2015), published study about equilibrium study of heavy metals adsorption on kaolin, they transformed raw kaolin to be Na-Kaolin to cause surface to surface arrangement of crystals which suport good adsorption process, kaolin fit well on Langmuir model and it characterized by XRD and BET surface area (Matłok et al. 2015).

Review zeolite, become very important materials, especially, in catalysis as metal carrier or support material, and low cost adsorbent in water treatment without any additive, due to its unique structure, in addition its flexible to be Na-zeolite by replacing extra framework cation, although it supports recycling by simple process.

1.9 Problem statement

The research concentrated on efficiency of zeolite as low cost adsorbent to remove (Cr^{3+}, Co^{2+}, Zn^{2+} and Fe^{2+}) from drilling mud wastewater, by natural and synthesize zeolites and natural kaolin.

1.10 research objective

The main objective of research is to study the efficiency of zeolites in the treatment of drilling mud wastewater from block-6 field plant Sudan.

1.10.1 Specific objective

1- To collect zeolite samples from different Sudanese ores.

2-To investigate physiochemical properties of zeolites.

3-To synthesized zeolite from fly ash waste.

4- To use natural and synthetic zeolite and kaolin to remove or reduce of (Cr^{3+}, Fe^{2+}, Co^{2+} and Zn^{2+}) from mud water.

5- To conduct isotherms studies (Langmuir and Freundlich) of the zeolites under investigate.

Materials and methods

2.1 Sampling

2.1.1 Samples collection

2.1.1.1 Natural Zeolites

The natural zeolites used in this study were collected from Gadarf state Wdkolly (Eastern Sudan 410km from Khartoum) it`s bounded by Latitudes 12˚45` - 14˚ 53˚ and Longitudes 35˚ 10` - 36˚ E, natural zeolite occur in vesicles and volcanic rocks around El-Garf town at J.Tawawi, J-UmmDebiba and Doka villages, these areas are mostly comprised of zeolites, zeolite occur in various sizes and shapes, calcite also occur in the area as second minerals, HCl used to distinguish between zeolites and cacite.

2.2.1.2 Kaolin samples

The samples of natural kaolin were collected from Elmerkhiat mountain North-West of Omdurman town. The kaolin lies near the surface or as out cropping, it can be traced about 10 km East-West direction in relatively narrow bands South of Elmerkhit mountains 15°37` Latitude and 32°19` Longitude it was coded as Ka. (M.A 1999).

2.2.1.3 Mud samples

Samples of drilling mud fluid were collected from block (6) Elfulla west kordofan state (800 km from Khartoum) moga location. All samples collected in 500 cm^3 polyethene bottles. The waste drilling mud is a stable colloidal mixture with high water content, and it is difficult to directly filter the liquid. Thus, an appropriate demulsifier should be added to destroy the stability 80% H_2SO_4, AlC_3, $CaCl_2$, and $Al_2(SO_4)_3$ were chosen as potential demulsifiers.

2.1.2 Samples preparation

2.1.2.1 Zeolites samples

Natural zeolites were washed with acid to remove impurities that block the pores, zeolite was immersed in 1.0M HCl for 5 hours. 5g of zeolite was placed with 50 cm^3 of 1 M NaCl solution for 24 hours at room temperature, the suspension was

agitated in hot plate stirrer, then filtered and washed with dionised water, the material was dried at 200˚C for 8 hours in an oven. Then zeolite become Na-zeolite.

2.1.2.2 Synthesis of Zeolite from fly ash

To synthesis zeolite from fly ash it's important to add alkali to fly ash. The collected samples were initially screened to eliminate larger particles and calcined at 800 ± 10 ºC for 2 h to remove the unburnt carbon and volatiles. The syntheses of zeolite from fly ash was followed according to the procedure reported by(Ruen-ngam et al. 2009). In a typical run, ten grams of fly ash was added to 10 g of sodium hydroxide, the mixture was burnt in air at 550 °C for one hour in furnace. The product was crushed and dissolved in 85 cm^3 distilled water then stirred for 25 hours at room temperature. To start the crystallization, the mixture was placed on autoclave for 2 hours at 90 °C. Dimethylamine (as organic template) was used to facilitate the crystallization process. The crystallized zeloite was washed several times with distilled water until the pH reached 10 and it was dried over night at 105 °C. The synthesized zeolite was coded as SZ.

However, another type of zeolite was prepared by treating fly ash with 12 M HCl for 10 hours, although 2M sodium hydroxide added to fly ash by 3:1 ratio, it was heated to boil for 2 hours, however the extract solution neutralized by 1 M HCl, white gel obtained after few minutes, under stirring at room temperature, whereas white gel saved in autoclave for 10 hours, then it washed and calcinated at 600 ˚C for 2hours. (Liu et al. 2013).

2.1.2.3 Kaolin Samples

The removal of some impurities from raw clay was first done by physical separation of dirt. The powdered, bulk, sample was soaked in de-ionized water for 48 h. The slurry was plunged and screened through a 150-200 µm mesh sieve and then allowed to settle. Water was siphoned and the clay was dried .(Olaremu 2015).

2.1.2.4 Mud samples

Preliminary screening tests were conducted with 200 cm^3 drilling mud by adding $AlCl_3$, $CaCl_2$, and $Al_2(SO_4)_3$ with a dosage of 5 g/L and 80% H_2SO_4 with a dosage of 9 g/L, respectively the samples were mixed with the demulsifier by a mechanical stirrer for 15 min(Hu et al. 2012)

2.2 Chemicals

Ammonium acetate 98% (CH_3COONH_4) CDH, India

Ammonium Chloride (NH_4Cl) 99%, CDH, India

Ammonium Iron(II)(Sulphate $(NH_4)SO_4.FeSO_4.6H_2O$) 98%, CDH, India

CDH, INDIA – Cobalt chloride 97%, ($CoCl_2.6H_2O$) Aloha, India.

CDH, INDIA - Hydrochloride acid (HCl) 35-38%, Loba Chem, India

Chromium (III) Chloride Dehydrate ($CrCl_3.6H_2O$) 93% Aloha, India.

Fly ash was obtained from Garri electricity station (North Khartoum).

Nitric acid (HNO_3) 64%, Loba Chem, India.

Sodium chloride (NaCl) 98%, CDH, India.

Sodium hydroxide (NaOH) 98% Loba chem India.

Zinc Chloride ($ZnCl_2$) 97%, Loba Chem, India.

2.3 Instruments

Atomic Absorption spectrometry (AAS) Savanta serial No AA7638GBC (Australia).

Autoclave model 23-200 Germany.

Hot stirrer Model: LMS-1003 Scott science UK.

Inductively coupled plasma (ICP) Thermo Scientific™ iCAP™ 7200 ICP-OES (Germany).

Infrared spectroscopy: (FT-IR 84005 Shimadzu Japan).

Muffle furnace Model: WACS-104 Korea.

pH-Meter model: JENWAY 3505 UK.

Scanning electron Microscope (SEM) Model: H-8100 England equipped with Energy Dispersive X-Rey fluorescence (EDX) SHMADZU VEGA3 Japan.

Specific surface area BET (Quantachrome Instruments German).

X-ray Diffraction (XRD) (Panan analytical X'Pert³ MRD (Netherlands).

X-ray fluorescence (XRF) (Axios max pan analytical (Netherlands).

2.4 Methods:

The characterization was done using X-ray diffraction which determine the structure as well as the purity. Total elemental analysis was performed by X-ray fluorescence and Infrared spectroscopy via frequencies of structure-sensitive bands Information regarding framework properties, – OH stretching whereas, specific surface area measured by BET adsorption- desorption method and Scan Electron Microscopy(SEM) to indicate external morphology. (Oliveira & Rubio 2007).

2.4.1 X-ray Diffraction

Samples of zeolites were ground into fine homogenous powder and put in holder and to obtain a flat surface placed in the diffractometer and exposed to X-rays. The wide-angle X-ray scattering of samples was measured using an X-ray diffractometer (D8 advance powder diffractometer) with Cu K α radiation. Diffraction patterns were collected at 5–90◦ using Cu K α radiation with a step size of 0.028˚, and CaF_2 as internal standard it was used Panan analytical X'Pert³ MRD, Copper Kα radiation at 45 kv/ 35 mA with a goniometer speed of 2°/ min .in the 2ɵ range scanning from 2° to 50° Fig. 2.1.

2.4.2 X-ray Fluorescence

The chemical composition of the samples was analyzed by X-ray fluorescence XRF, 10 grams of samples mixed to 0.4-gram cellulose, ground to give homogenous and analyzed using XRF.

2.4.3 Infrared spectroscopy

Spectrum of the main functional groups of the samples were indicated from the FT-IR. IR of all samples were obtained (in KBr pellets) in 4000 -400 cm^{-1} regions with a resolution of 4 cm^{-1}, by FT-IR.

2.4.4 Atomic Absorption Spectroscopy (AAS)

The concentration of remining metals such as (Cr^{3+}, Co^{2+}, Zn^{2+} and Fe^{2+}) determined by atomic absorption spectroscopy. Using standard procedures.

2.4.5 Scanning Electron Microscopy (SEM) & Electron dispersive X-ray (EDX)

The morphology of different crystalline phase of samples was investigated by scanning electron microscopy SEM linked with energy dispersive X-ray (EDX), as well as XRD, samples was coated with gold and analyzed with Scanning Microscope.

2.4.6 Determination specific surface area of Zeolite and kaolin

The specific surface area was calculated using the adsorption data of N_2-adsorption analysis by adopting the Brunaur, Emmett and Teller (BET) model in the relative pressures range of 0.05 to 0.35, the distribution of the pores and their average diameter were calculated from the adsorption data of N_2-adsorption analysis by adopting BJH model. The total pore volume was estimated on the basis of the amount of nitrogen adsorbed at a relative pressure (P/P^o) of ca. 1.0. The specific surface area was calculated using standard Brunaur, Emmett and Teller (BET) method for adsorption data in the relative adsorption range from 0.05 to 0.25 for ZN1 and ZN2, 0.05 to 0.35 for Ka.

2.4.7 Physical properties

The particle size of all samples between 150 to 200 µm it done by the sieving, the mechanisms of zeolite as cation exchange is participating ion through the internal channels and cavities or their hindered movement through the film of ordered water which exists on the surface of the zeolite. Although to indicate ion exchange capacity of the samples, covert to Na-zeolite and added 0.1M NH_4Cl for 2 hours, filtration and determined the concentration of NH_4Cl in the solution, ion exchange capacity confirmed.(Malekian et al. 2011), (Englert & Rubio 2005).

2.4.8 Batch study

Batch adsorption was performed four types of artificial ion solutions (Cr^{3+},Co^{2+},Zn^{2+} and Fe^{2+}), to regared concentration, pH and contact time.

adsorption experiments were carried out at room temperature, in polyethylene flask (100 cm^3).

about 40 cm^3 of aqueous solution added to 0.4 gram solid samples, kept on Hot stirrer to prevent any sedimentation and provide proper agitation. The final concentration in the supernant (liquid phase) was measured by AAS.

The removal percentages of heavy metal ions were calculated from equation (2.1).

$$\text{Metal removal\%} = \frac{C_0 - C}{C_0} * 100 \qquad (2.1)$$

Where C_o and C are initial and final concentration (mg/dm^3) of the metal ions solution in contact with the mass of zeolite.

The amount of Cr^{3+}, Fe^{2+}, Co^{2+} and Zn^{2+} adsorbed onto zeolite surface was determined using mass balance equation (2.2)

$$q_e = \frac{V(C_0 - C)}{m} \qquad (2.2)$$

Where (q_e) is the metal concentration on the zeolite (mg/dm^3) at equilibrium, (C) is metal concentration in solution (mg/dm^3) at equilibrium, (C_o) is initial metal concentration in solution (mg/dm^3), (V) is initial volume of metal solution used (cm^3), and (m) is mass of zeolite used. The final metal concentration in the supernant (liquid phase) was measured using atomic absorption.

Then the optimum condition of each parameter (pH, time) was used for the experiments of removing the heavy metals, i.e. Cr^{3+}, Fe^{2+}, Co^{2+} and Zn^{2+}, in mud samples.

2.4.8.1 The effect of pH

Aqueous phase pH governs the speciation of metals and also the dissociation of active functional sites on the sorbent, it has been identified as the most important variable affecting metal adsorption onto adsorbent, this partly because hydrogen ions themselves are strongly competing with adsorbate, Adsorption experiments were carried out in pH range of 2 to 8 keeping all other parameters constant in batch solutions contain initial concentrations 200 ppm using HNO_3 and NaOH to adjust pH. To study the effect of pH on adsorption capacity of zeolites the mechanism of adsorption at the Zeolite surface reflects the nature of physicochemical interaction of the metal ions in the solution and the active sites of the Zeolite (Pandey et al. 2009).

2.4.8.2 The effect of contact time

Time is an important parameter in adsorption process, the adsorption of metal ions Cr^{3+} onto adsorbents was invesegated (constant tempruture) as function of shaking time in the range of 10 to 120 minute. Three different concentrations, 100,150 and 200 ppm.

2.4.9 Adsorption isotherms:

Equilibrium data, commonly known as adsorption isotherms, are requirement for design an adsorption system, there are many adsorption models such as (Freundlich, Langmuir and Dubinin- Radushkevch …. etc) . However, Freundlich and Langmuir were used to describe the equilibrium between adsorbed metals ions on the samples cell (q_e) and metals ions in solution (C_e) at constant temperature. (Asnaoui et al. 2015).

2.4.9.1 Freundlich Adsorption Isotherm:

Freundlich model supposes that uptake or adsorption of ions occurs on heterogeneous surface by monolayer, these data often fit the empirical equation proposed by Freundlich:

$$q_e = K_f (C_e)^{\frac{1}{n}} \qquad (2\text{-}3)$$

Where K_f and n are Freundlich constants characteristic of the system. Whereas K_f and n are indicators of adsorption capacity and adsorption intensity, although equation (2.3) can be linearized in logarithmic form and the constants can be determined

$$Log(q_e) = LogK_f + \frac{1}{n} Log(C_e) \qquad (2\text{-}4)$$

The initial concentrations of (Cr^{3+}, Co^{2+}, Zn^{2+} and Fe^{2+}) were varied and adsorbent dose was kept constant in order to determine the equilibrium isotherms.

2.4.9.2 Langmuir Adsorption Isotherm

The Langmuir equation validating the monolayer sorption in a surface of a finite number of identical sites is given by Equation (2.5)

$$q_e = q_{\max} \frac{K_L C_e}{1 + K_L C_e} \qquad (2\text{-}5)$$

q_{max} ($mg.g^{-1}$) is the maximum amount of metal ions per unit weight of solid to form a complete monolayer on the surface bound at high (C_e), and K_L ($L.mg^{-1}$) is constant related to the affinity of the binding sites, however q_e represents a practical limiting adsorption capacity when the surface is fully covered with metal ions.

The above equation can be also linearized by the following process (Asnaoui et al. 2015).

$$\frac{1}{q_e} = \frac{1}{q_{\max} K_L C_e} + \frac{1}{q_{\max}} \qquad (2\text{-}6)$$

Results and Discussions

3.1 Physical properties

Main physical, properties are summarized in table (3-1) below

Table (3-1) summery of physical properties of zeolites and kaolin

Parameters	ZN1	ZN2	SZ	Ka
Cation exchange capacity meq g^{-1}	2.1	2.03	2.4	1.88
Particle size μm	150-200	150-200	150-200	150-200
Moisture content %	10	12	13	11

Table 3.1 shows the physical properties of zeolites and kaolin. ZN1 have low Moisture content (10%), for zeolite samples is almost similar to that of kaolin, particle size is identical for all samples range between 150- 200 μm. Average per exchange capacities of zeolite. (2.1) is higher (3.4%) than that of kaolin. From the table, natural zeolite and kaolin can be used for ion exchange.

3.2 Characterization and analysis

From the Fig 3.1, 3.2,3.3 and 3.4 show XRD pattern for ZN1, ZN2, SZ and modified fly ash.

3.2.1. X- Ray diffraction

XRD pattern of ZN1 diffraction signal observed clear at 2ɵ, three peak at 9.5˚, 22˚ and 29.5˚ it indicates that zeolite consisted mainly of Stablite 70% and others impurities such as quartz 15%. Fig (3-1)

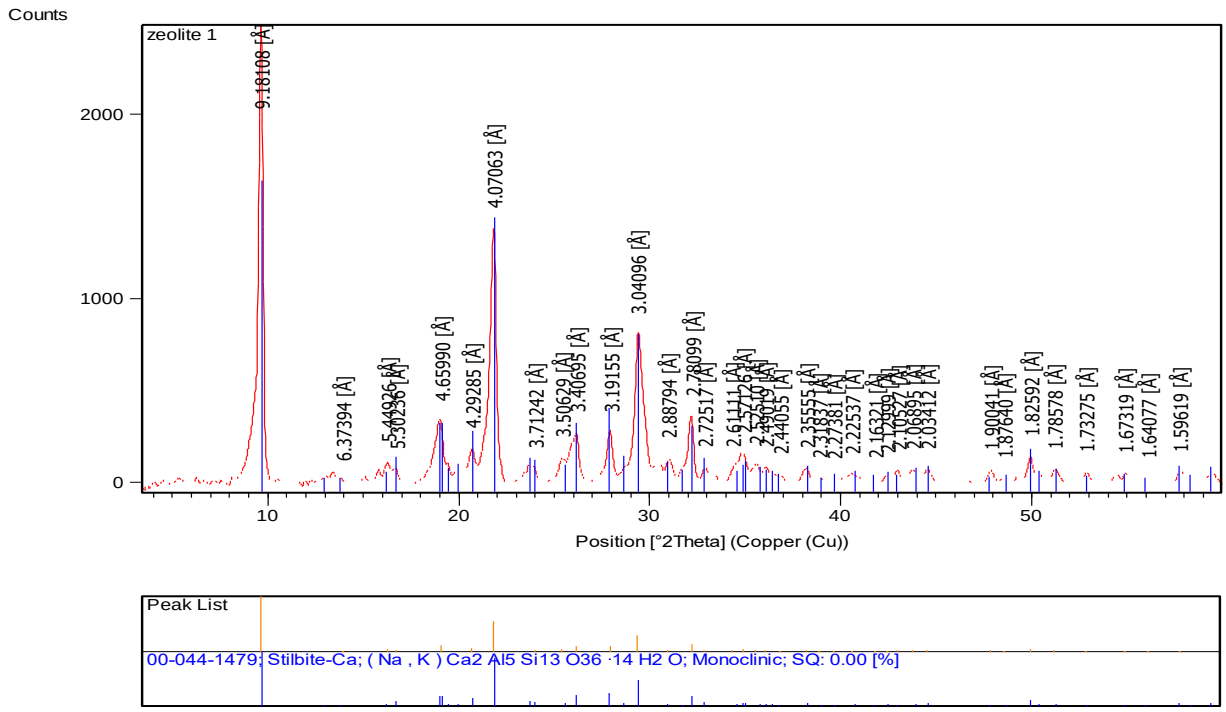

Fig (3-1) *Fig (3-4) XRD pattern of stablite ZN1*

For ZN2 XRD pattern of the sample is presented in Fig (3-2), the two major peaks were found in zeolite at 9.7˚ and 21.8˚ at 2ɵ corresponded to the Stellerite type, the remaining peaks in the pattern may be attributed to the presence Chabazite 23.5%. It demonstrate that natural zeolite have typical orthorhombic micro porous structure.(Treacy & Higgins 2001). The structure can be verified by observation of four distinct diffraction peaks indexed as, (020), (311), (060) and (319).in low 2ɵ region.

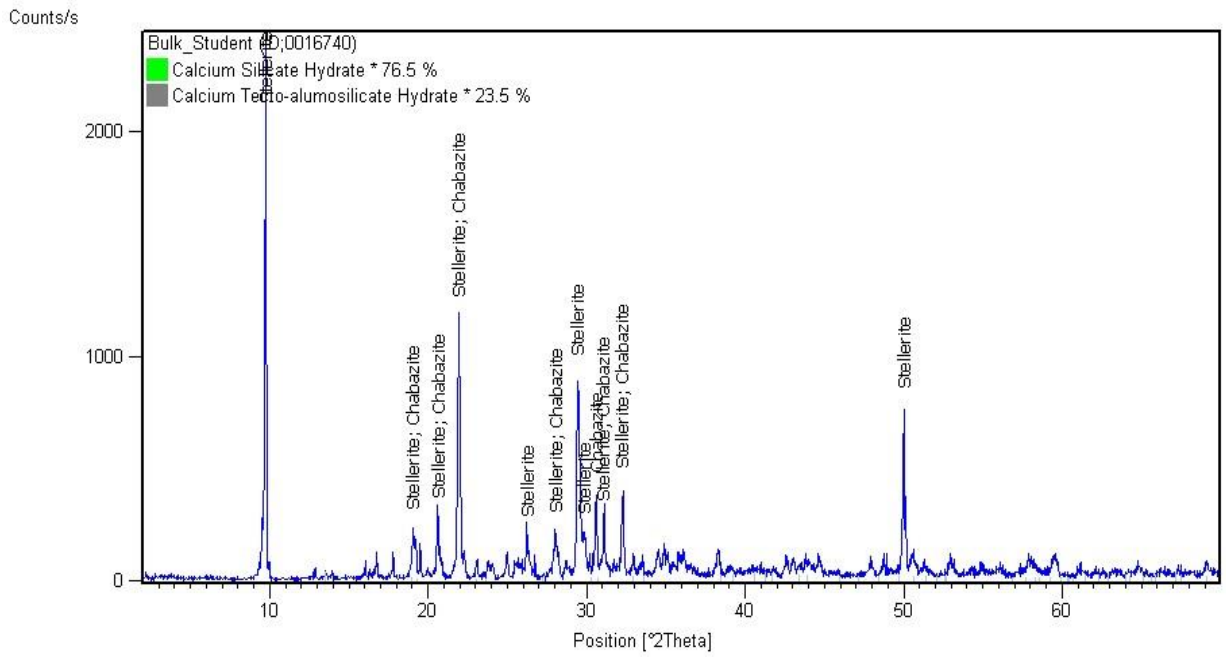

Fig (3-2) XRD pattern of Stellerit ZN2

However, XRD pattern of SZ have diffraction signals starting from 21˚, 27˚, 37˚ and 39˚, the Figure shows the crystal structure of mullite and quartz make the system silica dissolved, SiO_2 and Al_2O_3 can be activated, although the XRD pattern of SZ attributed to zeolite A, whereas the crystal system of SZ is hexagonal, $a = b \neq c$ and $\alpha = \beta \neq \delta$. The diffraction peaks indices are (011), (102) and (11-2).

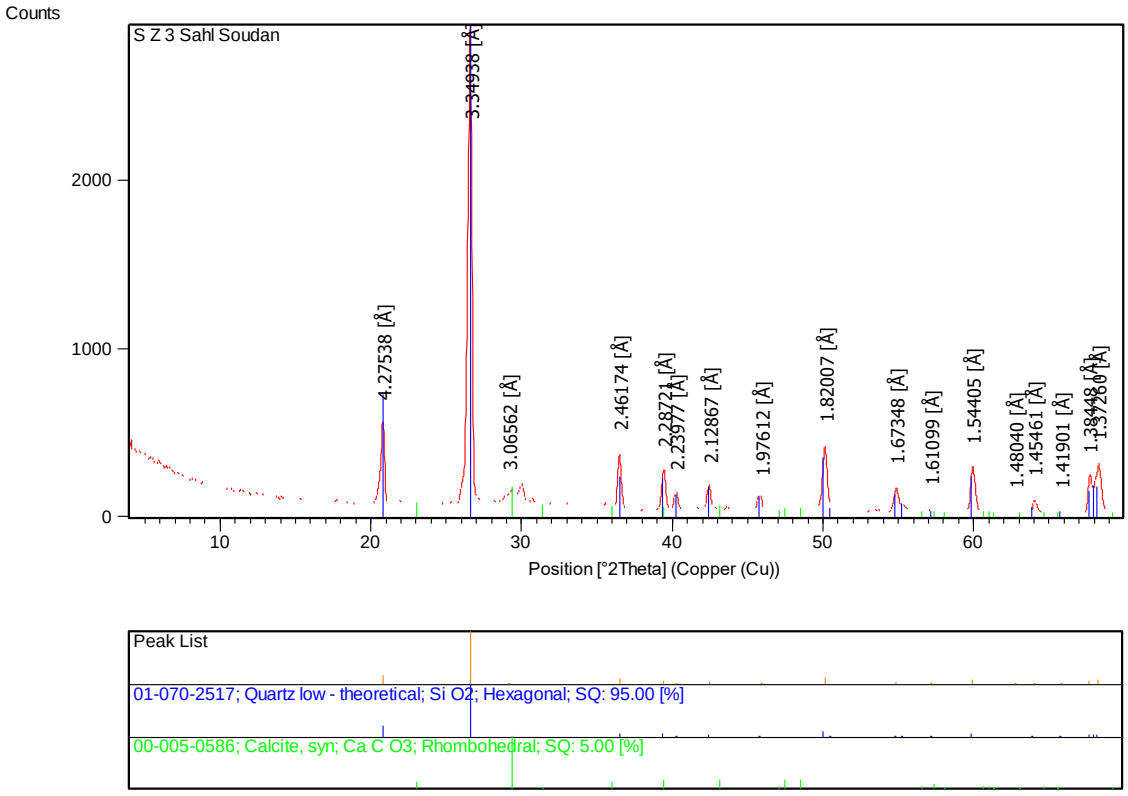

Fig (3-3) XRD pattern of Modified fly ash SZ

The XRD pattern of treated fly ash HCl solution by (white gel) shows clear crystal structure with diffraction signals 16˚, 24˚,29˚, and 38˚. With hexagonal crystal system.

It can be described as zeolite A.

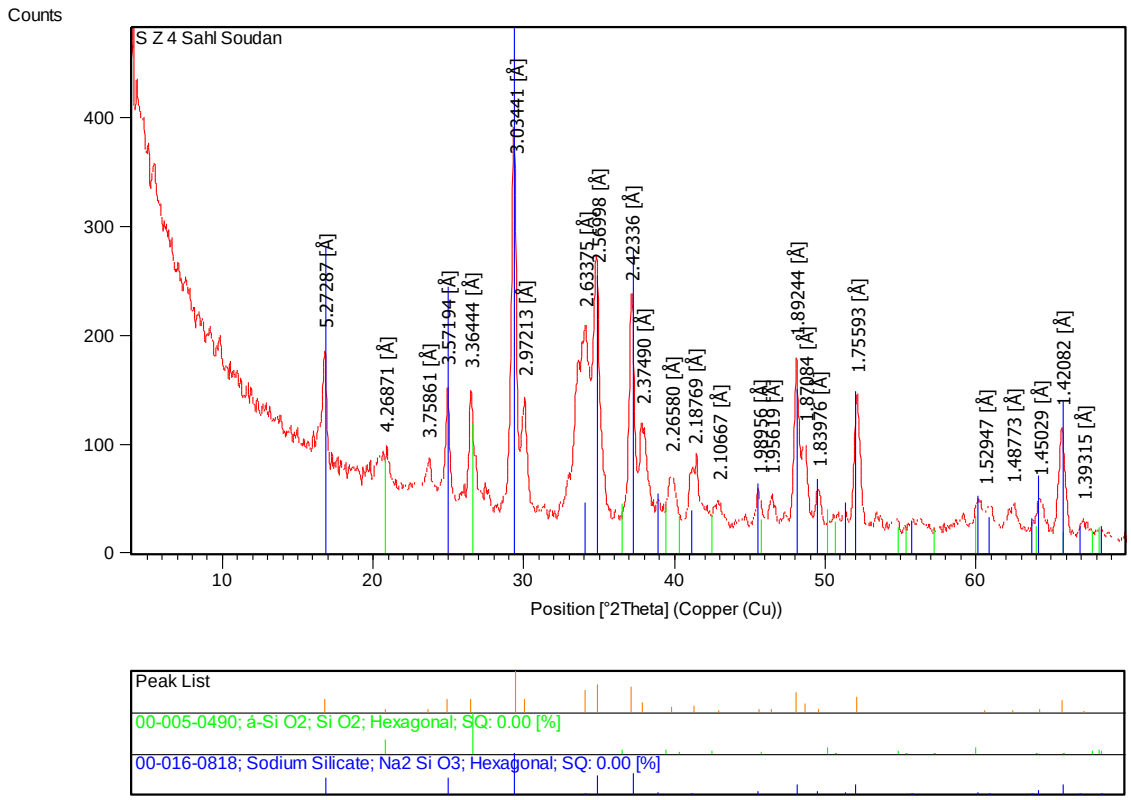

Fig (3-4) XRD pattern of Modified fly ash (solution)

XRD pattern in Fig (3-5) shows that Kaolin is the major compound it also contain other impurities like (Silicon oxide and Mica-Muscovite), with chemical formula $Al_2 (Si_2O_5) (OH)_4$ .The diffraction patterns obtained using (ICSD) as reference code is at 12.3°, 20.3°, 24.8°, 38.5°, 39.2°,50°,55° and 60° which corresponds to Kaolin and the other patterns indicated to other impurities .However the crystal system is similar to Triclinic which ($a \neq b \neq c$ and $\alpha \neq \beta \neq \gamma$).

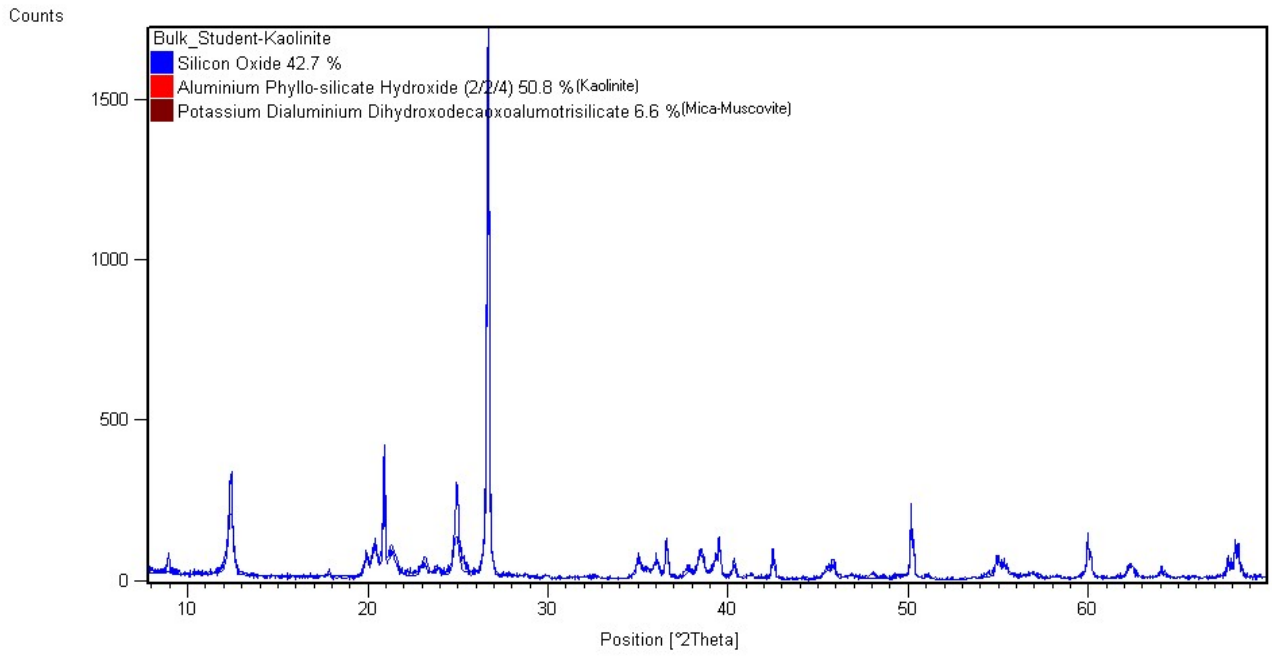

Fig (3-5) XRD pattern of Kaolin

3.2.2. Infrared spectroscopy

The FT-IR spectrum of ZN1 is shown in Fig (3-6), characteristic absorption peaks the range 439 cm^{-1} to 706.9 cm^{-1} wher deformation and mixed vibration of Si and Al are lattice, the strongest infrared absorption at 1026.06 cm^{-1} is attributed to valence vibration appear of (Al,SiO)-O bonds, the OH- group at 3448 cm^{-1} (Hou et al. 2012).

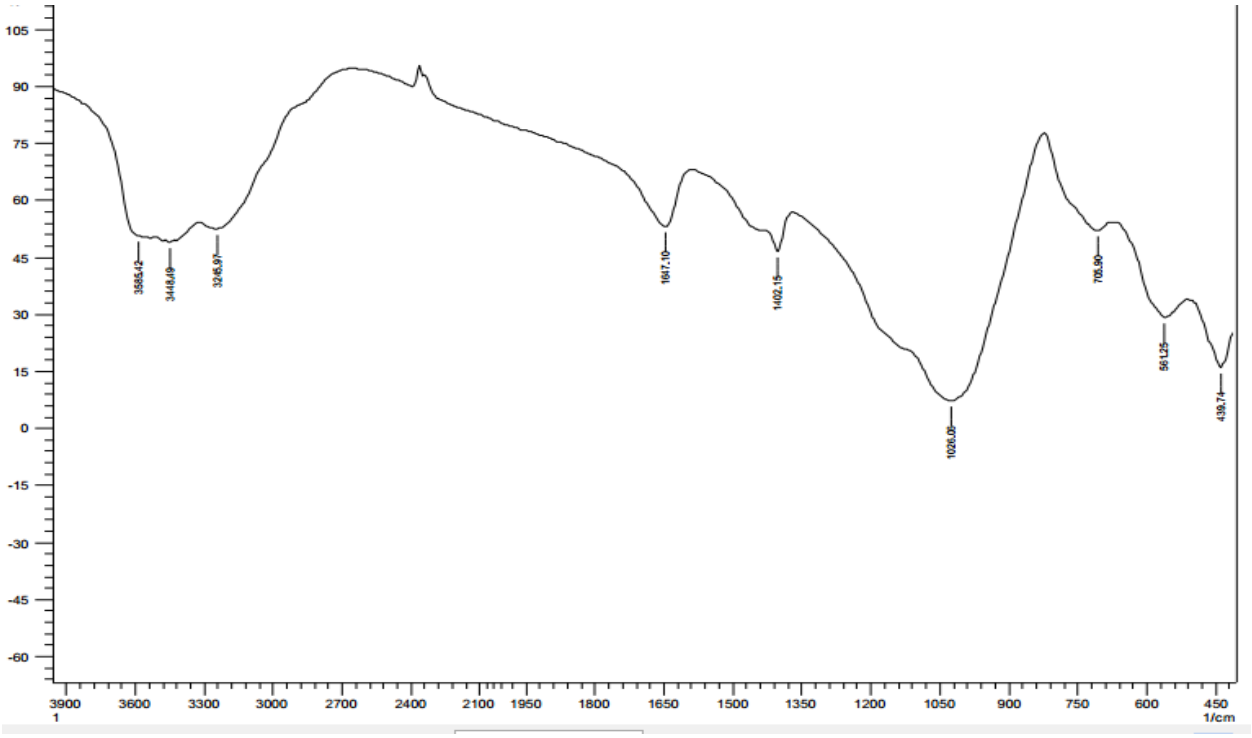

Fig (3-6) FT-IR of ZN1

The FT-IR spectrum of the ZN2 sample is shown in Fig (3-7). It is very obvious that the absorption bands at around 440cm^{-1} which is attributed to Silicon Aluminum lattic. The strongest infrared absorption band at 1020 cm^{-1} assigned to valence vibration of (Al,Si)-O bonds. OH- observed at 3568cm^{-1}, H_2O observed at 1645.17cm^{-1} (Hou et al. 2012).

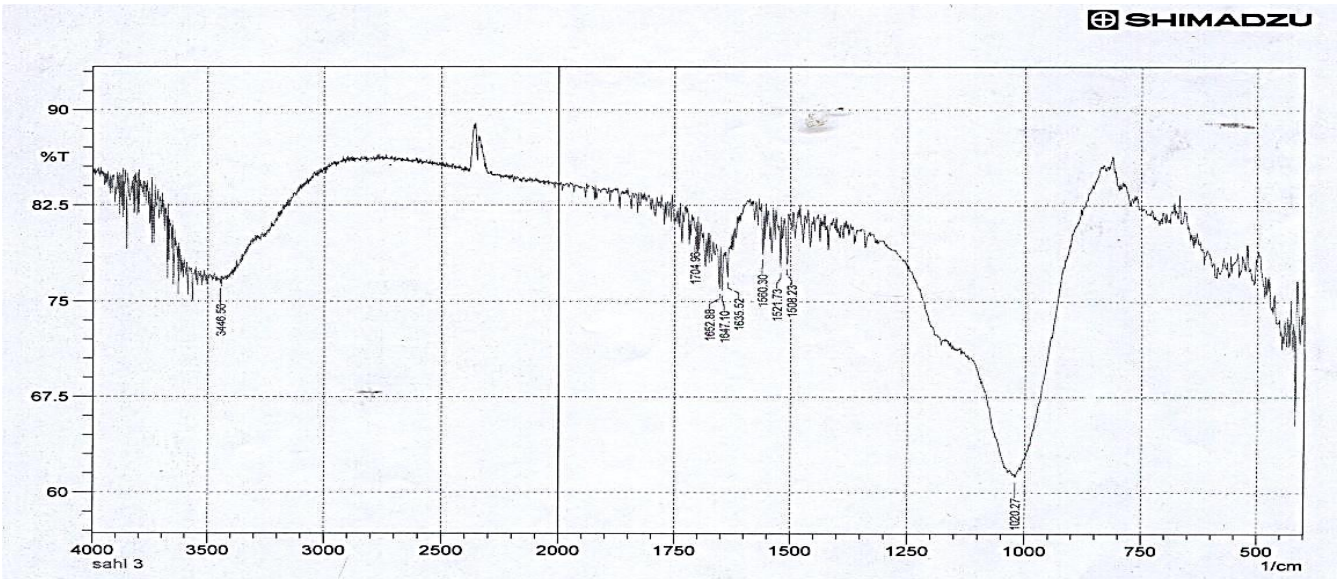

Fig (3-7). IR spectra of Natural zeolite ZN2

The infrared spectrum of Kaolin which is depicted in Fig (3-8) shows the existence of OH- bands of adsorbed water as well as of Al-O-H at around 3623 and 3696 cm^{-1}. The broad bands at 1107 and 1035 cm^{-1} are assigned to siloxane (Si-O-Si) stretching vibrations, whereas the shoulder at 915 cm^{-1} is assigned to Si-O stretching vibration of silanol (Si-OH). The peaks at 791, 692, 540, 469 and 427 cm-1 are attributed to framework of kaolin. (Olaremu 2015).

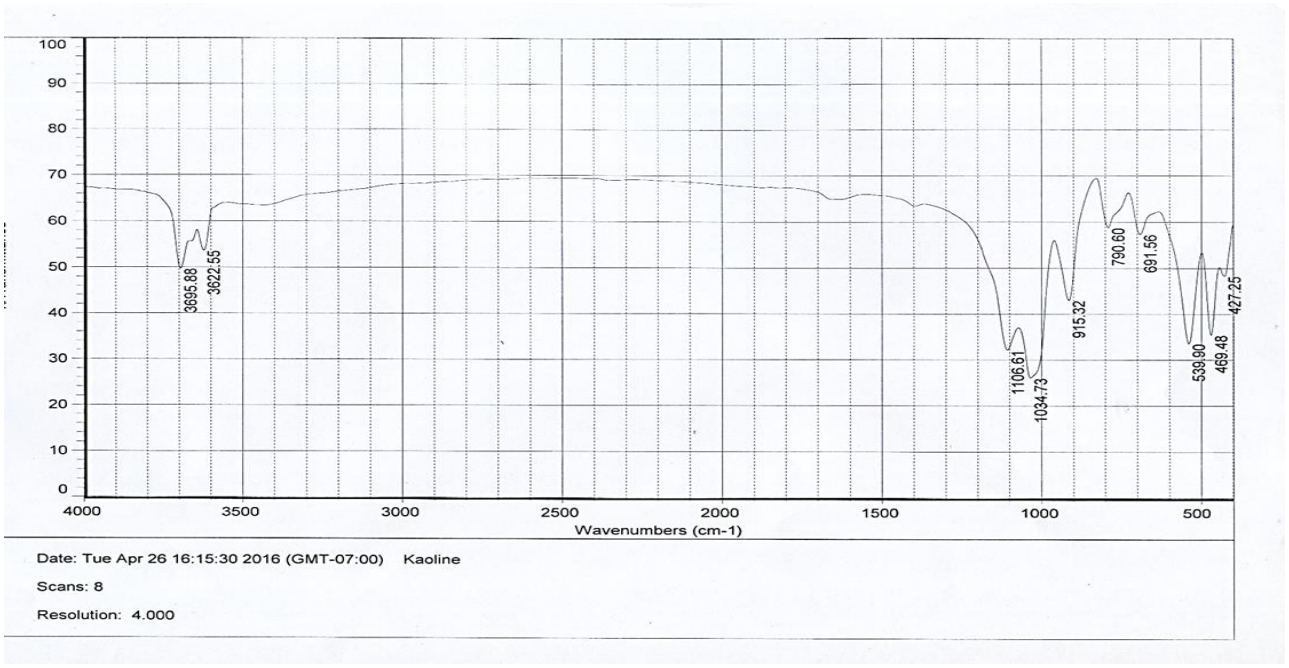

Fig (3-8) IR spectra of Kaolin Ka

Table 3.2: Summary of characteristic FT-IR absorption bands of natural zeolites, Kaolin and synthesized zeolite.

Function groups	ZN1	ZN2	SZ	Ka
Si,Al-O	439 cm^{-1}	440cm^{-1}	447.27cm-1	427.25cm^{-1}
Framework	698cm^{-1}	688.43cm^{-1}	681.53cm-1	691.65cm^{-1}
OH-	344cm^{-1}	3568cm^{-1}	3433.19cm-1	3695.88cm^{-1}
H_2O	1647cm^{-1}	1645cm^{-1}	1622.62cm-1	-

3.2.3 X-ray fluorescence

XRF analysis of samples is shown in Table 3.3 metals oxides of the natural samples ZN1, ZN2, SZ and Ka are rich of SiO_2 and Al_2O_3 and some impurities such as CaO, MgO, Na_2O, Fe_2O_3 and TiO_2.

Table (3-3) XRF value of ZN1, ZN2, Ka and fly ash

Compound	ZN1	ZN2	Ka	Fly ash	Unit
SiO_2	62.94	64.35	64.5	66.02	%
Al_2O_3	19.81	21.73	31.4	1.66	%
CaO	9.12	10.16	0.175	24.4	%
MgO	2.71	0.92	0.345	0.512	%
Na_2O	2.12	1.48	0.166	0.11	%
Fe_2O_3	2.28	0.59	1.119	1.76	%
TiO_2	0.287	0.013	1.442	0.24	%

3.2.4 Determination of specific surface area of samples

Nitrogen adsorption-desorption isotherms are used to determine specific surface area and pore size distribution, it conducted at liquid nitrogen at 77K. ZN1 and ZN2 are depicted in Fig (3-9) and (3-10). The finding indicate that isotherms resemble type (iv) of (BET) isotherm type may attributed to mesoporous or nonporous. However, type (iv) isotherms have their unique features adopted to IUPAC in (Sing & Evertt 1985). Type (v) attributed to monolayer and multilayer adsorption and it similar to type (ii) which give adsorptive on the same surface area of the adsorbent in non-porous form.

Hysteresis loop which known as an inherent property of capillary condensation, the point of equilibrium transition and condensation, at the vaporlike spinodal, which represents the true limit of stability of metastable adsorbed films. This conclusion correlates with the classical scenario of capillary condensation hysteresis,in open-ended cylindrical pores (Neimark et al. 2000), ZN1 and ZN2 their Hysteresis appearing in the multilayer range of physio-sorption isotherms,

which associated with capillary condensation in mesoporous, whereas two lines nearly horizontal and parallel over range of P/P˚.

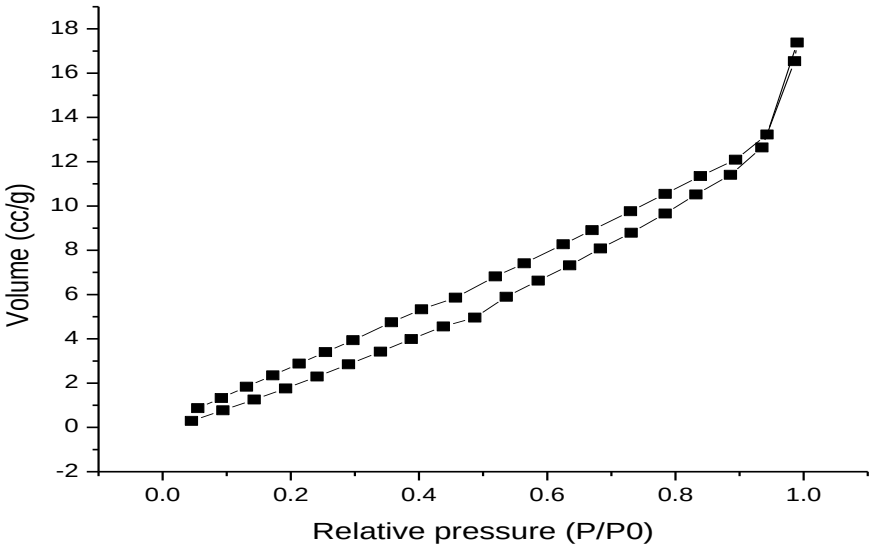

Fig (3-9) N_2 adsorption – desorption isotherm of natural zeolite ZN1

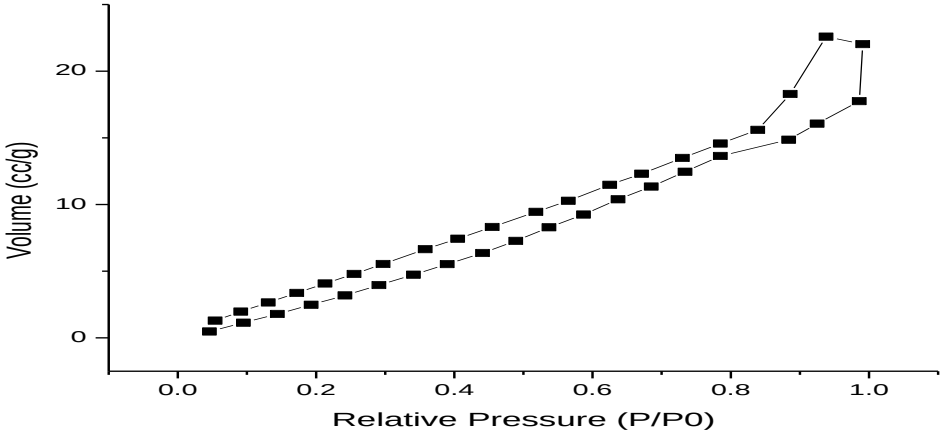

Fig (3-10) N_2 adsorption – desorption isotherm of natural zeolite ZN1

synthesized zeolite (SZ) isotherm Fig 3.11 obey the type (ii) isotherm which concave to the P/P˚ axis, almost linear and finally convex to the P/P˚. Although it indicates the formation of an adsorbed layer which increase progressively with increasing relative pressure until P/P˚ = 1, the knee of the isotherm is shape the uptake at point B is usually considered to represent of monolayer (Rouquerol Francoise, 1999). Whereas it obeys hysteresis loop number H_3, which does not

show any limiting adsorption at high P/P˚ is observed with aggregate such as (J) of plate- like particles giving rise to slit- shaped pore.

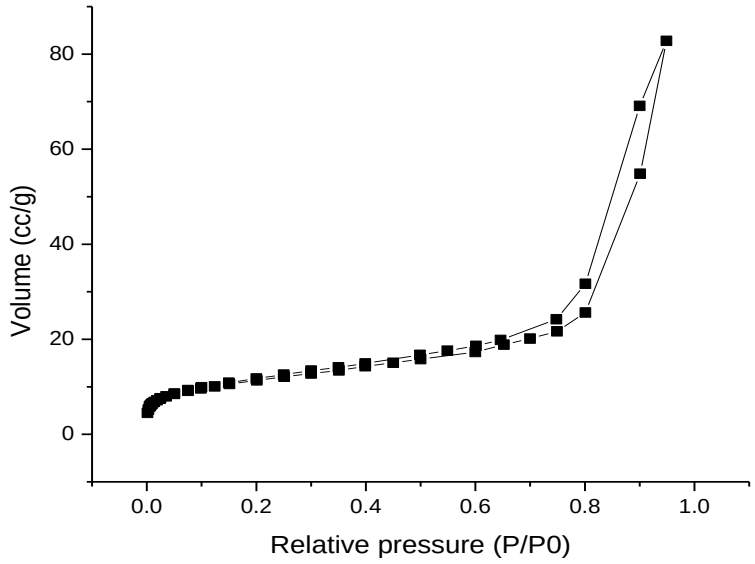

Fig (3-11) N_2 adsorption – desorption isotherm of Modified fly ash

Natural kaolin isotherm Fig 3.12 resembles type (IV) BET isotherm type, a characteristic of mesoporous materials. The capillary condensation usually observed at relative pressure (P/P˚) of 3- 5 with narrow, almost vertical and nearly parallel hysteresis pattern which is joined at intermediate relative pressures. The capillary condensation of this isotherm occurred at high relative pressure (P/P˚) of > 0.7. In addition, there is a limited uptake of N_2 sorbent over a range of high P/P˚. These parameters collectively indicate the existence of pores of high sizes which could result from voids between particles of non-porous or macro-porous materials. Surprisingly, the shape of the hysteresis loop does not resemble the ordinary shapes of typical mesoporous materials and hence provides more evidence of non-porous character, samples is similar to type H_3, typical of agglomerates of plate-like particles containing slit-shaped pores (Panda et al. 2010).

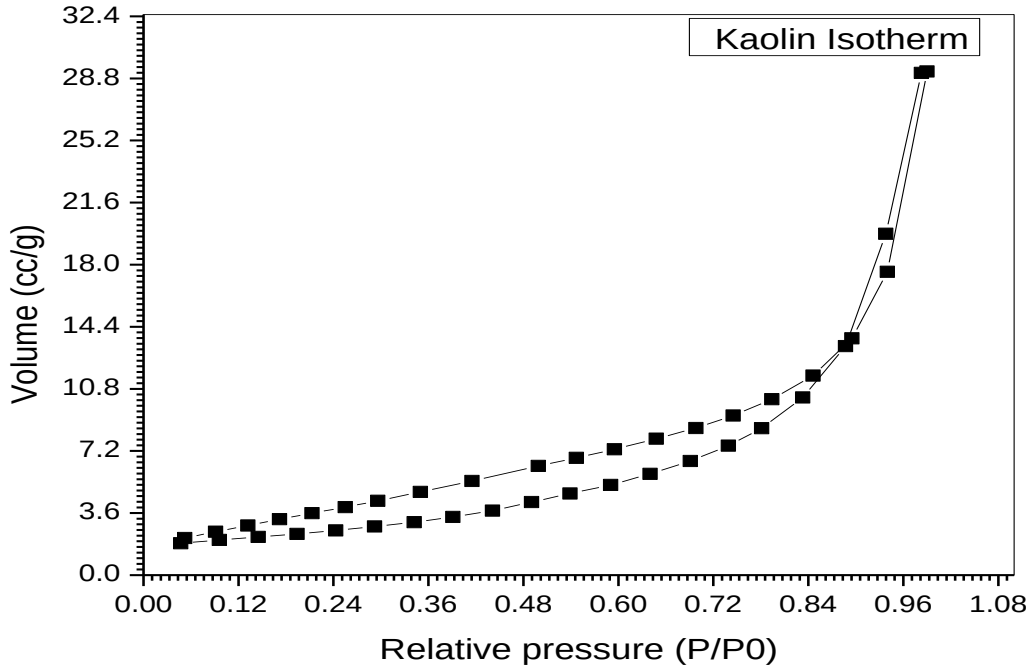

Fig (3-12) N_2 adsorption-desorption isotherm of Kaolin

However, it is generally accepted that the desorption isotherm is more appropriate than the adsorption isotherm for evaluating the pore size distribution of an adsorbent. The BJH method was originally developed for relatively coarse porous adsorbents having a wide range of pore sizes. The pore size distribution shows the material to be, mainly, mesoporous as the region within 2 - 50 nm had highest point. This is followed by microporous 0 - 2 nm and macroporous > 50 nm. Hence the order is mesoporous > micro pores > macro pores. Although the pore size distribution of ZN1 (11.88), ZN2 (12.69) SZ (13.8) nm and Kaolin (18.02) nm. The pore volume distribution data shown that the Ka > SZ > ZN1>ZN2 respectively (Olaremu 2015).

The specific surface area observed that of zeolites at (20.44 m^2/g) for ZN1, (26.88m^2/g) for ZN2 and (40.31m^2/g) for SZ are higher than Kaolin (14.73 m^2/g).

Table 4.4 below summary of specific surface area

Table (3-4) summarize N_2 adsorption

Samples	Surface area BET (m^2/g)	Total pore volume (cm^3/g)	Pore size (nm)
ZN1	20.44	0.00607	11.88
ZN2	26.88	0.00852	12.69
SZ	40.317	0.004	13.8
Ka	14.73	0.006	18.02

3.2.5 Scanning Electron Microscopy& Electron dispersive X-ray

Scanning electron microscopy (SEM) complement with other technique such as N_2 adsorption and XRD, however it indicates surface morphology linked with electron dispersive X-ray (EDX), in such context the technique used direct image.

The micrograph of ZN1 shows the crystallinity properties of the samples and when compared with XRD it indicates the hexagonal structure, when the micrograph of SEM linked to EDX, the spectrum shows presence of O, Si and Al as major component of ZN1.

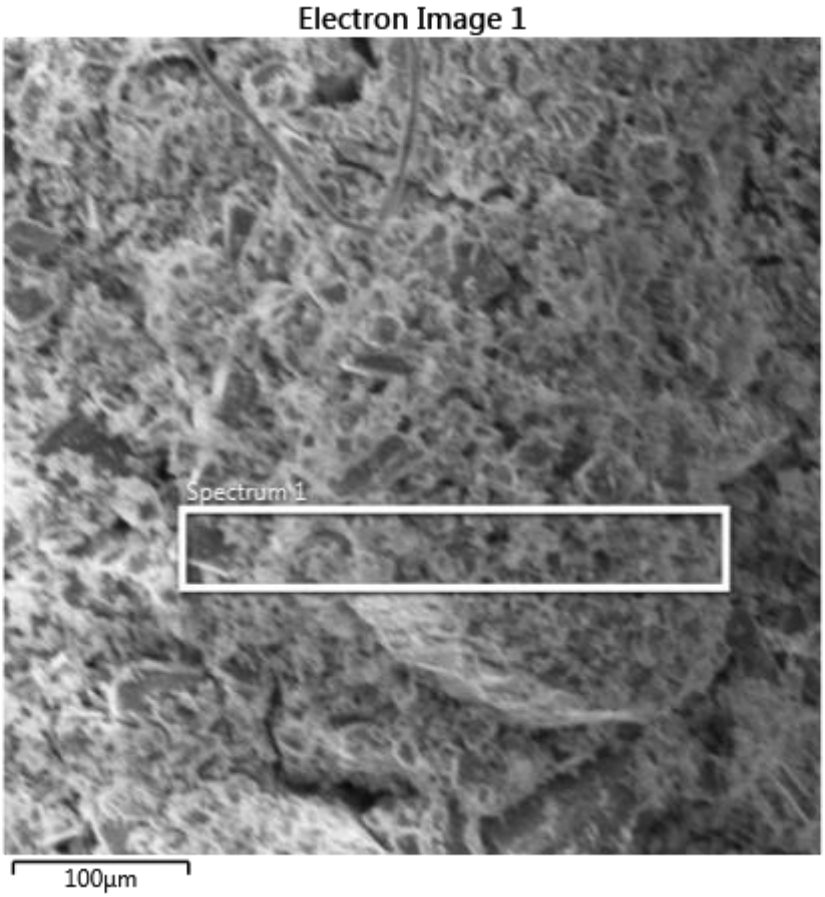

Fig (3-13) SEM of ZN1

The spectrum of EDX shows other elements of low content such as Ca, Fe, Na and Mg is part of ZN1 composition.

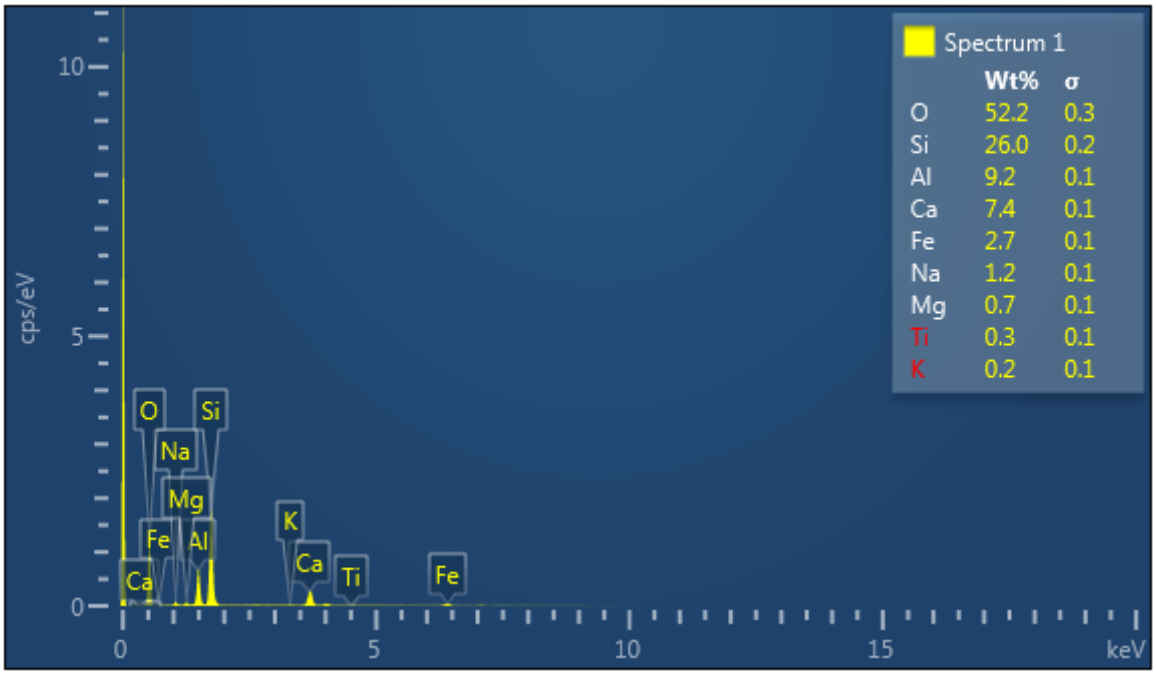

Fig (3-14) EDX of ZN1

The micrograph of ZN2 SEM indicated clearly the crystallinity and morphological feature of ZN2, the EDX analysis for four near spectrum (1,2,3 and 4) show variation in the percentage of main component of ZN2

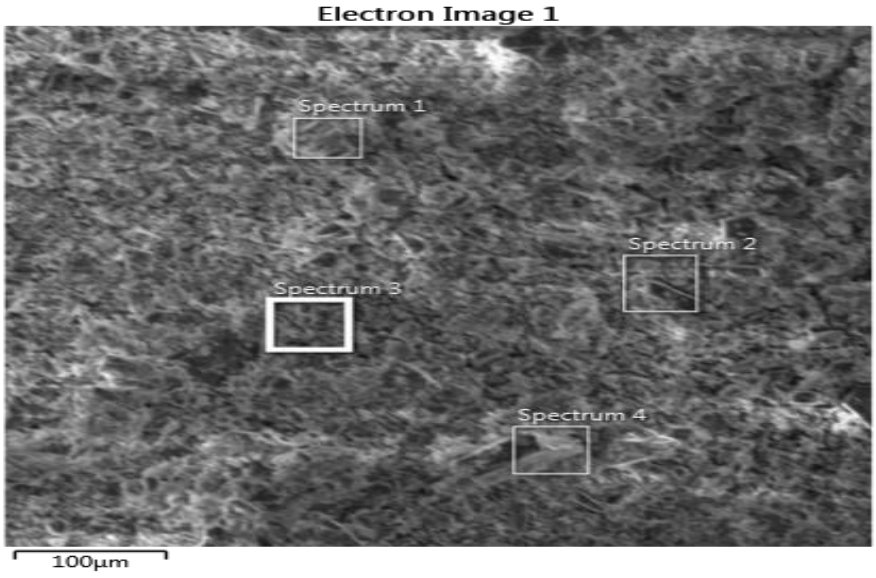

Fig (3-15) SEM of ZN2

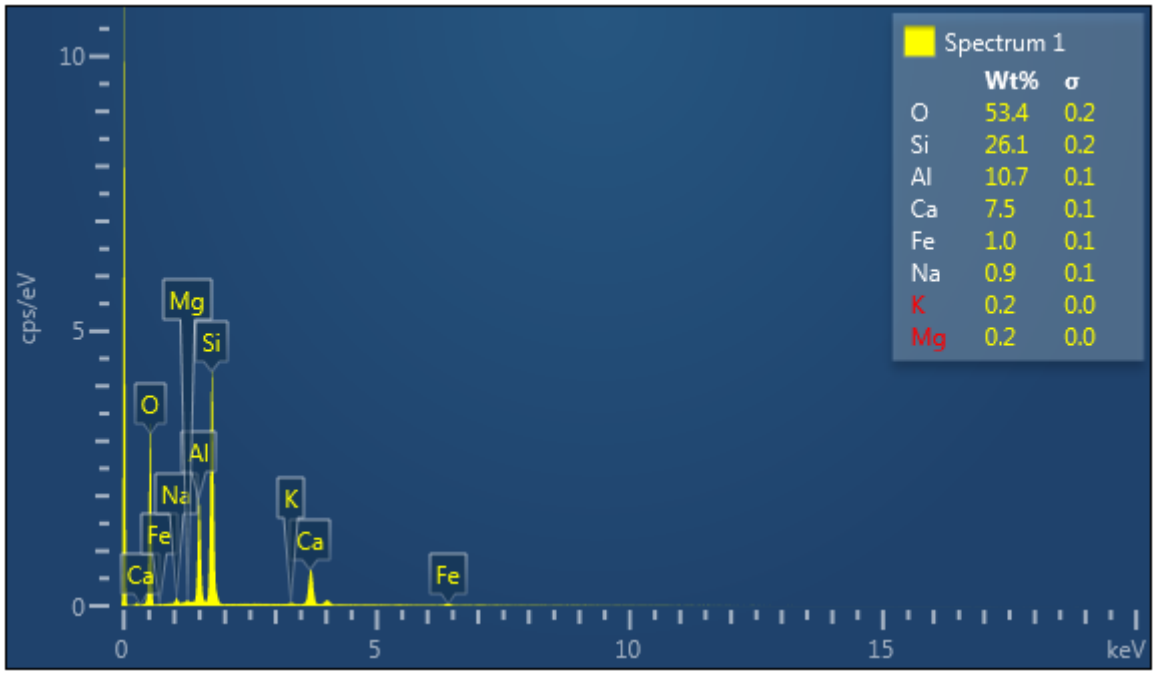

Fig (3-16) EDX of spectrum number one of ZN2

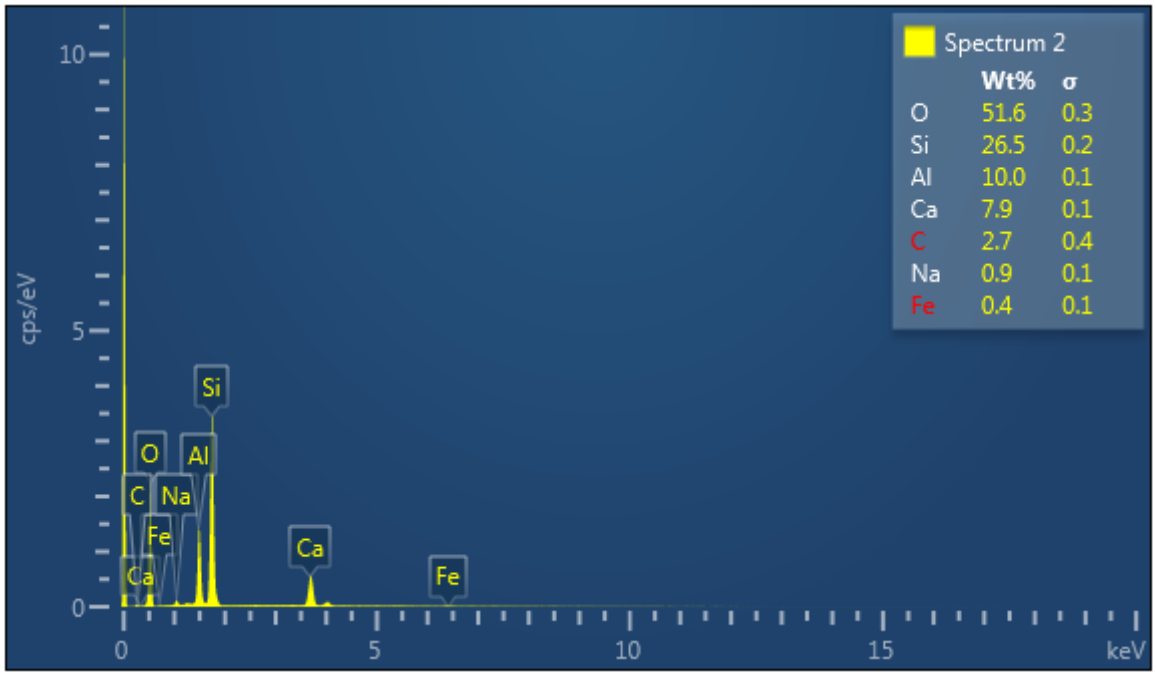

Fig (3-17) EDX spectrumnumber two of ZN2

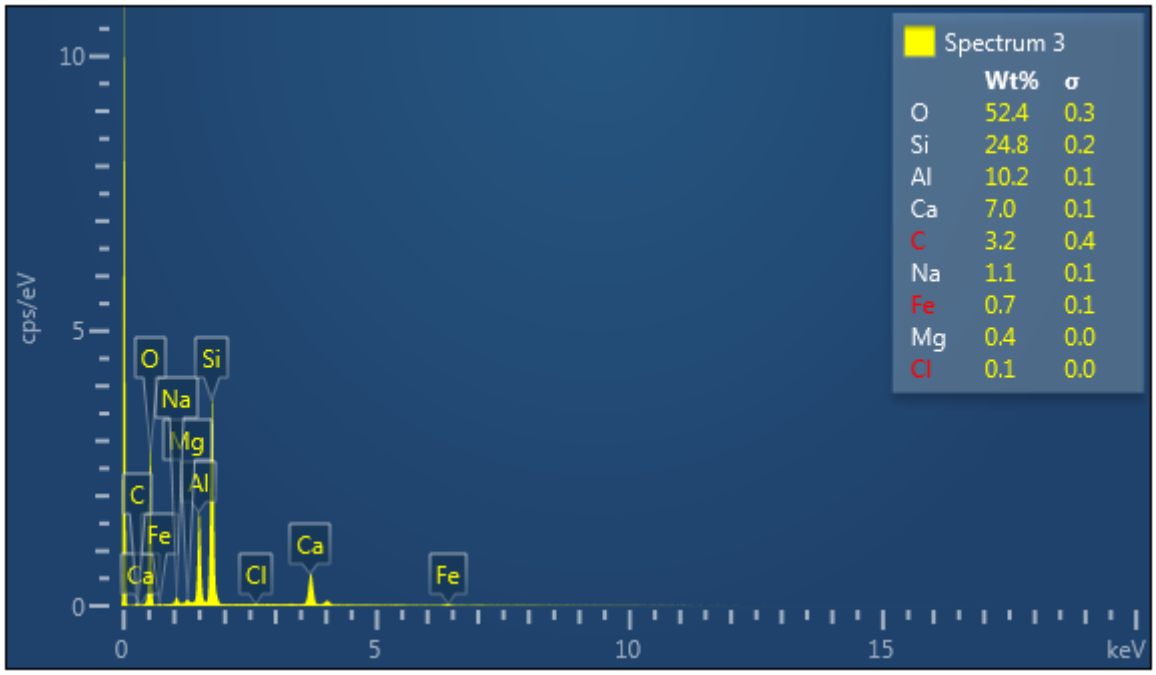

Fig (3-18) EDX spectrum number three of ZN2

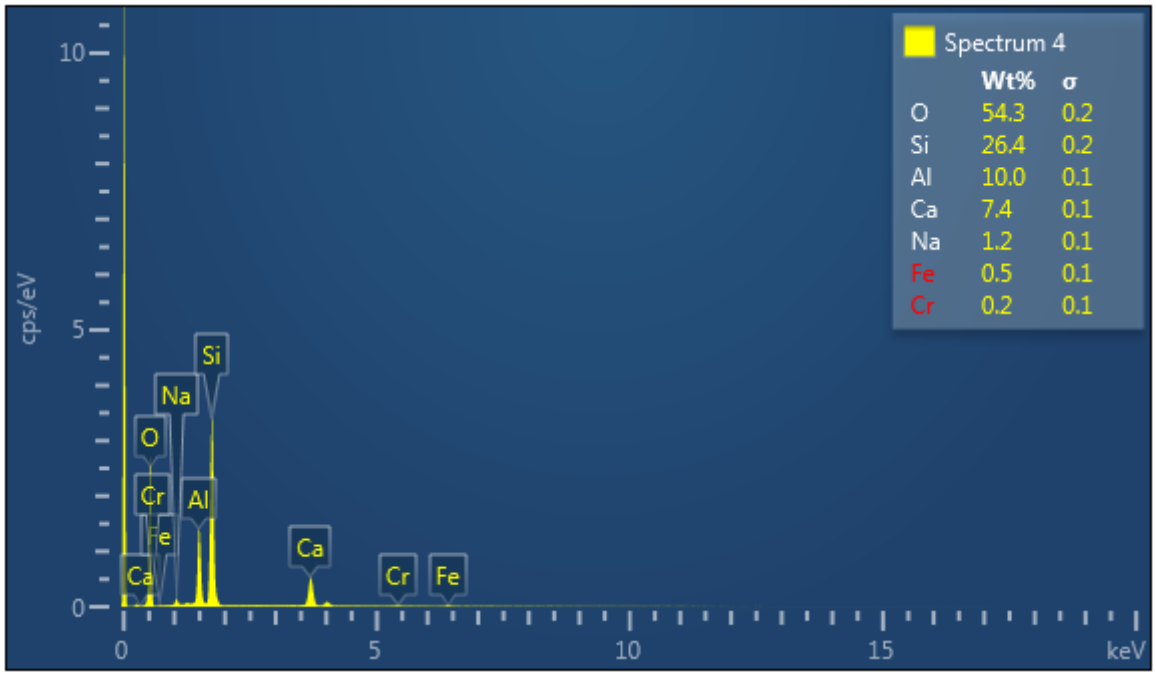

Fig (3-19) EDX spectrum number four of ZN2

The EDX spectrum of ZN2 Fig (3.16 – 3.19) show O, Si and Al are major component of ZN2 and percentage of Ca are constant among four spectrums.

The SEM micrograph of kaolin depicted in Fig (3-20- 3.24) provide good details regarding the morphology of the material. It also showed the presence of external surface area indicating the non-porosity or macro-porosity behavior of the Kaolin

material. The EDX spectra of these micrographs, which are illustrated in Fig (4), showed the presence of all elemental components of the Kaolin (O, Si, Al, Ca and Fe) with percentages consistent with the general chemical formula of the material.

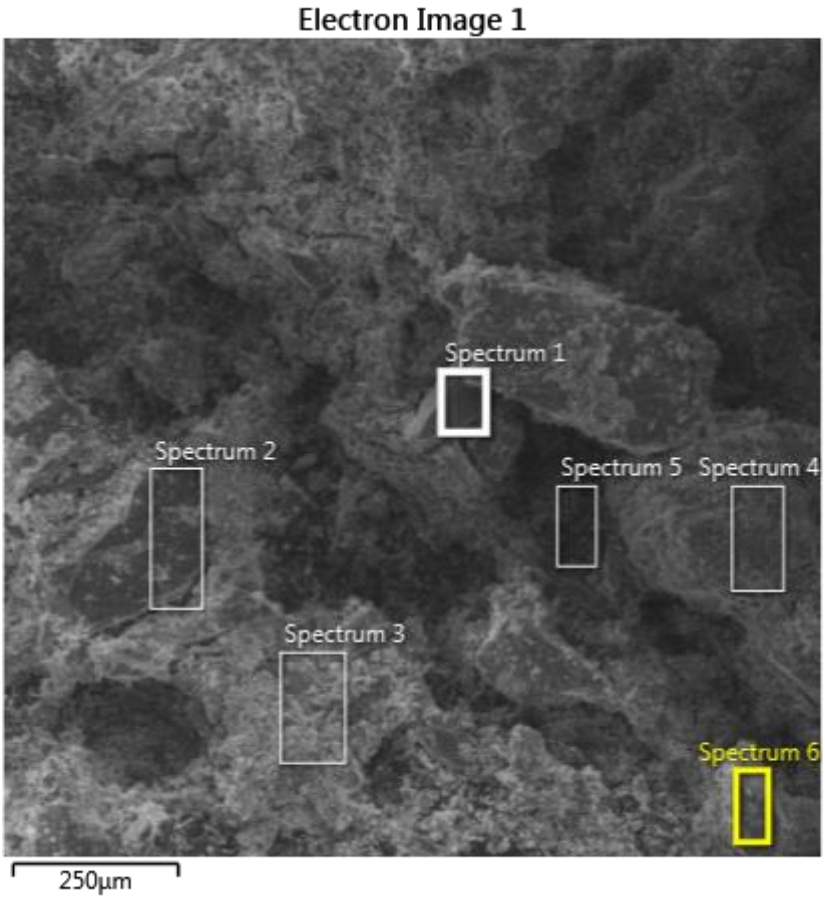

Fig (3-20) SEM of kaolin

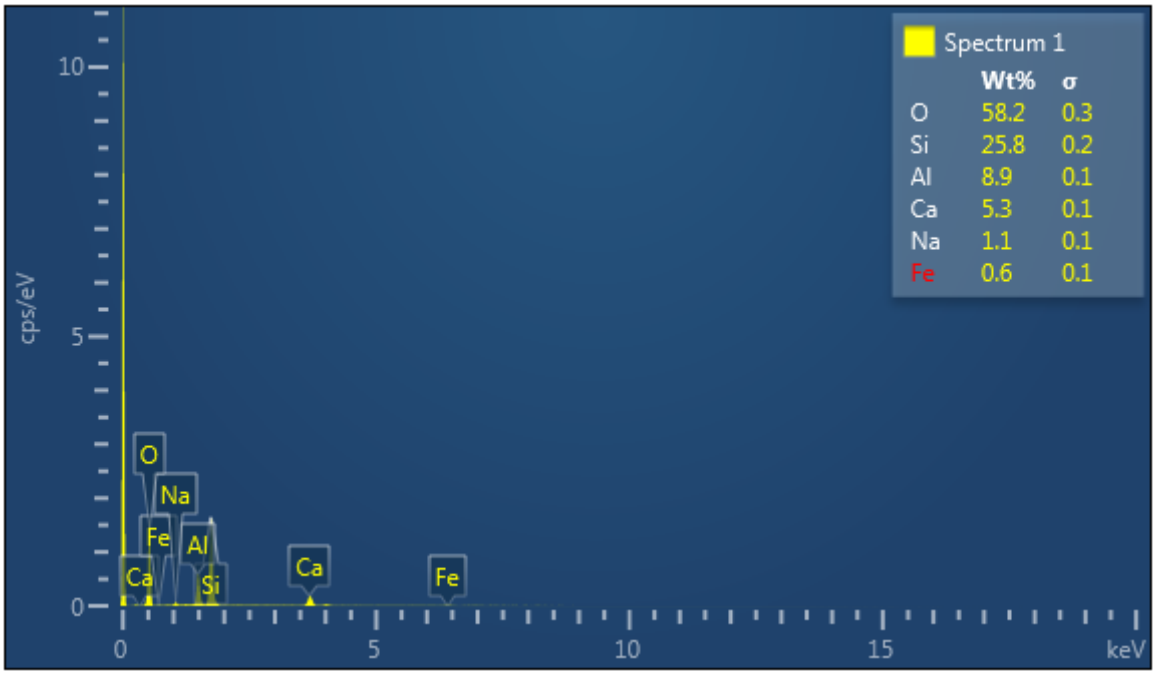

Fig (3-21) EDX spectrum number one of kaolin

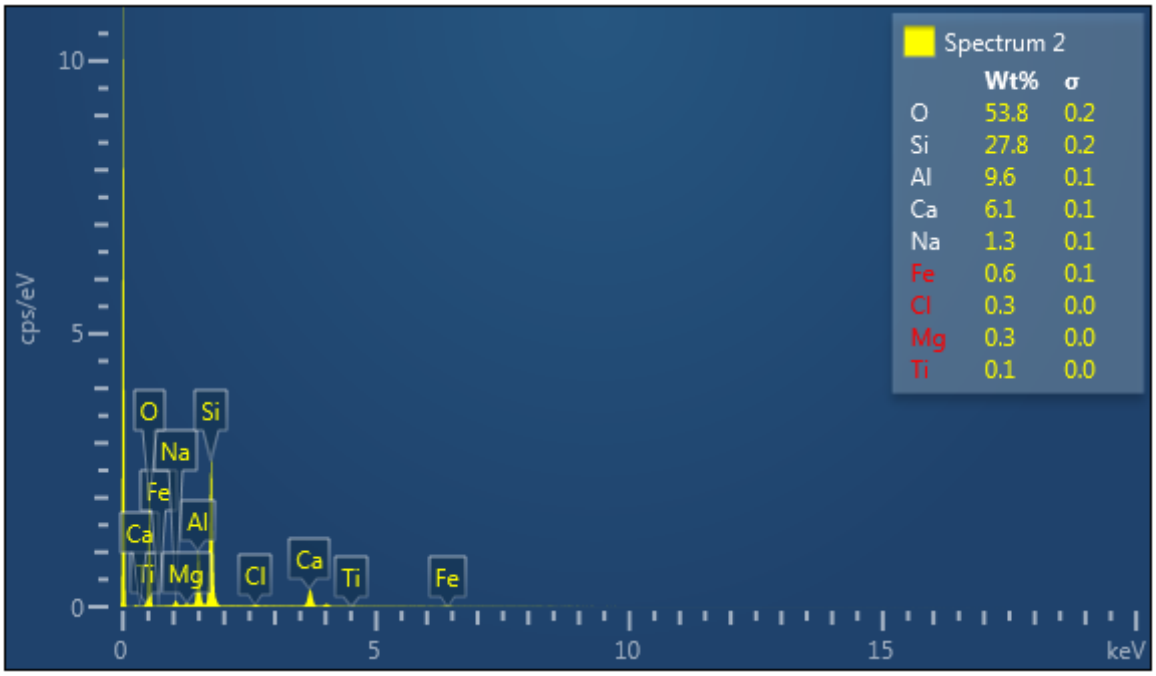

Fig (3-22) EDX spectrum number two of kaolin

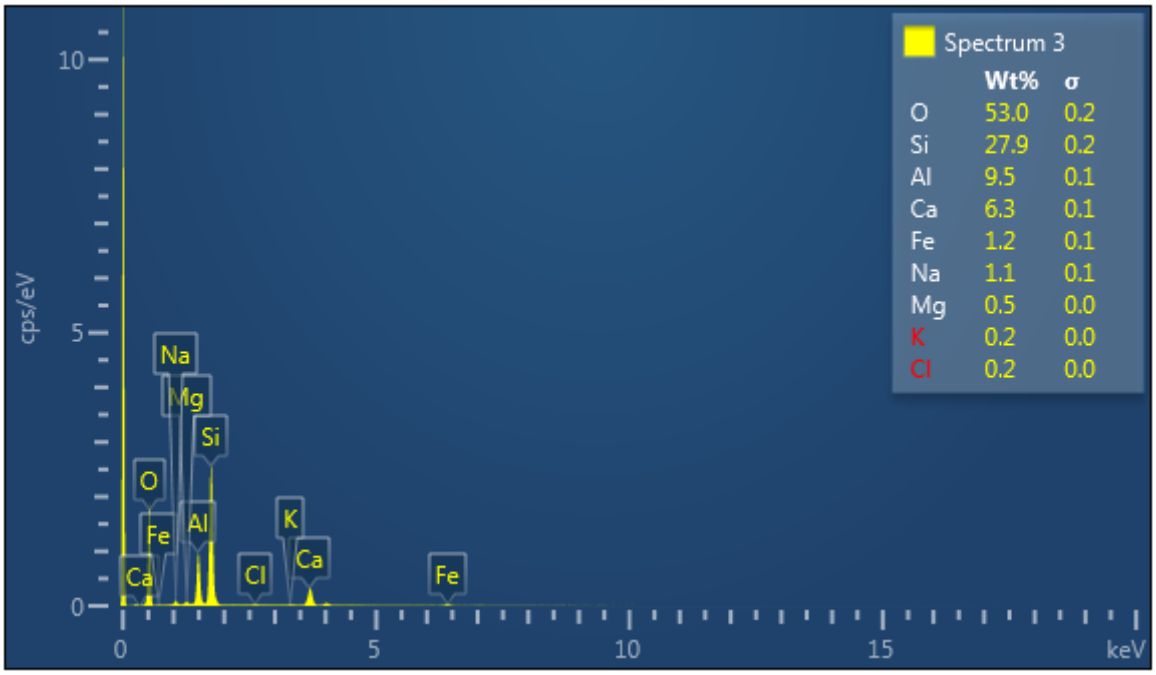

Fig (3-23) EDX spectrum number three of kaolin

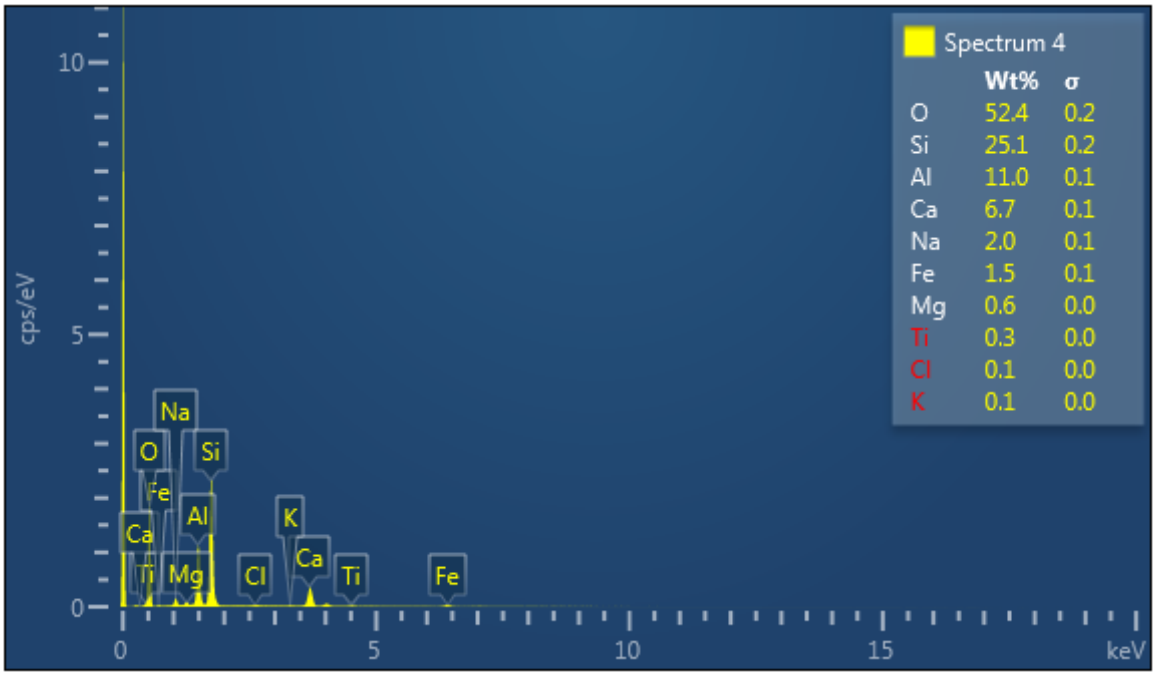

Fig (3-24) EDX spectrum four number of kaolin

3.3 Removal of heavy metals

To remove (Cr^{3+}, Co^{2+}, Zn^{2+} and Fe^{2+}) first from artificial solutions considering, suitable, parameters such as contact time and concentration (for Cr^{3+} only on ZN1 and ZN2), pH for of contain on ZN1 and ZN2).

However, used fluid mud solutions.

3.3.1 The effect of contact time

Time is very important factor for adsorption. The effect of contact time on the adsorption of Cr^{3+} on natural zeolites was investigated at different time intervals in range of 10 to 120 minutes, and the result are shown in Figures (3.25) and (3.26). The adsorption of Cr^{3+} has gradual increase with contact time until 40 minutes then the removal percent became constant (equilibrium is attained). Contact time started from 10 minutes.

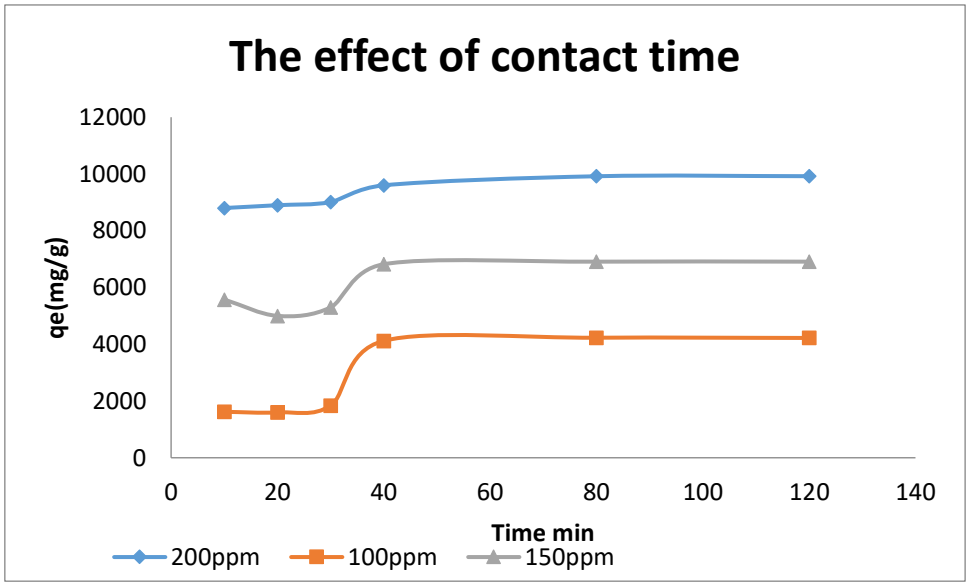

Fig (3-25) contact time of ZN2

The removal of Cr^{3+} was considerable after 40 min could be considered for optimum adsorption of Cr^{3+} on ZN1 and ZN2 sieve, the percentage removal was found to increase with increasing contact time, and attained the maximum value at 80 minutes, equilibrium started after this time, for ZN1 and ZN2 using Cr^{3+}

only, for concentrations the result shows that Cr^{3+} uptake of increases with increasing concentration of Cr^{3+} the maximum adsorption capacity is 200 ppm for ZN1 and ZN2. In addition most of following studies were carried out for one hour to five hours duration due to obtain the optimum equilibrium (Liu et al. 2013) and (Fornefett et al. 2016).

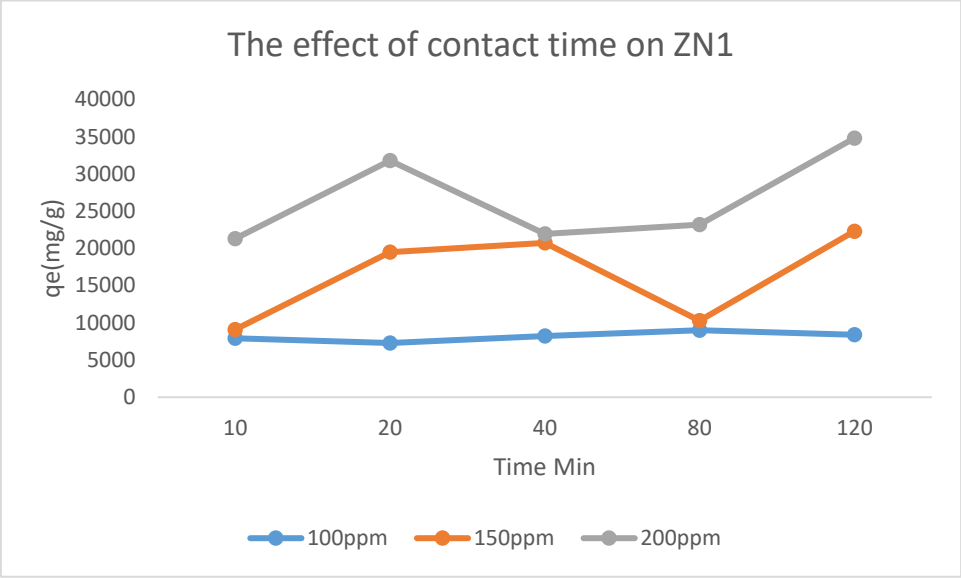

Fig (3-26) contact time of ZN1

3.3.2 The effect of pH

Acidity or basicity of solution, by pH is an important factor in the adsorption capacity of the adsorbent. The pH- dependence of adsorption processis due to the competition for the surface-active site between the metal and hydrogen ions in one side and consumption of the metal ions as metal hydroxide ion pairs or precipitations in another side of the pH scale (Fouladgar et al. 2015).

To study the effect of pH, solutions of (Cr^{3+}, Co^{2+}, Zn^{2+} and Fe^{2+}) prepared at different pH values ranging from 2 to 8, in order to determine the effect of pH on adsorption capacity of molecular sieve, at initial concentration of 200 ppm, it's evident that the adsorption capacity of Cr^{3+}, Co^{2+}, Zn^{2+} and Fe^{2+} on ZN1 and ZN2 affected by pH ranging from 2 to 8, as shown in Fig (3-27) and (3-28) respectively. adsorption capacities increase with increased solution pH, the optimum pH value appeared to be from 4.5 to 6 for Cr^{3+}, Co^{2+}, Zn^{2+} and Fe^{2+} removal.

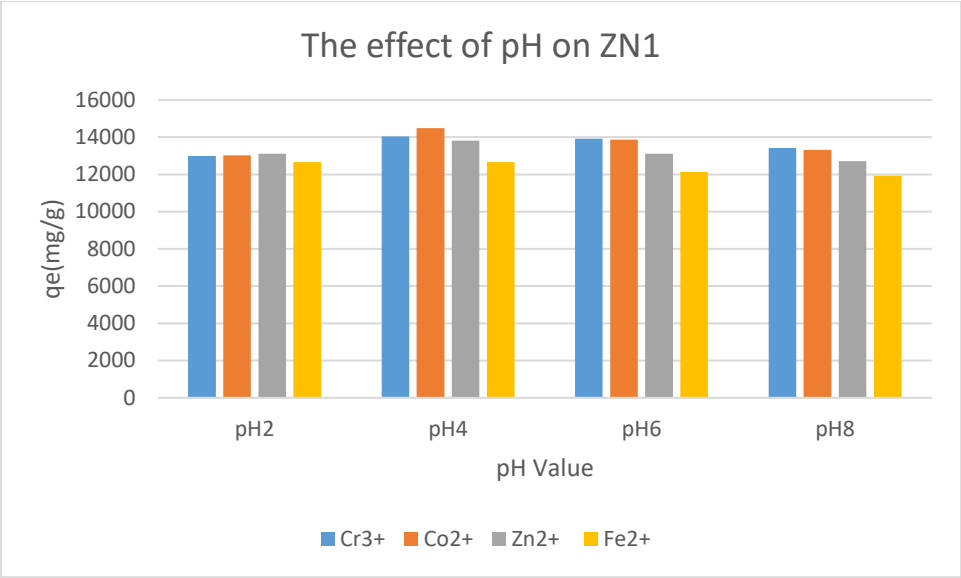

Fig (3-27) the effect of pHon ZN1

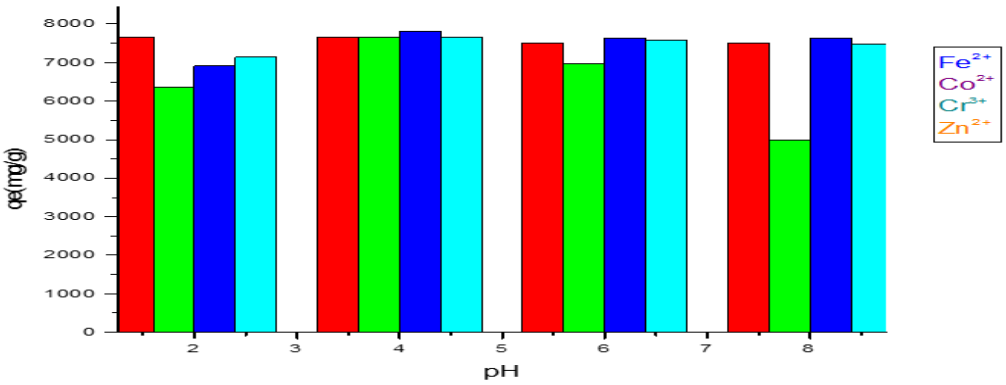

Fig (3-28) the effect of pHon ZN2

At lower pH (< 4.0) the for Cr^{3+}, Co^{2+}, Zn^{2+} and Fe^{2+} were free ions and hydrogen ions may have competed with ions for binding sites on the surface of adsorbent, (Zheng et al. 2000).

Some parameters interfere with adsorption mechanisms on to solid such as (electrostatic interaction, ion exchange, ion-dipole interaction, coordination by surface metal cation, hydrogen bonding and hydrophobic interaction. However, increasing ionic strength, as a consequence of addition of the base for pH adjustment, reduces the molar Gibbs free energy of the (hydrated) ions in solution, and decreases the electrostatic interactions between the cations in solution and the

alumina surface sites having negative charges, as well as increasing formation of [M^+, OH^-] ion-pair. Due to these bulk effects, the ions prefer to remain in solution, and thus, the removal efficiencies for both ions are expected to decrease ionic strength of the solution increases. At the same time, increasing [OH^-] concentration results in two chemical effects: first, adsorption of more OH^- on the positively charged Aluminum sites of the zeolite surfaces which results in a change in the nature of the surface and alters its tendency for absorption of ions, and second, displacement of the solubility equilibrium The relative contributions of each of the four processes described above on the removal efficiency depend on the nature of the metal M (i.e. its solution thermochemistry which depends on its interactions with the solvent molecules (Fouladgar et al. 2015).

3.4 Adsorption isotherms

Equilibrium data, Table 3.3. and 3.4 show the adsorption isotherms, are basic requirements for the design of adsorption systems. The uptake of each metal species increases with the initial metal concentration while the metal-removal efficiency decreased which was known as the loading effect, describing the extent to which the total number of sorption sites is occupied by the sorbate, Freundlich and Langmuir adsorption isotherms of (Cr^{3+}, Co^{2+}, Zn^{2+} and Fe^{2+}) ions obtained at the concentration (100 to 500ppm) at room temperature, Table (3-3) and (3-4).

This implies that (Cr^{3+} , Co^{2+} , Zn^{2+} and Fe^{2+}) is more like a monolayer adsorption process with heterogeneous distribution adsorption to be satisfactory when the value of Freundilch constant (n) is between 1 to 10. The findings illustrated that natural zeolites fit well with Freundlich isotherm, whereas that Synthesized zeolite obeyed Langmuir isotherm. For Kaolin, the result implies that the adsorption mechanism of Cr^{3+}, Co^{2+}, Zn^{2+} and Fe^{2+} could be described through formation of monolayer of metal ions on kaolin with heterogeneous distribution of adsorption, the result showed that the adsorption process of both Cr^{3+} and Zn^{2+} fit well with Fruendlich model and equilibrium adsorption capacity could be improved by increasing their concentration in the aqueous solution. The maximum capacity of

adsorbent (mg/g) (Q_{max}), and K_L is the Langmuir adsorption constant (L/mg). Cr^{3+}in ZN1 obtained high value of (Q_{max}) about (475 mg/g) with R^2 0.991.

	Metals	K(mg/g)	n	R^2
ZN1	Cr^{+3}	0.291	1.2	0.979
	Co^{2+}	0.65	3.46	0.926
	Zn^{2+}	1.19	5.64	0.883
	Fe^{2+}	1.09	7.98	0.982
ZN2	Cr^{+3}	0.13	2.69	0.756
	Co^{2+}	0.86	13.65	0.941
	Zn^{2+}	1.1	4.54	0.942
	Fe^{2+}	1.08	10.78	0.864
Ka	Cr^{+3}	1.39	2.67	0.951
	Co^{2+}	1.03	9.33	0.951
	Zn^{2+}	0.34	1.14	0.833
	Fe^{2+}	1.74	3.06	0.783
SZ	Cr^{+3}	3.69	0.36	0.759
	Co^{2+}	2.46	0.88	0.887
	Zn^{2+}	1.61	0.94	0.805
	Fe^{2+}	0.67	0.84	0.995

Table (3-5) Freundlich isotherms

n= slope, k= intercept

Table (3-6) Langmiur isotherm

	Metals	Q_{Max}(mg/g)	K(l/g)	R^2
ZN1	Cr^{3+}	475	0.007	0.991
	Co^{2+}	16.16	0.135	0.844
	Zn^{2+}	3.7	0.26	0.753
	Fe^{2+}	3.6	0.4	0.891
ZN2	Cr^{3+}	57.1	-0.072	0.531
	Co^{2+}	5.8	0.44	0.982
	Zn^{2+}	4.9	0.2	0.842
	Fe^{2+}	4.5	0.34	0.906
Ka	Cr^{3+}	3.8	0.011	0.891
	Co^{2+}	5.2	2.84	0.734
	Zn^{2+}	2.85	0.18	0.708
	Fe^{2+}	5.5	0.007	0.851
SZ	Cr^{3+}	37.9	0.184	0.759
	Co^{2+}	110.6	2.64	0.887
	Zn^{2+}	262.1	0.15	0.924
	Fe^{2+}	149	0.023	0.998

n= slope, k= intercept

Table (3-7) observe the mechanisms of adsorption (Zhou 2006)

R^2 Value	Type of isotherms
$R^2 > 1$	Unfavorable
$R^2 = 1$	Linear
$0 < R^2 < 1$	Favorable
$R^2 = 0$	Irrevesible

3.5 Removal of heavy metals from drilling fluid water

The water of drilling fluid waste is rich of heavy metals such as (Cr^{3+}, Co^{2+}, Zn^{2+}, Fe^{2+}, Cd^{2+}, Hg^{2+}, Pb^{2+} and others).Is useing two kind of natural zeolite, natural kaolin and synthesized zeolite to remove heavy metals at room temperature, for 80 minutes, pH 5, and ratio of solid liquid about 1:100.

Synthesize zeolite show Excellent efficiency for the removal of heavy metals (99%, 97%, 98% and 80%) respectively for (Cr^{3+}, Co^{2+}, Zn^{2+} and Fe^{2+}), however ZN1 and ka have low average uptake, about 66.6%, 80%, 50% and 77 for ZN2, whereas ka has uptake 72.8%, 78.6%, 77.9% and 34%, respectively for ((Cr^{3+}, Co^{2+}, Zn^{2+} and Fe^{2+}), table (3-6) summary of heavy metals removal.

Table (3-8) removal of metal ions using zeolites and kaolin

	Cr^{3+}	**Co^{2+}**	**Zn^{2+}**	**Fe^{2+}**
ZN1	**66.6%**	**80%**	**50%**	**77%**
ZN2	**83.8%**	**96.8%**	**38.4%**	**38.3%**
SZ	**99%**	**97%**	**98%**	**80%**
Ka	**72.8%**	**78.6%**	**77.9%**	**39%**

The adsorption depend on metal charge and size as well as broad distribution of pore size of adsorbent, on the other hand Cobalt competes other ions, this different

solid indicat. In addition metals ions appear in solution as ion hydrate, cobalte ion have small hydrated size about 4.23A° having high resoponse to adsorpe first through porous (Nightingale 1959).

In multi-ion system sorption of ions, gradually, decreases with increasing concentration of ions in the solution. The removal of heavy metals increased with the increase in the specific surface area of zeolite, this is attributed to the availability of a greater number of sorption sites for heavy metals bonding. However, some studies have reported that the increase in specific surface area does not necessarily increase sorption, the specific surface area of porous materials such as zeolite can be divided into the external and internal specific surface areas. The internal specific surface area is governed by the size and distribution of pores; the findings show synthesized zeolite have high capacity attributed to high surface area about (40.317 mg/g).

Table (3-9) adsorption process with other studies

Zeolite type	**Selectivety**	**References**
Clinoptilolitic	$Pb^{2+} > Cd^{2+} > Zn^{2+}$	(Minceva et al. 2007)
Clinoptilolite	$Co^{2+} > Cu^{2+} > Zn^{2+} > Mn^{2+}$	(Erdem et al. 2004)
Modyfite Clinoptilolite	$Cd^{2+} > Pb^{2+} > Cu^{2+} > Zn^{2+}$	Jia Wen et al, 2016
Zeolite X	$Cu^{2+} > Zn^{2+}$	(Wang et al. 2009)
stablite	$Co^{2+} > Cr^{3+} > Zn^{2+} > Fe^{2+}$	Present study
Stellerite	$Co^{2+} > Cr^{3+} > Zn^{2+} > Fe^{2+}$	Present study
Synthesis zeolite	$Cr^{3+} > Zn^{2+} > Co^{2+} > Fe^{2+}$	Present study
Kaolin	$Co^{2+} > Zn^{2+} > Cr^{3+} > Fe^{2+}$	Present study

3.6 Conclusions

Oil industry has a harmful effect on environment, especially drilling fluids, which assists the drilling operation, however some metals dissolve in the drilling solution, it contains hazardous materials, such as heavy metals and radioactive metals. The present study focused to remove some heavy metals such as (Cr^{3+}, Co^{2+}, Zn^{2+} and Fe^{2+}) from drilling mud fluids by natural, synthesized zeolites and kaolin since infield processes concentrate only on biodegradable treatment. Zeolites, natural or synthesized, and kaolin are important low cost materials for water and waste water treatment due to their high ion exchange capacity and high performance adsorption of cations in aqueous solution.

Natural zeolites converted to Na-zeolite by soaking in sodium chloride solution. Synthesized zeolite made from fly ash and kaolin without modification. Instrumental techniques were used to characterize zeolites and kaolin.

The study was conducted at different conditions such as pH, contact time and concentrations, were optimized for high removal efficiency for artificial solutions of (Cr^{3+}, Co^{2+}, Zn^{2+} and Fe^{2+}). The percentage removal was found to increase with increasing contact time, and attained the maximum value at 80 minutes, equilibrium started after this time, for ZN1 and ZN2 used Cr^{3+} only, for concentrations the result shown the uptake of Cr^{3+} increase with increasing initial concentration of Cr^{3+} the maximum adsorption capacity of 200 ppm for ZN1 and ZN2. The effect of pH value on the adsorption of (Cr^{3+}, Co^{2+}, Zn^{2+} and Fe^{2+}) on ZN1 and ZN2 was determined by stirred 200ppm of standards aqueous solutions at 80 min and contestant temperature, the result indicate that the increase of adsorption increasing of pH value, the maximum adsorption capacity found between 4 to 6 at pH value.

The optimization parameters used to remove (Cr^{3+}, Co^{2+}, Zn^{2+} and Fe^{2+}) from mud drilling solution by ZN1, ZN2, SZ and Ka.

. The selectivity of removing found in ZN1 $Co^{2+} > Cr^{3+} > Zn^{2+} > Fe^{2+}$ for ZN2 $Co^{2+} > Cr^{3+} > Zn^{2+} > Fe^{2+}$ for SZ $Cr^{3+} > Zn^{2+} > Co^{2+} > Fe^{2+}$ and for Ka was $Co^{2+} > Zn^{2+} > Cr^{3+} > Fe^{2+}$. synthesized zeolite showed high efficiency for removing (Cr^{3+}, Co^{2+}, Zn^{2+} and Fe^{2+}) from mud drilling solution according to its surface area.

In addition, the equilibrium data fit well to Fruendlich and Langmuir models. Zeolites and kaolin were shown high affinity to remove (Cr^{3+}, Co^{2+}, Zn^{2+} and Fe^{2+}) from aqueous solutions.

3.7 Recommendation

1/ Using zeolites and kaolin as low cost materials for water purification.

2/ Choosing zeolites and kaolin as starter material for synthesis nano composite materials under hydrothermal conditions.

3/ Characterization of zeolites and kaolin samples by advanced technique such as Nuclear magnetic resonance (NMR), transition electron microscope (TEM) and Thermogravimetric analysis (TGA).

4/ Synthesis of zeolite from waste garbage.

5/ Assessment of physio-chemical properties of ground water around oil field periodically.

6/ Provide zeolites and kaolin as efficient catalysis due to size and pore size.

7/ Mapping and survey of natural zeolite in Sudan.

References

Afkhami, F. et al. (2013) Impact of oil excavation activities on soil metallic pollution, case study of an Iran southern oil field. *Environmental Earth Sciences*, 70(3), pp.1219–1224.

Akimkhan, A.M. (2012) Structural and Ion-Exchange Properties of Natural Zeolite. *Ion Exchange Technologies*.

Anthony R. West (2014) *Solid State Chemistry* second., New Delhi, India: wiley.

Asnaoui, H., Laaziri, A. and Khalis, M., 2015. Study of the kinetics and the adsorption isotherm of cadmium(II) from aqueous solution using green algae (Ulva lactuca) biomass. *Water Science and Technology*, 72(9).

Auerbach, M. (2003) *Zeolite Science and it`s technology*, NewYork: Marcel Dekker, Inc.

Bein, T, M. (2005). Advanced applications of zeolites. *Studies in Surface Science and Catalysis*, pp.263–288.

Cejka, J. et al. (2007). *Studies in Surface Science and Catalysis 168: Introduction to Zeolite science and practice*,

Colella, C. (2005). Zeolites and Ordered Mesoporous Materials: Progress and Prospects. *Studies in Surface Science and Catalysis*, 157, pp.13–40.

Corma, A. and Martinez, A. (2005). Zeolites in refining and petrochemistry. *Studies in Surface Science and Catalysis*, vol 3.

Duong D. Do. (1998). *Adsorption analysis eqilibera and Kinetics* First Edit., London: Emerical collge press.

Dyer, A. (2005). Ion-exchange properties of zeolites. *Studies in Surface Science and Catalysis*, vol 157, pp.181–204.

Elbrir. Fatima A, Yasin. Sahl, A.M., 2015. The removal of some metals by natural and modified zeolite from oilfield produced water. , 2(7), pp.57–62.

Englert, A.H. and Rubio, J., 2005. Characterization and environmental application of a Chilean natural zeolite. , 75, pp.21–29.

Erdem, E., Karapinar, N. and Donat, R. (2004). The removal of heavy metal cations by natural zeolites. *Journal of Colloid and Interface Science*, (2).309–314.

Fansuri, H., Pritchard, D. and Zhang, D. (2008). Manufacture off low-grade zeolites from fly ash for fertlliser appllications research report 91 Authors : Muresk Institute , Curtin University of Technology.

Flanigen, E.M., Broach, R.W. and Wilson, S.T. (2010). Histry of zeolite. *wiley-Netherland*.

Fornefett, I. et al. (2016). Adsorption of sucrose on zeolites. *Green Chem.*, 18(11),3378–3388.

Fouladgar, M., Beheshti, M. and Sabzyan, H., 2015. Single and binary adsorption of nickel and copper from aqueous solutions by -alumina nanoparticles: Equilibrium and kinetic modeling. *Journal of Molecular Liquids* (2) .1060–1073.

Gougazeh, M. and Buhl, J.C. (2014). Synthesis and characterization of zeolite A by hydrothermal transformation of natural Jordanian kaolin. *Journal of the*

Association of Arab Universities for Basic and Applied Sciences, 15(1),35–42.

Hou, J., Yuan, J. and Shang, R. (2012). Synthesis and characterization of zeolite W and its ion-exchange properties to K^+ in seawater. *Powder Technology*, 226,222–224.

Hu, K. et al. (2012). Novel Sequential Treatment Methodology for Disposal of Water-Based Waste Drilling Mud. *Environmental Engineering Science*, 29(7),669–676.

Ibrahim, H.S., Jamil, T.S. and Hegazy, E.Z. (2010). Application of zeolite prepared from Egyptian kaolin for the removal of heavy metals: II. Isotherm models. *Journal of Hazardous Materials*, (182), 842–847.

Kazemimoghadam, M. (2010). New nanopore zeolite membranes for water treatment. *Desalination*, (13), 176–180.

Kheiralla, K.M., Mohamed, N.E. and Ibrahim, A.E. (2012). Reservoir characterization using multi geophysical data for Cretaceous sediments in the Shelungo Oil Field, Muglad Rift Basin, Sudan. *Comunicacoes Geologicas*, (2), 5–11.

Kim, S.J. et al. (2015). Ion exchange of zeolite membranes by a vacuum "flow-through" technique. *Microporous and Mesoporous Materials*, (4), 170–177.

Kokotailo, G.T. and Fyfe, C.A. (1995). Zeolite Structure Analysis With Powder X-Ray Diffraction and Solid-State Nmr Techniques. (1), 3–10.

Lirong, D. et al. (2013). Petroleum geology of the fula sub-basin, Muglad basin, Sudan. *Journal of Petroleum Geology*, 36(1), 43–59.

Liu, M. et al. (2013). Applied Surface Science Synthesis , characterization , and mercury adsorption properties of hybrid mesoporous aluminosilicate sieve prepared with fly ash. *Applied Surface Science*, 273, 706–716.

M.A, E., (1999). Occurence and chcracrtization of kaolin deposits in the Sudan. *Journal of Khartoum University*, (1).

Makeen, Y.M. et al. (2015). Organic geochemical characteristics of the Lower Cretaceous Abu Gabra Formation in the Great Moga oilfield , Muglad Basin , Sudan : Implications for depositional environment and oil-generation potential. *Journal of African Earth Sciences*, (103),102–112.

Malekian, R. et al. (2011). Ion-exchange process for ammonium removal and release using natural Iranian zeolite. *Applied Clay Science*, 51(3), 323–329.

Matłok, M., Petrus, R. and Warchoł, J.K., (2015). Equilibrium Study of Heavy Metals Adsorption on Kaolin. *Industrial & Engineering Chemistry Research*, 54,6975–6984.

Minceva, M., Markovska, L. and Meshko, V. (2007). removal of Zn^{2+} , Cd^{2+} and Pb^{2+} from binary aqueous solution by natural zeolite and granulated activated carbon. *Macedonian Journal of Chemistry and Chemical Engineering*, 26(2), 125–134.

Mohamed, R.M., Mkhalid, I.A. and Barakat, M.A. (2015). Rice husk ash as a renewable source for the production of zeolite NaY and its characterization. *Arabian Journal of Chemistry*, (1), 48–53.

Munthali, M.W. et al., (2014). Proton adsorption selectivity of zeolites in

aqueous media: Effect of Si/Al ratio of zeolites. *Molecules*, (12), 20468–20481.
Neimark, A. V, Ravikovitch, P.I. and Vishnyakov, A. (2000). Adsorption hysteresis in nanopores. (2),1493–1496.
Nightingale, E.R. (1959). Phenomenological Theory of Ion Solvation. Effective Radii of Hydrated Ions. *Journal of Physical Chemistry*,(9),1381–1387.
Olaremu, A. (2015). Physico-Chemical Characterization of Akoko Mined Kaolin Clay. *Journal of minerals and materials characterization and Engineering*.353–361.
Oliveira, C.R. and Rubio, J. (2007). New basis for adsorption of ionic pollutants onto modified zeolites. *Minerals Engineering*,(6), 552–558.
Panda, A.K. et al. (2010). Effect of sulphuric acid treatment on the physico-chemical characteristics of kaolin clay. *Colloids and Surfaces A: Physicochemical and Engineering Aspects*,(13) 98–104.
Pandey, P. et al. (2009). Batch Adsorption Studies for the Removal of Cu (II) Ions by ZeoliteNaX from Aqueous Stream. *Proceedings of the World Congress on Engineering and Computer Science*, (2),20–22.
Rouquerol Francoise, R.L. and S.K. (1999). *Adsorption by Powders and porous solids, principle, methodology and application*, France. Academic press.
Ruen-ngam, D. et al. (2009). Zeolite formation from coal fly ash and its adsorption potential. *Journal of the Air and Waste Management Association*, (10),1140–1147.
Shaw, R. et al. (2016). Surface Engineered Zeolite: An Active Interface for Rapid Adsorption and Degradation of Toxic Contaminants in Water. *ACS Applied Materials and Interfaces*, (19), 12520–12527.
Sing, K. and Evertt, D. (1985). international union of pure commission on colloid and surface chemistry including catalysis reporting physisorption data for gas/ solid system with Special Reference to the Determination of Surface Area and Porosity. (4), 603–619.
Tataurova, Y. et al. (2012). Surface-selective solution NMR studies of functionalized zeolite nanoparticles. *Journal of Physical Chemistry Letters*, (3), 425–429.
Treacy, M.M.J. and Higgins, J.B. (2001). Collection of simulated XRD powder patterns for zeolites. *Elsevier*, .13-20.
WANG, C. et al. (2009). Evaluation of zeolites synthesized from fly ash as potential adsorbents for wastewater containing heavy metals. *Journal of Environmental Sciences*,(1), 127–136.
Wang, S.and Peng, Y. (2010). Natural zeolites as effective adsorbents in water and wastewater treatment. *Chemical Engineering Journal*,(1), 11–24.
Zheng, S. et al. (2000). Synthesis, characterization and photocatalytic properties of titania-modified mesoporous silicate MCM-41. *J. Mater. Chem.*,(3),723--727.
Zhou, L. (2006). *Adsorption - Progress in fundamental and application research*,

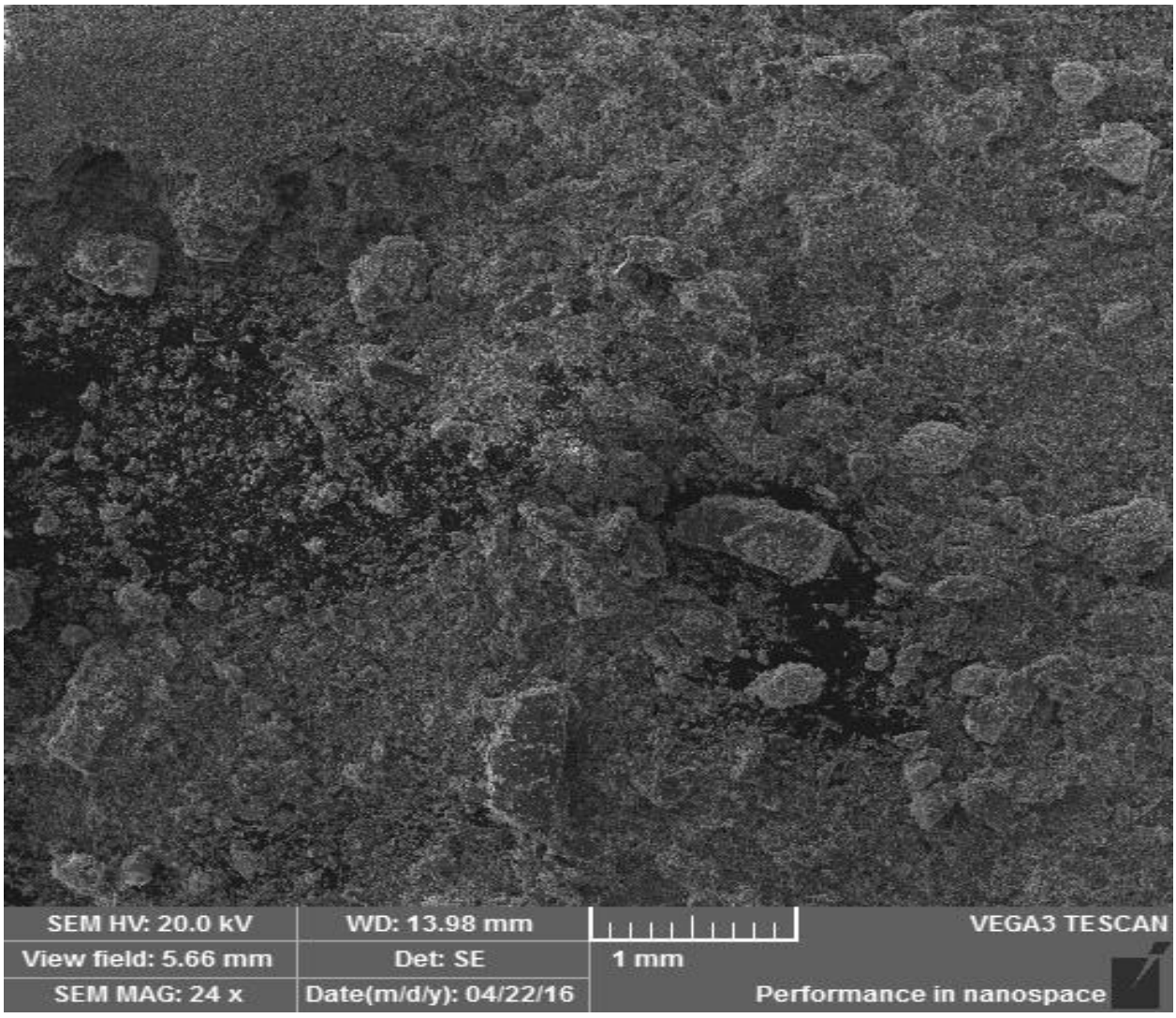

Fig (5-1) ZN1 magnification 24 time

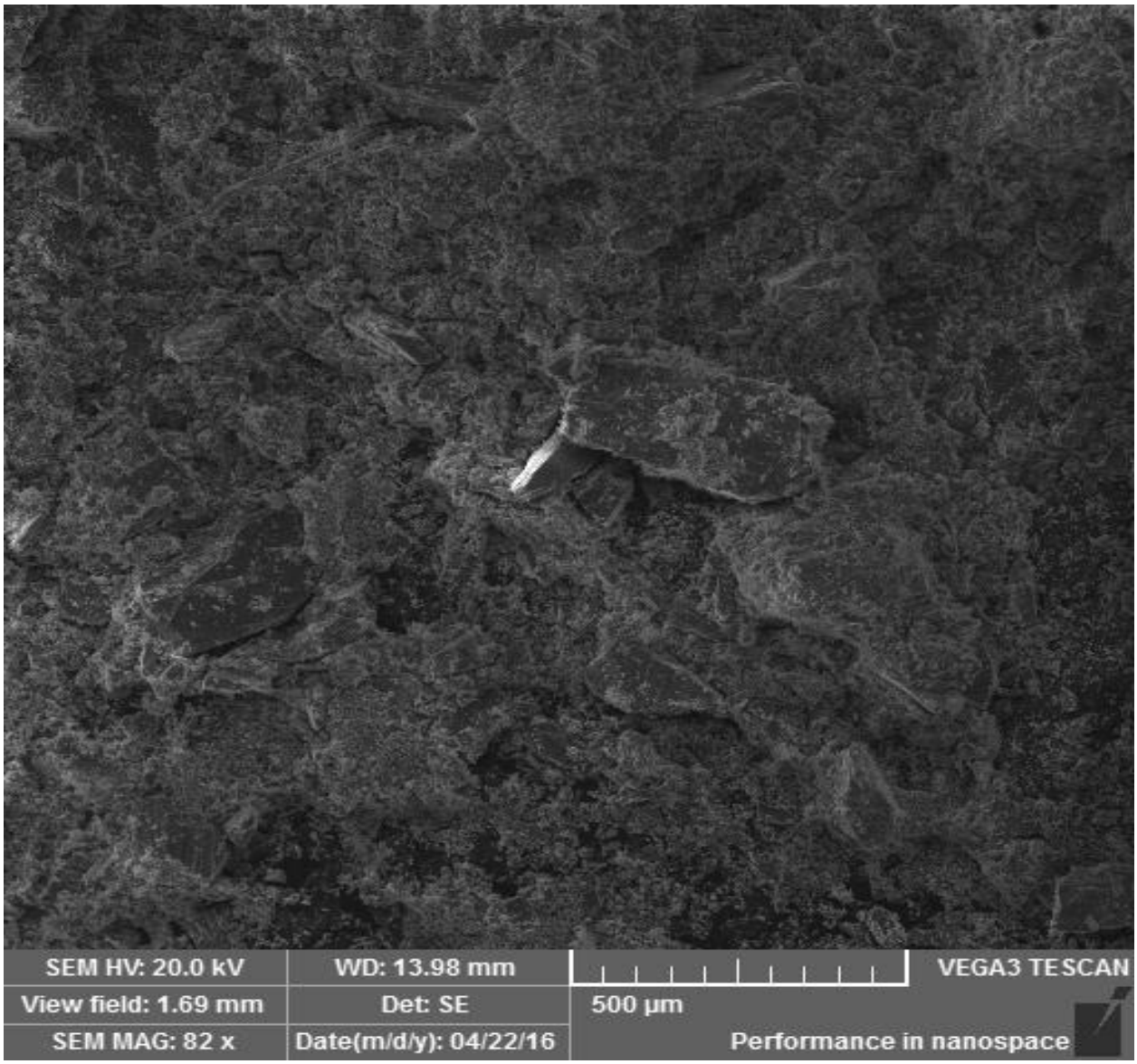

Fig (5-2) ZN1 magnification 82 time

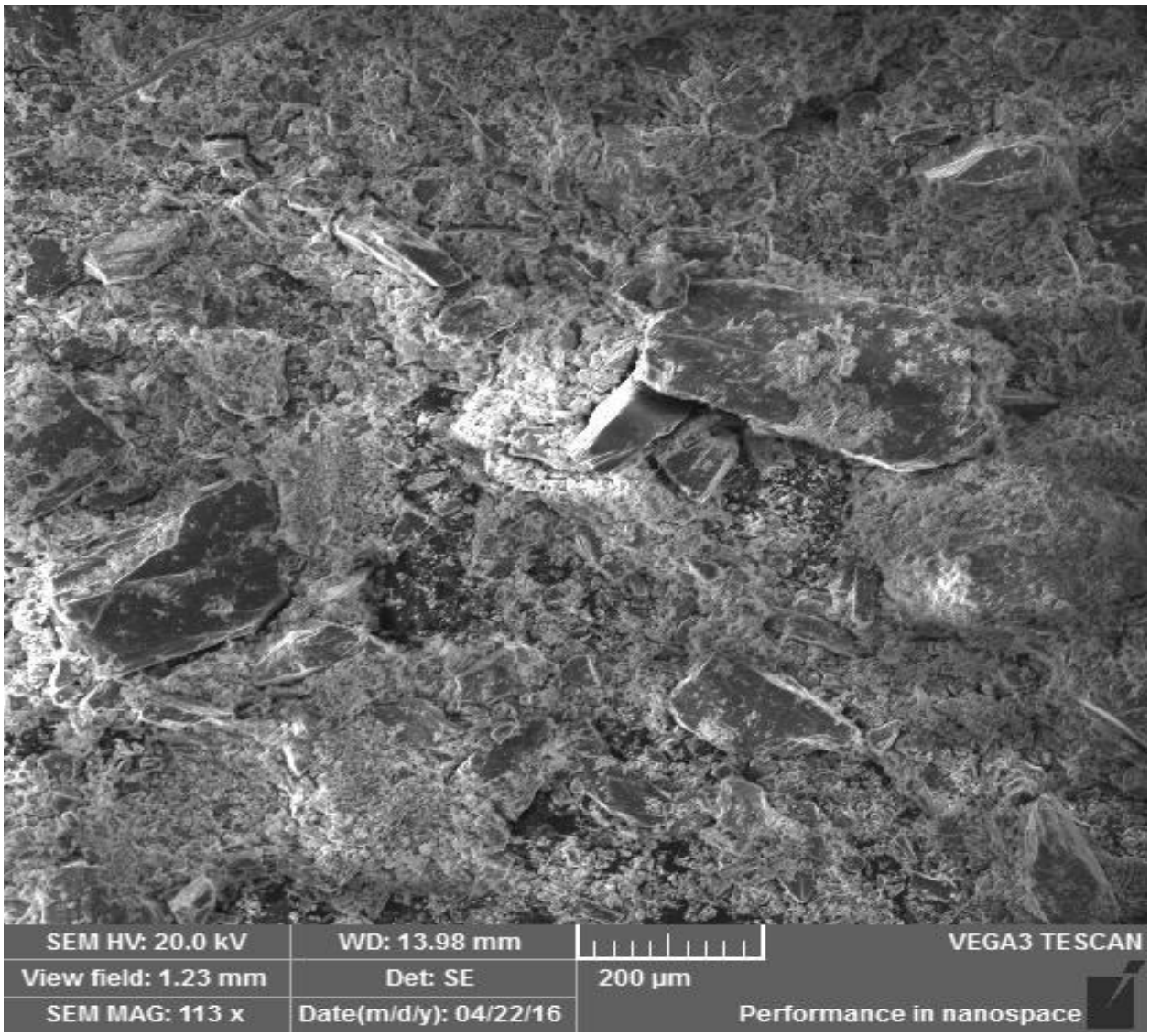

Fig (5-3) ZN1 magnification 113 time

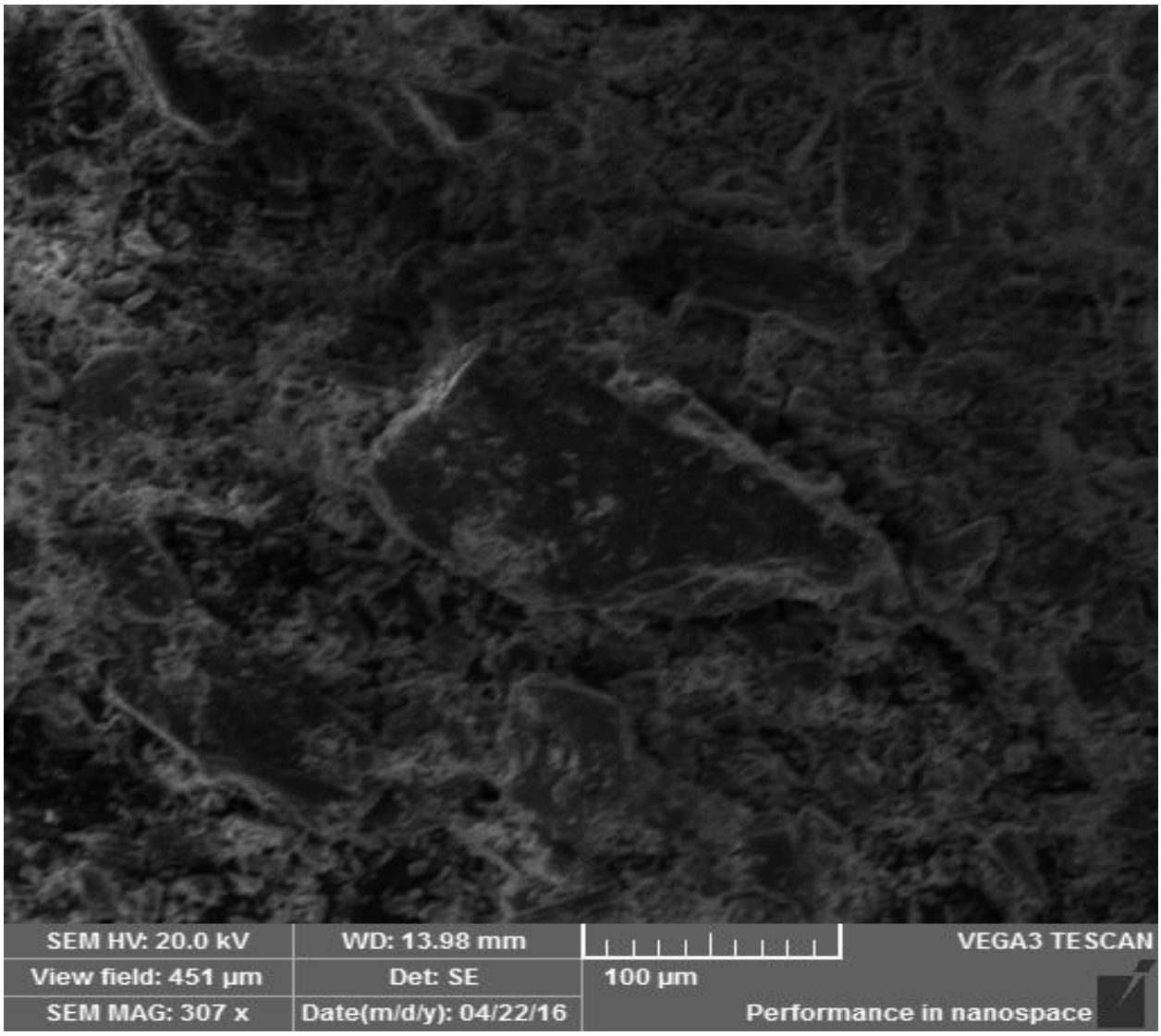

Fig (5-4) ZN1 magnification 307 time

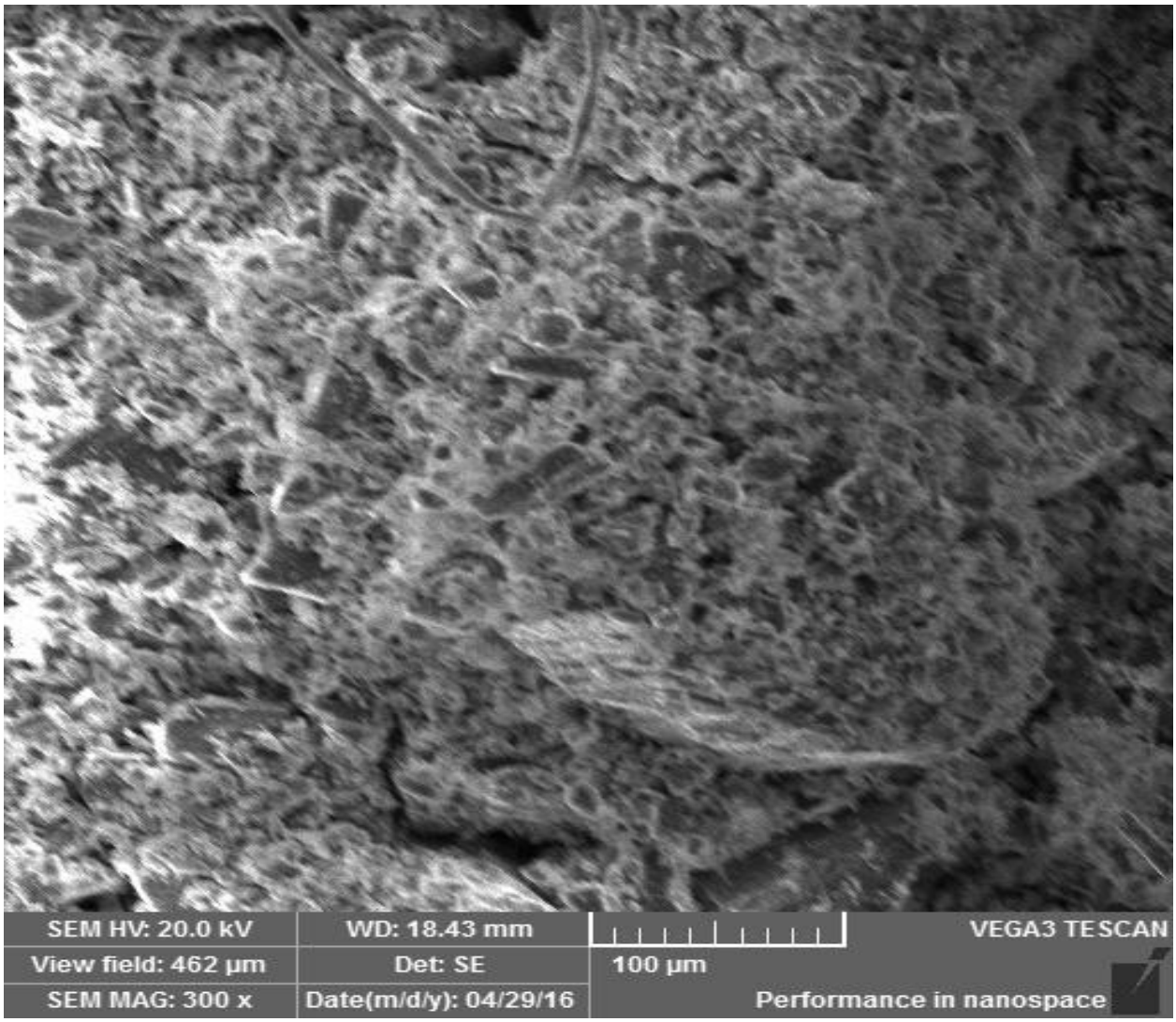

Fig (5-5) ZN1magnification 300 time

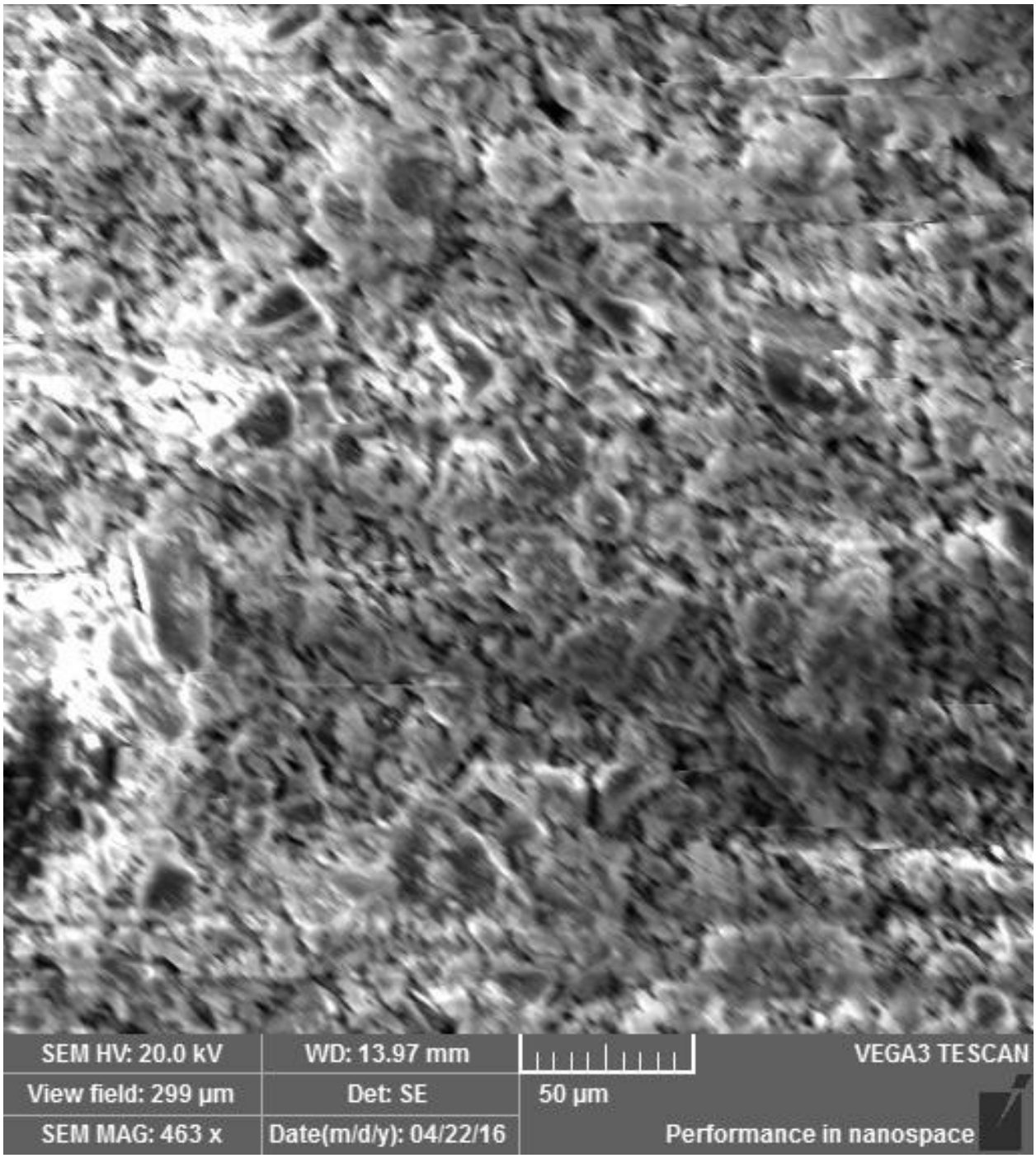

Fig (5-6) ZN2 magnification 463 Time

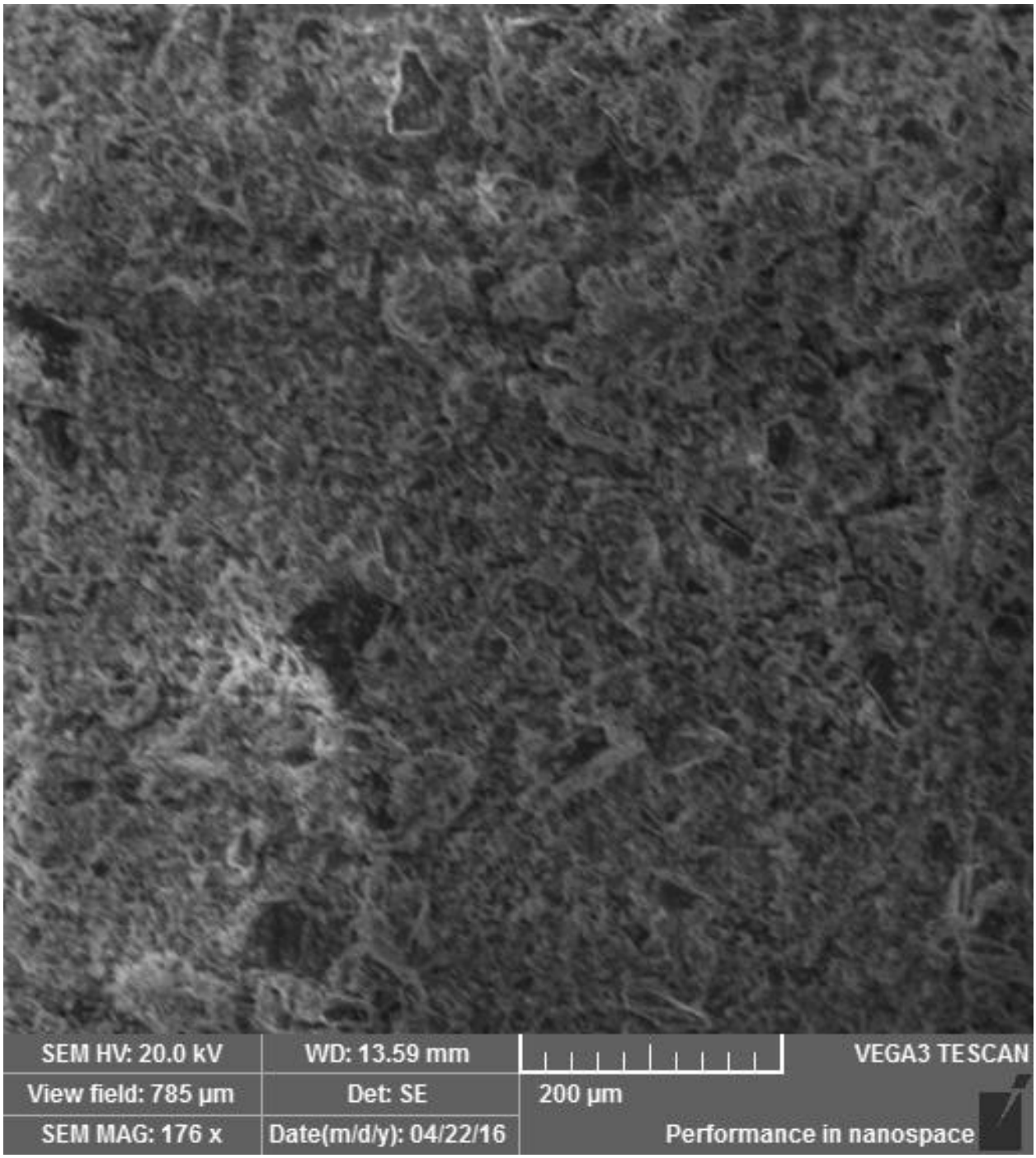

Fig (5-7) ZN2 magnification 176 time

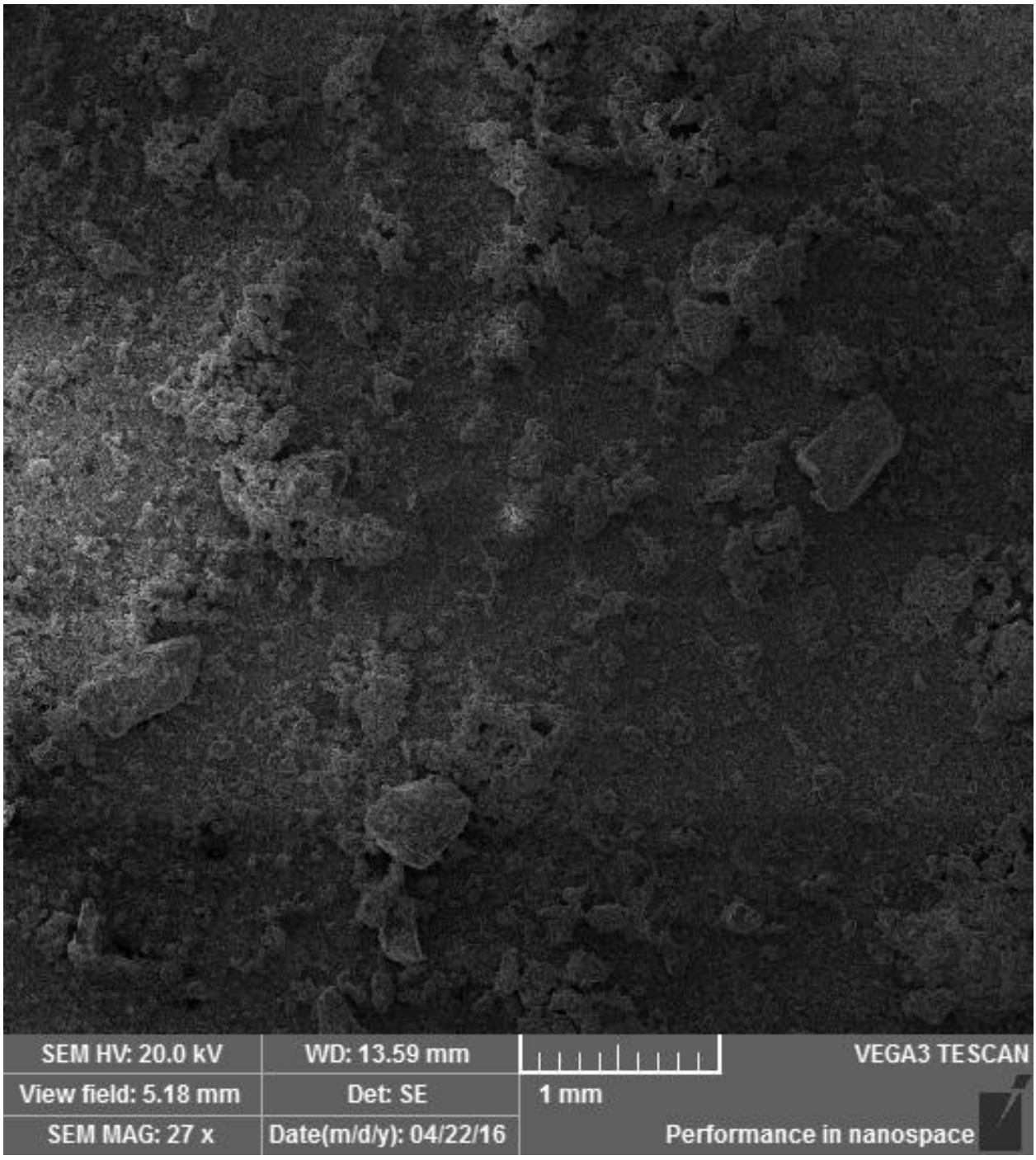

Fig (5-8) ZN2 magnification 27 time

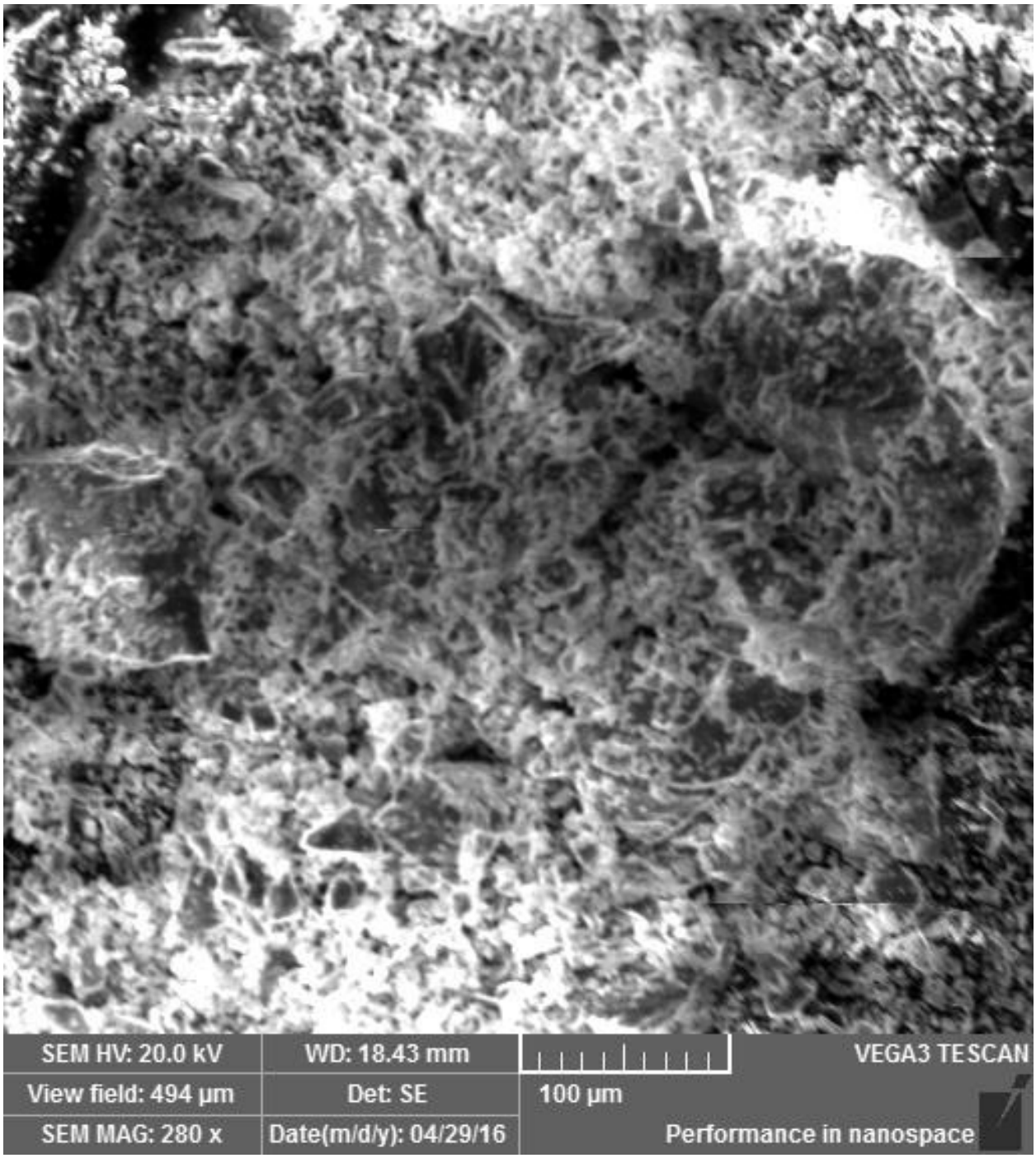

Fig (5-9) ZN2 magnification280 time

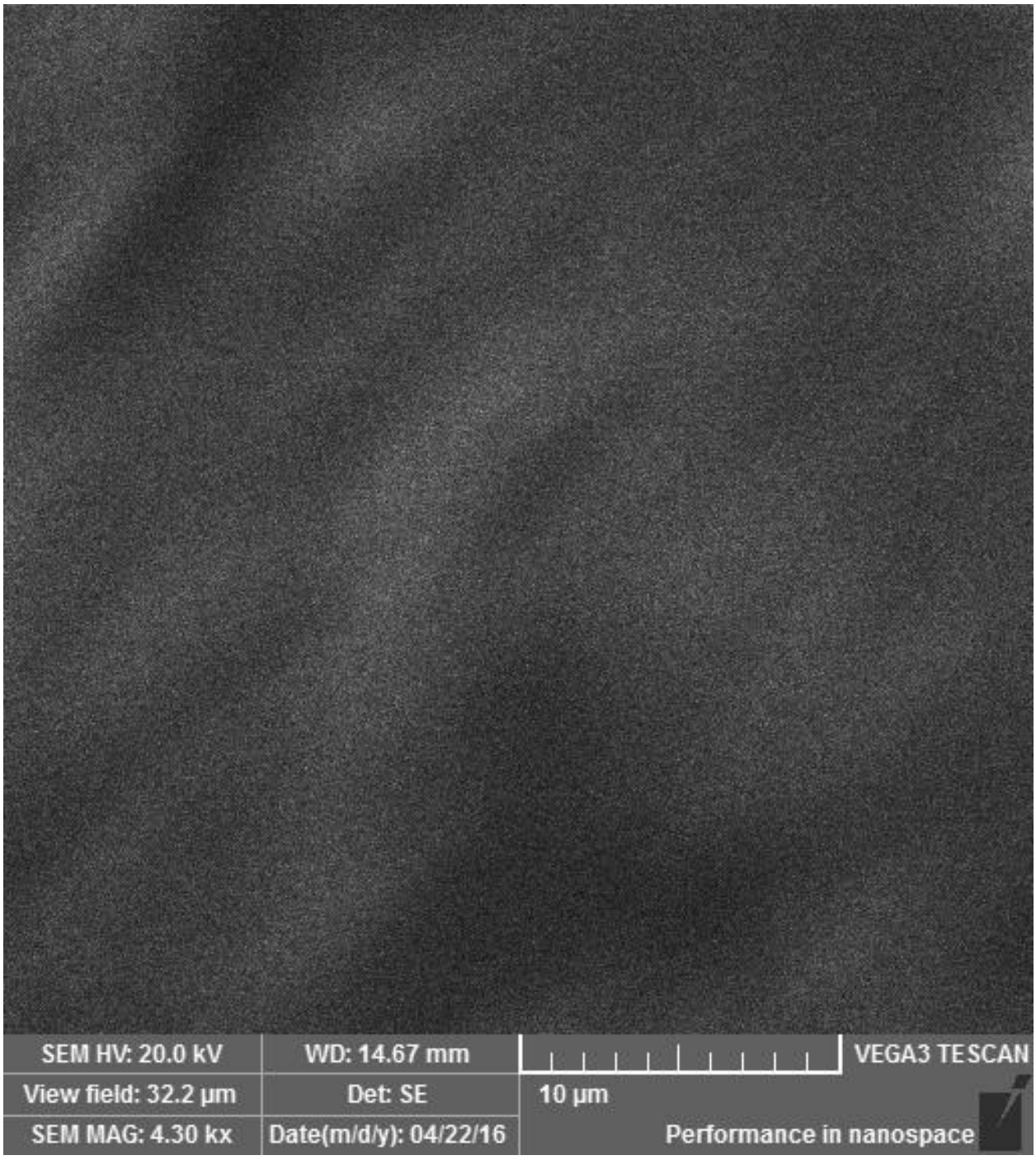

Fig (5-10) Ka magnification 4.30 time

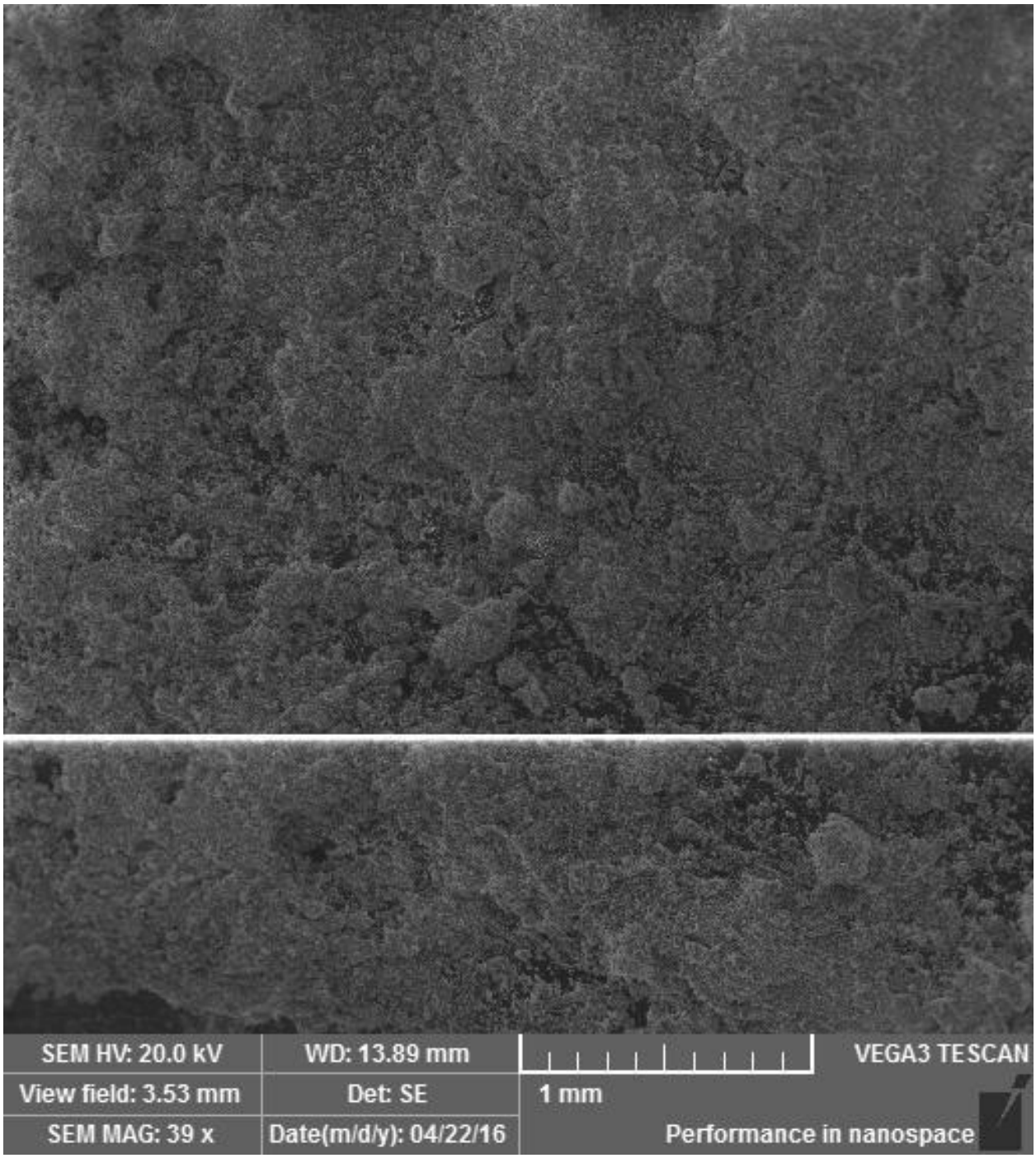

Fig (5-11) Ka magnification 39 time

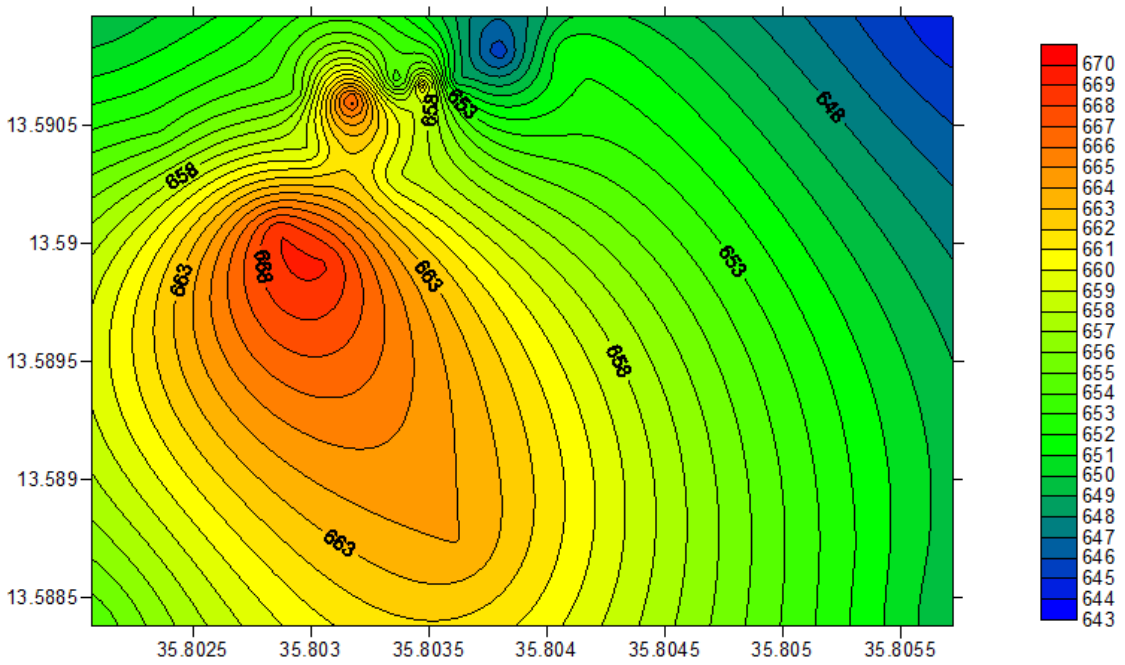

Fig (5-12) Cantor map of zeolite collected

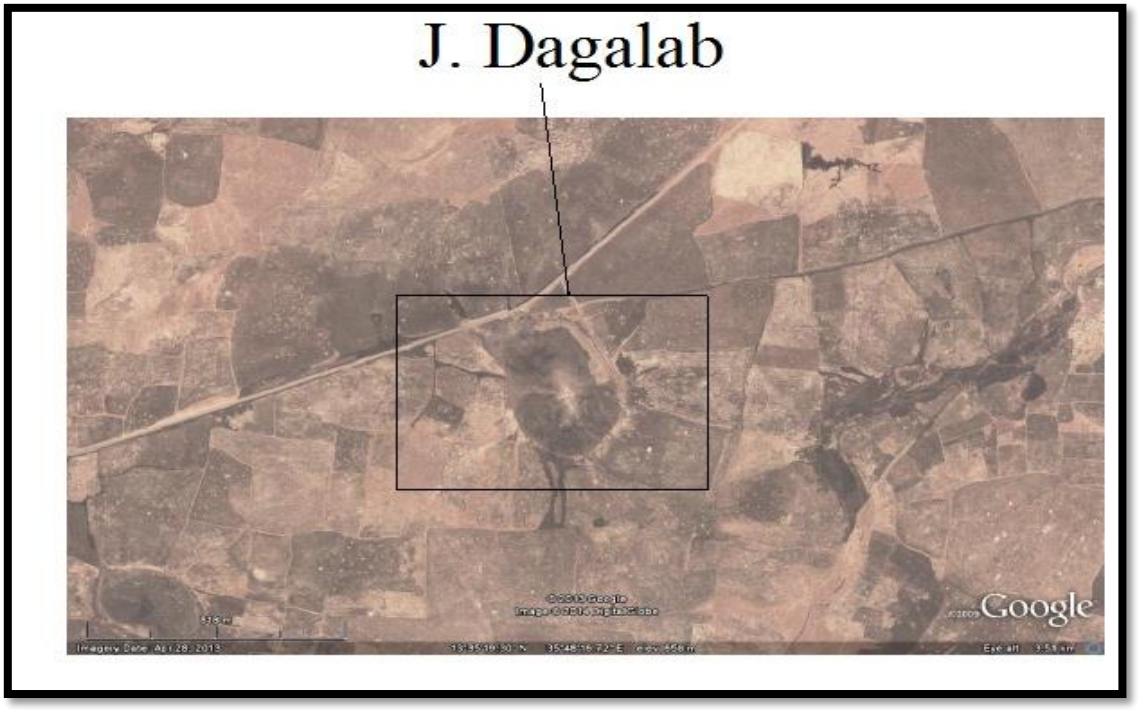

Fig (5-13) satellite map of zeolite collected

Fig (5-14) Fluid mud samples location

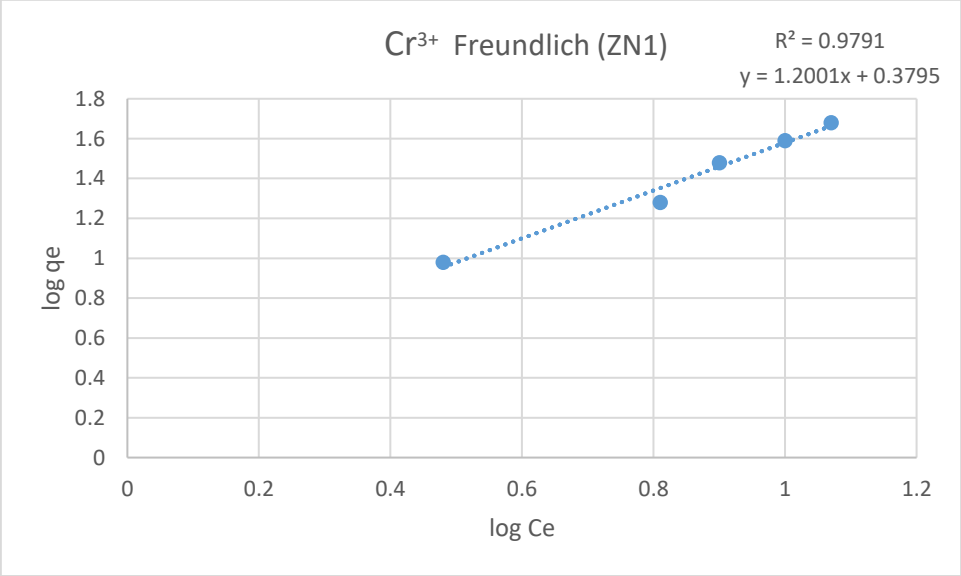

Fig (5-15) Cr^{3+} Fruendlich isotherm of ZN1

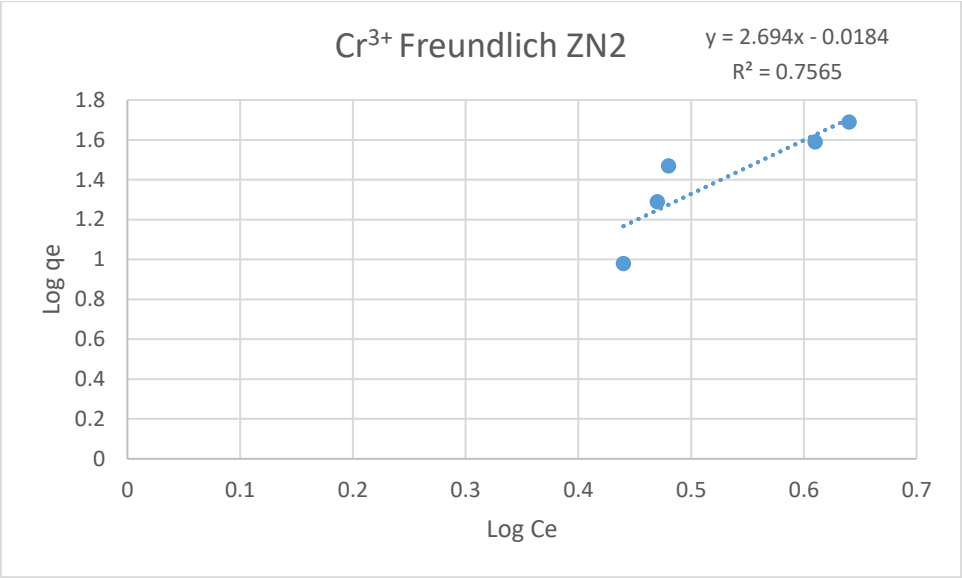

Fig (5-16) Cr^{3+} Fruendlich isotherm of ZN2

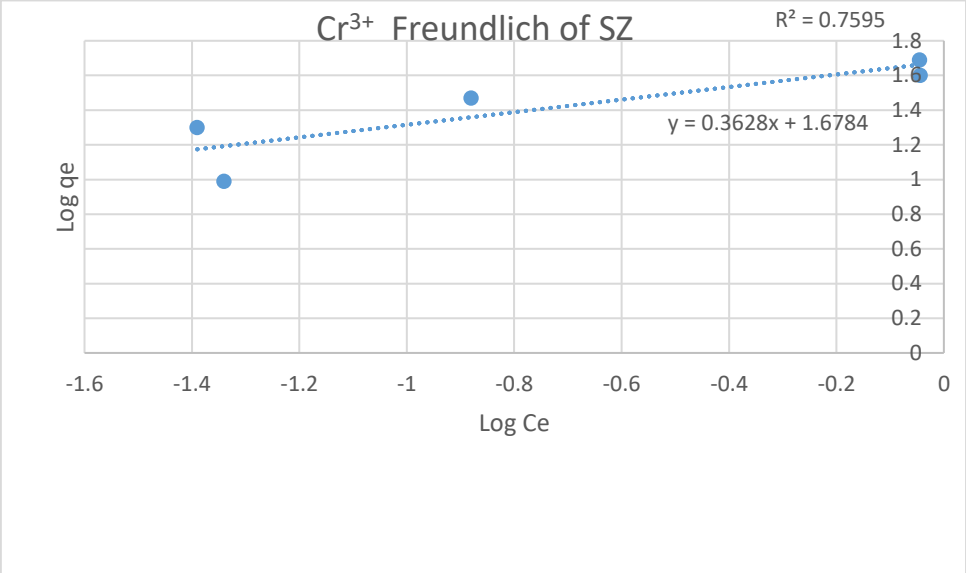

Fig (5-17) Cr^{3+} Fruendlich isotherm of SZ

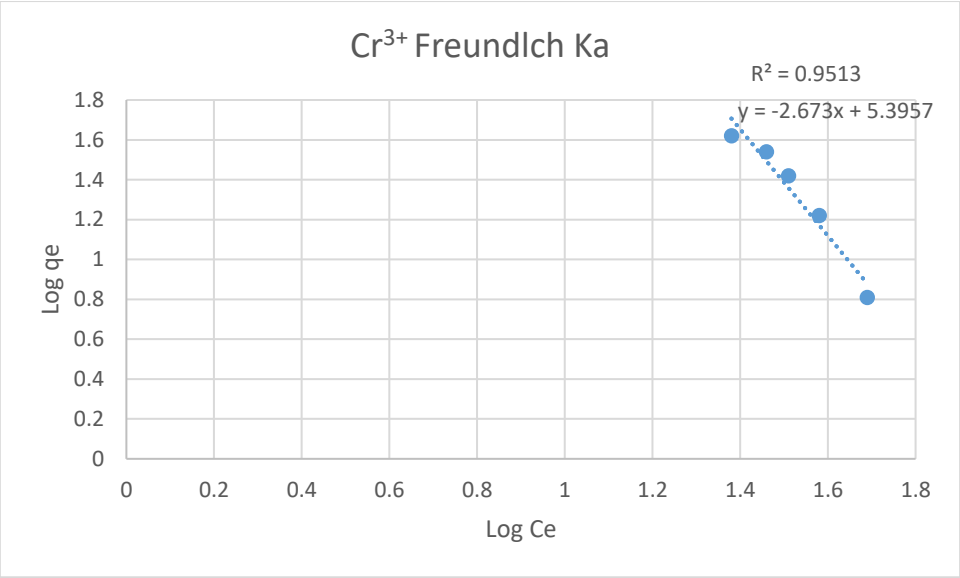

Fig (5-18) Cr^{3+} Fruendlich isotherm of Ka